SPACE SCIENCES LABORATORY

California U

UNIVERSITY CALIFORNIA

BERKELEY CALIFORNIA

SPACE SCIENCES LABORATORY

UNIVERSITY OF CALIFORNIA

Berkeley 4, California

INVESTIGATION OF DYNAMIC STRESSES

IN DETONATION TUBES

by

R. D. Wing

M. C. de Malherbe

A. J. Laderman

A. K. Oppenheim

Faculty Investigator

ABSTRACT

35353

This work reports a study made of the stresses induced in a thin cylindrical tube by int.rnal blast loading from a detonation wave. A method for the prediction of the cylinder's stress response has been developed on the basis of a simple dynamic model of the vibrating system and an approximate expression for the shape of the blast loading wave. The results are demonstrated to compare satisfactorily with experimental stress measurements.

This investigation was associated with an experimental study of detonation phenomena in hydrogen-oxygen mixtures contained in large diameter cylindrical vessels. The safety of the vessel is critically dependent upon the magnitude of the hoop stresses induced in the cylinder walls by the detonation process. A strain measuring system utilizing semiconductor strain gauges was employed to monitor the stresses, and these results, in conjunction with the theoretical stress predictions, provided a satisfactory check on the state of stress in the metal.

TABLE OF CONTENTS

NOMENCLATURE

C_2 - Constant (for strain gauges).

E - Young's Modulus of Elasticity.

F - Force

$G.F$ - Gauge Factor (for strain gauges).

h - Thickness of cylinder.

H - Step function.

k - Spring constant.

L - Length of cylinder.

m - Mass.

p - Pressure.

r - Radius

$\ddot{r}$ - Radial acceleration

R - Reflected wave pressure ratio

R - Electrical resistance

s - Sensitivity

s - Transform variable

t - Time

T - Decay time

u - Displacement

Greek Symbols

α - Temperature expansion coefficient

γ - Ratio of specific heats

ϵ - Strain level

δ - Non-linearity

θ - Angular measure

ρ - Density

ϕ - Dynamic time function

S - Stress

η - Efficiency

ω - Natural frequency

z - Axial length

Subscripts

o - Initial condition

m - Maximum

z - Axial

θ - Hoop

FIGURES

Figures for Appendices

INTRODUCTION

This work describes an experimental and analytical investigation of stresses induced in dynamically loaded cylindrical pressure vessels. The program was associated with studies of gaseous detonation conducted at the Propulsion Dynamics Laboratory, University of California, Berkeley. As part of these studies, observations were made in detonating hydrogen-oxygen mixtures contained in a 2 ft. diameter x 20 ft. long stainless steel cylindrical vessel.

To provide an adequate margin of safety, it was decided to restrict operation of the vessel so that the maximum stress induced by the explosion would not exceed the yield stress of the material. This was to be accomplished by placing an upper limit on the initial pressure of the mixture for each condition of initial temperature and composition. A series of detonation tests were to be performed, at successively increased values of initial pressure, until the maximum stress, deduced from strain measurements made at selected locations on the vessel, approached the yield condition.

The dynamics of thin-walled cylinders have been studied by a number of investigators, and among the first reported works are the classical treatises of Lord Rayleigh (1) and Love (2). These early references, however, are of limited application since they are concerned with cylinders having infinitely thin walls. A more useful and up-to-date treatment of thin-shell

theory can be found in the authoritative text of Timoshenko (3).

There are essentially two indepenaent ways in which a thin cylinder responds to dynamic excitation. These are demonstrated in Fig. 1 where they are classified a (a) extensional vibrations, and (b) bending modes.

Extensional vibrations, (a), are set up as a direct result of symmetrical excitation in the radial and axial directions. There is only a single mode of oscillation in each instance, that is to say, the radial and axial vibrations take place at their corresponding fundamental frequencies. The amplitudes of vibration are not only dependent on the geometry of the vessel, the point of application of the load, and its magnitude, but are highly sensitive to the duration and pulseshape of the load.

The bending modes, (b), are systems of combined axial and radial harmonic flexural vibrations. There are an infinite number of modes for both the axial and radial directions and hence an infinite number of combinations of these modes constituting this aspect of the cylinder's motion. The relative amplitudes of the various modes are dependent on boundary conditions such as the shell geometry and the method of excitation. In the present application the excitation of the cylinder was radially symmetric so effects from the bending modes were negligible. The treatment of flexural vibrations in thin cylinders by Arnold and Warburton (4), which was extended by Mixson and Herr (5) to include the effect of internal static pressures in the cylinders, provides a satisfactory background for this part of the analysis and is presented here in Appendix I.

The extensional response of a pressure vessel to a single pulse was discussed in recent papers by Baker (6), and Hodge (7).

Baker developed the basic equations of motion for a thin sphere subjected to a linearly decaying radial pressure pulse, accounting for both elastic and plastic shell deformation. In the elastic range the differential equations of motion are linear and may be solved by Laplace transform techniques in a manner similar to that for other vibrating systems, i.e. single degree of freedom spring-mass or inductance-resistance networks. Consideration of these analogous systems permits the attainment of solutions for a variety of pulse loading wave-shapes. A comprehensive treatment of such solutions is given in reference (8). The analysis by Baker for the plastic range becomes fairly complex, and, in spite of a highly simplified model, it leads to non-linear differential equations of motion which must be solved by numerical techniques.

Hodge (7) considers only the plastic deformation of thin cylinders since his primary concern was the point of ultimate failure. The paper is of interest, however, in that a variety of blast-loading waveshapes are considered, giving a notable expansion of applications.

Since it was specified earlier that the vessel was not to be stressed beyond its yield point, the present analysis is restricted to the elastic range. Theoretical stress predictions based on the dynamic behavior of a simple dynamic model are correlated to experimental measurements of strain obtained by use

of semiconductor strain gauges on the outer surface of the vessel.
Theoretical and experimental agreement is shown to be satisfactory,
thus establishing a useful design approach for future situations
of this kind, which might include, for example, the design of
safety vessels for proof testing of high pressure equipment, or
the design of rocket motor thrust chambers where the design must
provide for the possibility of internal explosions. It should
be noted that application of this theory is not restricted to
cylinders. A simple change of the coordinate system or the
boundary conditions of the equations would make the method appli-
cable to almost any mathematically definable thin shell design.

THEORY

The dynamic response of the vessel is determined from the equations of extensional motion of a cylindrical surface under the action of a radially acting force which are derived in generalized form by Timoshenko (3).

Figure 2 shows the segment of cylinder considered, a curved-face rectangle of width $r d\theta$ and length dz. A time varying pressure impulse, $p(t)$, acts radially outwards on the element, giving rise to two major stresses, an axial stress, σ_z, and a hoop stress, σ_θ. Bending stresses caused by $p(t)$ will be negligible provided that the analysis is restricted to long uniform cylinders and that end effects are not considered. Static stresses which result from a pressure difference across the walls of the cylinder are neglected, but may be accounted for in the general stress system by simple addition in the event they acquire significant magnitude.

Before proceeding, some realistic forms of dynamic loading are examined. This particular investigation calls for an examination of blast-type loadings, which, generally speaking, are considered as a single application of a large force for a very short period of time. Such loadings are specified analytically in terms of their peak pressure, p_m, and total time of duration or decay, T. Several blast-type loading pulse-shapes are shown in Fig. 3, arranged in order of successively better approximations to the measured wave shapes of typical blasts.

The rectangular step function, (A), provides the simplest boundary conditions for solution of the equations of motion, but is the least accurate representation of a typical blast load. The pulses with linear and exponential decays, (B) and (C), can generally be used as good approximations to the loading pulse-shape, and provide reasonably straightforward solutions to the equations of motion. The best approximations to a blast load, (D) and (E), are unfortunately in too complex a mathematical form to permit easy matching to experimental results, i.e. there is considerable difficulty involved in finding the best values of the constants for the mathematical forms when matching experimental data.

In the following analysis, the linear decay pulse, (B), has been used as an example throughout. Experience has shown that this waveshape approximates well to the type of blast loading associated with gaseous detonation processes. In Appendix II, solutions to the equations of motion are given for the other waveshapes shown in Fig. 3.

Consider, now, the hoop and axial stresses induced in the cylinder by a pressure loading function $p(t)$. In this example it is taken as sawtooth wave shape, pulse (B) as shown in Fig. 3, which is given by:

$$p(t) = \begin{cases} p_m(1 - t/T) & \text{for } 0 \leq t \leq T \\ 0 & \text{for } t \geq T \end{cases}$$

where T is the total time of duration of the pulse, and p_m its maximum pressure.

Hoop Stress σ_θ

Figure 2 shows a small segment of cylinder under the action of a radial pressure $p(t)$, giving rise to a hoop stress σ_θ . In order to find the radial acceleration, $\ddot{r}$, from $\Sigma F_r = m\ddot{r}$, the radial forces may be equated thus giving us the equation of motion:

$$-2\sigma_\theta \left(\sin \frac{d\theta}{2}\right) h dz + p(r d\theta dz) = \rho h r d\theta dz \, d^2u/dt^2 \tag{1}$$

which, upon simplification becomes:

$$\ddot{u} + \omega^2 u = p(t)/\rho h \tag{2}$$

The complete solution to equation (2) may be found in Appendix II, but here only the final results will be quoted.

When $p(t)$ is given by the sawtooth function, ( ), the hoop stress, determined by the method of Laplace transform is:

$$\sigma_\theta = \left(p_m r/h\right) \phi_\theta \tag{3}$$

where

$$\phi_\theta = \begin{cases} \left[1 - t/T - \cos\omega_\theta t + \dfrac{\sin\omega_\theta t}{\omega_\theta t}\right] & 0 \le t \le T \\[2ex] \left[\left(\dfrac{1-\cos\omega_\theta T}{\omega_\theta T}\right) \sin\omega_\theta t - \left(1 - \dfrac{\sin\omega_\theta T}{\omega_\theta T}\right)\cos\omega_\theta t\right] & t \ge T \end{cases} \tag{4}$$

and r is the cylinder radius, h its thickness, and ω_θ its natural hoop frequency of vibration.

It should be noted that the solution for σ_θ is composed of two parts—a parameter $\left(p_m r/h\right)$ corresponding to the hoop stress

induced in a thin cylinder by a static internal pressure of magnitude, p_m , and a dynamic time function, ϕ_θ , representing the correction to σ_θ required for the specified time variant loading.

Axial Stress

Axial vibrations of the vessel are set up when the detonation wave reflects from the end wall at the end of the cylinder opposite to the ignitor. In this case the response of the vessel can be compared ideally to the motion of a spring-mass-system, Fig. 4, where:

the spring constant of cylinder = $k = AE/L = 2\pi r h E/L$

the mass of system = mass of the end-flange = m

The equation of motion for this system is:

$$m\ddot{x} + k\ddot{x} = F(t) \tag{5}$$

where here $x = U_z$, the displacement from equilibrium position. For the sawtoothed impulse example, the R.H.S. of Eq. (5) is:

$$F(t) = p(t)A = \begin{cases} R\pi r^2 p_m \left(1 - t/T\right) & \text{for } 0 \leq t \leq T \\ 0 & \text{for } t > T \end{cases}$$

where R accounts for the difference in peak amplitudes between the incident and reflected pressure pulses. Thus, if p_m is the incident wave peak pressure, then the reflected wave will have a peak pressure of Rp_m.

When dealing with the reflection of detonation waves from a solid end wall, theoretical prediction of the value of R is

virtually impossible due to the complexity of the interaction process. R must then be found by comparing direct measurements of pressure taken at the side wall and end wall of the cylinder. The case may arise, however, of a simple (non-reactive) shock wave undergoing the reflection process and, for this case, gasdynamic theory can provide an estimation of the value of R . The shock reflection process is depicted in the space-time plane, Fig. 5.

Using the form given by reference (9), the ratio of the reflected to incident wave pressures is:

$$\frac{P_2 - P_0}{P_1 - P_0} = 1 + \frac{7}{6\, P_0/P_1 + 1} \quad \text{for} \quad \gamma = 1.4$$

where P_0 is the pressure of the gas at rest, P_1 the pressure behind the incident shock wave, and P_2 the pressure behind the reflected wave.

In terms of the incident wave pressure ratio, then, R can be expressed as:

$$R = P_2/P_1 = \frac{8\, P_1/P_0 - 1}{P_1/P_0 + 6}$$

The equation of motion, (5), can then be written in the form:

$$d^2 u_z/dt^2 + k u_z/m = R\pi r^2 p_m(t)/m \tag{6}$$

which by comparison to Eq. (2) leads, by inspection, to the

following expression for the axial stresses:

$$\text{Axial stress,} \quad \sigma_z = \frac{R p_m r}{2h} \cdot \phi_z \tag{7}$$

where

$$\phi_z = \begin{cases} \left[1 - t/T - \cos \omega_z t + \frac{\sin \omega_z t}{\omega_z T} \right] & for \quad 0 \leqslant t \leqslant T \\[4mm] \left[\left(\frac{1 - \cos \omega_z T}{\omega_z T} \right) \sin \omega_z t - \left(1 - \frac{\sin \omega_z T}{\omega_z T} \right) \cos \omega_z t \right] & \\ & for \quad t \geqslant T \end{cases} \tag{8}$$

ω_z being the natural axial frequency of vibration of the cylinder. As was the case with the hoop stress, it can be seen that the solution is comprised of two parts - one a static parameter corresponding to the axial stress that would be induced in a cylinder loaded with a static pressure of magnitude ($R p_m$) and the other a dynamic loading function ϕ_z , giving the correction to σ_z for the given dynamic load.

Apart from the solutions for the hoop and axial stresses just considered, Appendix II gives the solutions for the other wave-shapes shown in Fig. 3. In each case it is found that the solution is in the same form, a static stress parameter multiplied by a dynamic loading function. Graphs are given in the Appendix of these functions for most of the loadings considered. the plots being on a non-dimensional amplitude-time coordinate system.

EXPERIMENTAL APPARATUS

Test Vessel

Figure 6 shows a side elevation of the detonation tube, a 20 ft. long x 2 ft. diameter stainless steel cylinder of 3/8" wall thickness, closed at one end by a solid plate, and at the other by a removable flange. The vessel is supported at three places, as indicated on the drawing. A viewing section of glass portholes intended for Schlieren visualization of the flow extends alond nearly half the length of the cylinder. In addition, the vessel is tapped in numerous locations with ports to accept pressure transducers, ionization pick-ups, thermocouples, etc.

Provision is made for heating and cooling the vessel in order to run tests in the range -200 to +200°F, this being effected by electric heating rods attached to the vessel's outer skin and a liquid nitrogen spray cooling system. The instrumented vessel is shown in Fig. 7.

The procedure for running detonation experiments was to first evacuate the vessel to a pressure of a few microns of Hg, next fill with a pre-mixed charge of hydrogen and oxygen to the desired initial pressure, then to initiate the detonation prccess with a small charge of solid explosive. A detonation wave would be quickly established and travel down the length of the vessel to be ref'ected at the far end wall.

Of the many instruments used in these tests to observe the detonation process, only the pressure and strain recorders are

of direct interest here, although temperature measurements were required in conjunction with the strain measurements and ionization pick-ups were needed to trigger this instrumentation.

Pressure Measurement

The pressure-time history of the detonation waves at 2 ft. intervals along the length of the vessel and at the end wall was recorded by a series of piezo-electric pressure transducers. The particular transducers used were Kistler type 601 quartz crystal pick-ups, with a sensing element 1/8" diameter, a pressure range of 1 - 5000 psi, a sensitivity of $0.5\mu\mu$ Cb/psi, and a rise time of 3 μsec. The output from the transducers were recorded using Tektronix 535 and 551 oscilloscopes.

Strain Measurement

Measurements of the strains produced in the detonation tube were made using strain gauges located at a number of points on the outer surface of the vessel. A few gauges were attached at critically stressed points (on corner welds and around the entrance ports), but these were solely for safety reasons and need not be further considered here. The remaining gauges were affixed at locations 6 ft., 14 ft., and 18 ft. from the closed end, on reasonably uncluttered parts of the vessel's skin where surface discontinuities would not affect the results. At each location the gauges were mounted in pairs, one to read axial and the other radial strains at each of the measuring stations.

Choice of the strain gauge instrumentation lay essentially between:

(a) Wire grid gauges of a special type having their backing strip and insulation made of a suitable material to withstand the wide range of temperatures over which the tests would be conducted. It is necessary, when using this type of gauge, to amplify their output considerably - this requirement for amplifiers unfortunately increasing the overall cost of the instrumentation quite considerably.

(b) Semiconductor strain gauges for which no additional amplification is necessary - the output from this type of gauge is sufficient to permit direct connection to be made to an oscilloscope with high sensitivity amplifiers.

The semiconductor system was chosen as being most suitable for this application , and Baldwin-Lima-Hamilton type SPB2-18-12 strain gauges were selected. Full details of the installation and calibration of the gauges is given in Appendix II.

The recording system for preservation of permanent records of the strain history were obtained using Tektronix 535 or 551 oscilloscopes equiped with Polaroid cameras. The complete strain recording system is shown in outline in Fig. 8.

EXPERIMENTAL RESULTS

The series of stress measurements reported here was run using stoichiometric mixtures of hydrogen and oxygen in the pressure range 100 to 200 mm Hg. Simultaneous readings were taken from the pressure and strain gauges during each test, the outputs being recorded on oscilloscopes (and preserved by photographs) which were triggered at the time of passage of the detonation wave by ionization probes. Measurement of the time intervals between successive pressure traces permitted the detonation wave to be traced as it passed down the cylinder and was reflected at the end wall. Such a trace is shown on the time-distance plane in Fig. 9. In this case, the triggering ionization probe was at station 2, and the wave's passage plotted from pressure records made at stations 3, 5, 7, and 9 which are shown in Fig. 26, together with strain records made at stations 3, 7, and 9. Figure 10 is typical of measurements made at 100 mm Hg initial pressure; a typical set of measurements for 200 mm Hg is given in Fig. 11; Fig. 12 shows further results for 100 mm Hg, the oscilloscope sweeptime being extended in this case to show better the low frequency axial vibrations.

Analysis of the pressure records for a number of experiments made at the same initial conditions permits plotting of the variation of the peak wave pressure along the detonation tube (Fig. 13).

Similarly the reflected wave pressure is found from
the pressure records made at the end wall of the vessel.
These are plotted as a function of initial mixture pressure,
Fig. 14. Figures 13 and 14 clearly indicate the effect of
using the Primacord explosive to initiate the detonation
process - the detonation wave is "overdriven" by the explosive
charge, resulting in wave pressures generally higher than those
predicted by the Chapman-Jouguet detonation theory, reference (9).

ANALYSIS AND DISCUSSION

The dynamic response of the cylinder in terms of the hoop and axial stresses can be predicted from Eqs. (3) and (7) provided the specific boundary conditions can be supplied. These conditions are:

(a) ω_θ and ω_z, the hoop and axial natural frequencies of the vessle, respectively, which may be found from the physical dimensions and material properties of the cylinder.

(b) the equation for the pressure loading function, $p(t)$, here assumed to be a sawtooth pulseshape.

(c) the magnitude of the peak wave pressure, which may be obtained directly from Figs. 13 and 14.

(d) the decay time of the pressure pulse, also obtained from the pressure records in the manner explained in Fig. 15.

Evaluating these, in order, for the case in question:

(a) the expression for the natural hoop frequency, ω_θ, is given by Eq. (A2.5) in Appendix II:

$$\omega_\theta = \sqrt{E/\rho r^2}$$

where for type 304 stainless steel,

E = 29 x 10^6 psi

ρ = 0.287 lb/in^3

r = the mean radius of the cylinder = 12.19 in.

so that

$$\omega_\theta = 16,316 \text{ radians/sec} = 2,597 \text{ cycles/sec.}$$

The axial natural frequency, ω_z, is given by Eq. (A2.16), Appendix II as:

$$\omega_z = \sqrt{k/m} = \sqrt{\frac{2\pi r h E}{mL}}$$

where

m = mass of vessel end cap = 940.7 lb

L = length of vessel = 240 in.

h = wall thickness of vessel = 0.375 in.

then

$$\omega_z = \sqrt{\frac{2\pi \times 12.19 \times 0.375 \times 29 \times 10^6 \times 386}{940.7 \times 240}}$$

$$= 1,1935 \text{ radians/sec} = 191 \text{ cycles/sec.}$$

(b) pressure loading function,

$$p(t) = \begin{cases} p_m(1 - t/T) & 0 \leq t \leq T \\ 0 & t \geq T \end{cases}$$

(c) peak pressure, p_m. In order to permit use of the response curves (shortly to be obtained) for a range of peak pressures, p_m is taken as unity.

(d) decay time, T, of pressure pulse. The experimental results obtained from the present test shows that the range $0.1 < T < 10.0$ milliseconds.

Substituting these values in Eqs. (3) and (4), (7) and (8) yields the appropriate expressions for the hood and axial stresses.

Hoop Stress

$$\sigma_\theta = \left(Pm\, r/h\right)\phi_\theta = \frac{Pm \cdot 12.19}{0.375}\; \phi_\theta \quad p.s.i. \tag{3}$$

where

$$\phi_\theta = \begin{cases} \left[1 - t/T - \cos(16.316\,t) + \dfrac{\sin(16.316\,t)}{(16.316\,T)}\right] \\ \qquad\qquad\qquad\qquad\qquad \text{for } 0 < t < T \\[2mm] \left[\left(\dfrac{1-\cos 16.316\,T}{16.316\,T}\right)\sin(16.316\,t) - \left(1 - \dfrac{\sin 16.316\,T}{16.316\,T}\right)\cos(16.316\,t)\right] \\ \qquad\qquad\qquad\qquad \text{for } t > T \end{cases} \tag{4}$$

and both t and T are to be given in milliseconds.

The calculation of ϕ_θ is almost identical to the calculation of $\phi(t)$ which is given in detail in Appendix II. The computer program for this computation, as shown in Table 1, is for a range of pulse decay times from $1.0 \leqq T \leqq 10$ milliseconds. Figure 16 shows the resulting computer output, which is in the form of a graph of ϕ_θ versus time t yielding a family of curves for the various values of decay time, T. Figure 17 shows a similar plot of ϕ_θ for the range of decay times $0.1 \leqq T \leqq 1.0$ milliseconds. Values of ϕ_θ obtained from these curves may be substituted directly into Eq. (3) to obtain the actual value of the hoop stress, σ_θ.

Axial Stress

Equation (7) gives:

$$\sigma_z = \frac{R\,p_m\,r}{2h} \cdot \phi_z$$

$$= \frac{(R\,p_m)\,12.19}{0.75} \cdot \phi_z \quad p.s.i.$$

where, from Eq. (8),

$$\phi_z = \begin{cases} \left[1 - t/T - \cos(1.1935t) + \dfrac{\sin(1.1935t)}{1.1935\,T}\right] & 0 \leq t \leq T \\[4mm] \left[\left(\dfrac{1-\cos(1.1935\,t)}{(1.1935T)}\right)\sin(1.1935\,t)\right. \\[4mm] \left. -\left(1 - \dfrac{\sin(1.1935\,t)}{(1.1935T)}\right)\cos(1.1935\,t)\right] & t \geq T \end{cases}$$

where again both t and T are to be specified in milliseconds.

In the same manner as for the hoop stress ϕ_z has been computed for a range of decay times $1.0 \leq T \leq 10$ milliseconds using an electronic computer. The resulting graph is shown in Fig. 19, where ϕ_z against time, t. Values of ϕ_z obtained from this graph may be substituted directly into Eq. (7) to obtain the actual value of axial stress, σ_z.

COMPARISON OF THEORY AND EXPERIMENT

Results for the dynamic stresses in the cylinder are
now available in two forms which will be compared in detail.
These are (a) purely experimental strain measurements, and
(b) theoretical stress predictions which are still partly
experimental in that they depend upon the pressure measurements
to obtain the input waveshape.

Comparison of Measured and Predicted Frequencies of Vibration

Collected measured values of the natural hoop and axial
frequencies are given in Table 2 together with the corresponding
calculated values. The form of the loading function does not
appear in the expressions for the vessel's natural frequencies -
Eqs. (A2.5) and (A2.16) in Appendix II. However there are
several other ways in which inaccuracies may be expected to
appear in these values, for example:

a) Variations are to be expected in the steel manufacturer's
   quoted values of the cylinder material's properties,
   not only for the vessel as a whole, but also from
   point to point in the material.

b) Dimensional accuracy in the cylinder's skin thickness,
   h , is known to be poor. The nominal thickness of
   3/8" may vary by as much as $\pm$ 1/16" which, for the
   axial frequency, would result in considerable variation
   from the calculated value. The hoop natural frequency
   is independent of skin thickness, provided this dimension

is very small compared with the cylinder's radius.

c) In measurement of the mass of the vessel's end cap
in order to find the axial natural frequency, it
is difficult to determine how much of the mass of the
end flange and clamping bolts should be included, an
additional problem being the welding between the
cylinder and end flange which has obliterated the
transition point and locally increased the cylinder's
"spring-constant".

Comparison of Measured and Predicted Maximum Stress Amplitudes

The experimental and predicted values of the maximum
tensile stress amplitudes are presented in Table 3, and shown
graphically in Fig. 19.

Predicted values require specification of the input loading
function, which was found in each case by reference to the rele-
vant pressure record, using the sawtooth approximation to
specify the function mathematically. Use of Figs. 16, 17 and
18 for the hoop and axial dynamic time functions led immediately
to the predicted values of the maximum stresses.

a) Hoop stress

In comparing the experimental and predicted values, it
will be seen that there is good agreement for the results
obtained at position 9, but values measured at position 7 fall
approximately 25% below the predicted values. This variation
is most probably due to an artificial strengthening of the

cylinder in the vicinity of position 7 by either an increase in the skin thickness or through the ribbing that supports an outer skin around the vessel.

b) Axial stress

Here there is considerable variation between experimental and calculated results. In each case the measured value is between 1/5 and 1/10 of that calculated. The discrepancy indicates that the transfer of energy between the end cap and cylinder walls is considerably less efficient than was anticipated. More light is thrown on this result by comparison of the dynamic waveforms, which are discussed in the following section.

Comparison of Dynamic Waveforms

a) Hoop stress

In Fig. 20 are reproduced the measured strain gauge outputs from Test CD 149 together with the calculated curve shown to the same scale from Fig. 16. As may be seen, agreement is good or the first 0.7 milliseconds, after which time the arrival of the reflected shock wave adds an additional loading to the system. The effect of the additional stressing due to the reflected shock wave could be included into the analysis, but the results for the time preceding the arrival of the reflected shock give all the data required.

Normally, as may be seen from the analytical and experimental results, the most serious stressing occurs in the first half cycle of the dynmaic response, when the dynamic loading

function, ϕ_θ, tends toward its upper limit of 2.0. In this particular case, however, a second loading pulse in the form of the reflected shock wave, was added to the motion before the effect of the first loading pulse had decayed, consequently cuasing the most serious stressing to occur during the first cycle of the response corresponding to the arrival of the second loading pulse.

The good agreement between the predicted and measured waveforms and peak amplitudes for the hoop stresses (at location 9) is satisfying, since it is these hoop stress that will cause the ultimate failure of the cylinder. The axial stresses, as measured, are only 50 to 60% of the hoop stress magnitudes. In any general stress system the component stresses must be summed, taking the Poisson's ratio effect into account, in order to find the magnitude of the maximum stress. Here, however, the two component stresses take place on different time scales and consequently never require their additive effect to be accounted for. The hoop stresses are excited first, reaching peak amplitude after approximately 0.2 milliseconds, and are substantially decayed by the time the axial stresses have reached maximum amplitude approximately 12 milliseconds later. Thus, the record on the axial strain gauge AA, shown together with the hoop record, BB, in Fig. 20 is purely a Poisson's ratio effect, given by:

$$\epsilon_z = (-0.29)\, \epsilon_\theta \tag{9}$$

b) Axial stress

The strain record for axial motion shown in Fig. 12, s recorded by gauge AA, may be compared with the calculated curve for axial response from Fig. 18, using the particular curve for a 2.0 millisecond decay time. The calculated curve, it may be seen, is almost exactly a pure sine wave of peak amplitude $\phi_{z\,(max)}' = 1.0$.

Examination of the experimental trace shows that from the second cycle onward the response is sinusoidal. The first cycle, however, is of considerably less amplitude, indicating a relatively slow transfer of energy from end plate to cylinder. This effect, and the diminution in stress amplitude noted previously would indicate that the simple model for axial motion (Fig. 4) should be somehow improved to account for the energy transfer from end plate to cylinder.

The gradual buildup of response amplitude is typical of the response of a two mass - two spring system, which could here be used as a model by considering the flange securing bolts as the second spring. Such a model is shown in Fig. 21, but is not examined in detail since it has already been determined that, in this case, the axial stressing does not produce the critical stresses in the cylinder.

CONCLUSIONS

A theory predicting the dynamic response of a cylindrical vessel under the action of a symmetric radial blast load has been developed. In addition, experimental data have been obtained for the dynamic stress response, the tests having been carried out on a 20 ft. long x 2 ft. diameter cylinder loaded by internal detonation of a mixture of hydrogen and oxygen. The response waveforms and peak stress loading in the critical hoop direction show close agreement between theory and experiment.

An important aspect of the experimental work was the use of semiconductor strain gauges - a relatively new technique for stress analysis. In evaluation of these gauges it must be said that their performance was most satisfactory, and apart from their tedious calibration requirements, represent a very significant step forward in strain gauge technology.

REFERENCES

1. Lord Rayleigh, <u>The Theory of Sound</u>, Dover, New York, 1040 pp, (1945).

2. Love, A.E.H., <u>The Mathematical Theory of Elasticity</u>, 4th ed., Dover, New York, xviii + 645 pp. (1944).

3. Timoshenko, S., <u>Theory of Plates and Shells</u>, McGraw Hill Co., New York, xiv + 580 pp., (1959).

4. Arnold, R.N. and Warburton, G.B., "The Flexural Vibrations of Vibrations of Thin Cylinders", Proc. Inst. Mech. Eng.A, <u>167</u>, 1, 62-74 (disc. 74-80), (1953).

5. Mixson, J.S. and Herr, R.W., "An Investigation of the Vibration Characteristics of Pressurized Thin-walled Circular Cylinders Partly Filled with Liquid", N.A.S.A. Tech. Rept. No. R-145, 1962.

6. Baker, W.E., "The Elastic-Plastic Response of Thin Spherical Shells to Internal Blast Loading", J. Appl. Mech., <u>27</u>, 139-144, May, 1960.

7. Hodge, P.G., "The Influence of Blast Characteristics on the Final Deformation of Circular Cylindrical Shells", J. Appl. Mech., <u>23</u>, 4, 617-624, 1956.

8. Ayre, Robt. S., "Transient Response to Step and Pulse Functions", Vol. 1, 54 pp. <u>Shock and Vibration Handbook</u>, Ed. by Cyril M. Harris and Charles E. Crede, McGraw Hill, New York (1961).

9. Courant, R., and Friedrichs, K.O., <u>Supersonic Flow and Shock Waves</u>, Interscience, New York, xvi + 464 pp. (1948).

10. Mason, W.P., Forst, J.J., and Tornillo, L. M., "Recent Developments in Semiconductor Strain Transducers", I.S.A. Preprint No. 15-NY60, (1960).

11. Dorsey, J., "Semiconductor Strain Gauge Handbook", Parts I and II, Baldwin-Lima-Hamilton (1963).

APPENDIX I

HARMONIC FLEXURAL VIBRATIONS

There are, as was explained in the Introduction, two salient
types of vibration pertaining to cylindrical shells: (a) exten-
sional vibrations, as have been examined in the preceding text,
and (b) bending or flexural modes.

It is evident that whereas the extensional vibrations, (a),
depend upon extension and some slight amount of bending, the
flexural modes, (b), are associated only with bending and do not
produce any appreciable extension or contraction of the surface
midway between the inside and outside cylinder walls. Practical
experience shows that a cylinder can easily be deformed by pressing
it inward at the periphery (for example at two opposite points,
illustrating the 2nd radial mode ...see Fig. 1). The operation
is clearly one associated with bending alone, since any extension
of the middle surface would require considerable force to produce
it.

The effect of any impulse loading on a cylinder will be to
excite both forms of vibration, the relative vibrational amplitudes
for a given cylinder being a function of the magnitude, the wave-
shape, and the point of application of the load. Taking each
vibrational form in turn, the type of loading to which each is
most susceptible can be examined.

Bending modes are, of course, most easily excited by a periodic force, especially when the frequency of the excitation is the fundamental or some harmonic natural frequency of the cylinder. In this case resonance can produce a rapid buildup of response amplitude leading eventually to the cylinder's failure. However, we are here only concerned with impact loadings, where the condition of resonance is never encountered.

Flexural vibrations, then, will not cause serious stressing of the vessel in this application, and, in fact, could be neglected if their effect did not show in the strain and pressure records. While producing almost no strain in the middle surface of the cylinder, some effect will be detectable on the inner or outer surfaces, so it is to be expected that these vibrations will appear as high frequency signals superimposed on the strain gauge records of extensional vibrations.

It is of interest to note that the piezo-electric pressure transducers used in these tests will also be susceptible to flexural vibrations. These transducers are acceleration sensitive through the inertia induced piezo-electric effect, so that, as these transducers are rigidly attached to the cylinder walls, flexural vibrations will induce an additional signal superimposed onto the response to the pressure pulse.

The acceleration induced signal on both strain gauge and pressure records was generally disregarded in analysis of data as the amplitudes involved were always small. The signal could be distinguished easily from the signal corresponding to other data

by the frequencies at which it appeared; these were easily found under test conditions by recording the output from a microphone positioned near the vessel, the creation of sound waves at the same frequencies being another direct consequence of this form of vibration.

Theory of Harmonic Vibrations

If m is the number of the radial mode (= half the number of nodes), and n the number of waves standing in the axial length of the tube, any combination of n and m can combine to form a vibration pattern, with external factors such as surface discontinuities, vessel supports, etc., determining which vibrational patterns will be present and in what proportions.

From the external conditions in this instance, it is possible to predict that (a) due to the three point method of support of the vessel (see Fig. 6) it is probable that the <u>even</u> axial modes will predominate (i.e. m = 2,4,6, etc.); (b) the method of excitation being an axially moving stress pulse, it is equally likely for the radial mode to be any of those possible, probably the <u>higher</u> frequencies being excited more easily than the low.

The following theory follows the approach of Arnold and Warburton (4), which itself is an adaptation of Love's classic theory (2). The effect of the static pressure difference across the walls of the cylinder is discussed by Mixson and Herr (5), but calculation of the effect in this instance showed that it could be neglected with no loss of accuracy to the analysis.

As it stands, the vessel under consideration is somewhat awkward to analyze since one end is closed by a disc-like integral closure and the other by a flange and associated removable end cap. The end conditions play an important role in determining the axial vibration mode and must be carefully considered. Arnold and Warburton account for end conditions by a factor modifying the value of λ, the wavelength factor, which, for freely supported ends is:

$$\lambda = \frac{\pi a m}{l} \qquad (A1.1)$$

where a is the mean cylinder radius, l the cylinder length, and m the number of the axial mode.

The other extreme case is the condition of fixed ends, when the wavelength factor becomes:

$$\lambda = \frac{\pi a}{l} \left(m + 0.3 \right) \qquad (A1.2)$$

Somewhere between these two cases lie the flanged and the drum-closed end conditions. Experimental evidence led to the following empirical expression to account for these:

$$\lambda = \frac{\pi a}{l} \left(m + 0.3^{-2h/d} \right) \qquad (A1.3)$$

where h is the wall thickness of the cylinder and d is an "equivalent diameter" for the end flange such that

$$d = d_1 \left[\eta^2 - 1 \Big/ \frac{1+\mu}{1-\mu} \eta^2 + 1 \right]^{1/3}$$

where η = flange outer radius/flange inner radius, d_1 is the flange

thickness, and μ is Poisson's ratio.

Equation (A1.3) is the expression for a flanged end, and does not account for the removable end cap which, however, has been shown experimentally to have negligible effect on the wavelength factor.

In addition to λ, the wavelength factor, Arnold and Warburton define a frequency factor, Δ, given by:

$$\Delta = 4\pi^2 f^2 \left(\frac{\rho a^2 [1-\mu^2]}{Eg} \right) . \tag{A1.4}$$

where f is the vibrational frequency, ρ the material density, and E the modulus of elasticity.

Re-arranging (A1.4) to give an expression for frequency, f, and substituting the following values for the cylinder used in this experiment:

a	= 12.19 in.		μ	= 0.29
l	= 240 in.		E	= 2 x 10^6 psi
d_1	= 2.85 in.		h	= 0.375 in.
h	= 1.295		d	= 1.565 in.

then
$$f = \frac{\sqrt{\Delta}}{2\pi}\sqrt{\frac{Eg}{\rho a^2(1-\mu^2)}}$$

$$= (2.70 \cdot 10^3)\sqrt{\Delta} \quad c.p.s.$$

and
$$\lambda = 0.1595 \, [m + 0.1855]$$

The frequency factor, Δ , is determined from the following equation, derived in the Appendix to Arnold and Warburton's paper, (4):

$$\Delta = \frac{K_0}{K_1} + \left(\frac{K_0}{K_1}\right)^2 \frac{K_2}{K_1} \tag{A1.5}$$

where $K_0 = 0.325\lambda_e^4 + 0.355\beta\left[(\lambda_e^2 + n^2)^4 + n^4(1 - 8\lambda_e^2 - 2n^2)\right]$

$K_1 = 0.355(\lambda_e^2 + n^2)^2 + 1.271\lambda_e^2 + 0.355n^2 + 1.355\beta(\lambda_e^2 + n^2)^3$

$K_2 = 1 + 1.355(\lambda_e^2 + n^2)$

with $\beta = h^2/12a^2$ $(= 0.79 \times 10^{-4}$ in this instance).

Now, using Eqs. (A1.3 - A1.5) an example is given of the calculation of the lowest vibrational frequency, that is, where the axial mode number, $m = 1$, and the radial mode number, $n = 2$.

The wavelength factor for $m = 1$ is:

$$\lambda_e = 0.1595 \ (1+0.1855)$$
$$= 0.1891$$

The K coefficients, leading to the value of Δ , and ultimately to the frequency, f , are, for $n = 2$:

$K_0 = (0.325 \times 1.281 \times 10^{-3}) + (0.355 \times 0.79 \times 10^{-4})$
$$[(4.0358)^4 - 4.59 - 128 + 16]$$
$$= (4.16 \times 10^{-4}) + (4.12 \times 10^{-3}) = \underline{4.538 \times 10^{-3}}$$

$K_1 = 0.355(4.0358)^2 + (1.271 \times 3.58 \times 10^{-2}) + (0.355 \times 4)$
$$+ \ 1.355 \times 0.75 \times 10^{-4}(4.0358)$$
$$= 5.76 + 0.0455 + 1.420 + 0.0070 = \underline{7.232}$$

$K_2 = 1 + 1.355(4.0358) = \underline{6.46}$

Then $\Delta = 0.628 \times 10^{-4}$

and $f = \dfrac{10^4 \sqrt{\Delta}}{3.7} = 67.8$ cycles/second.

The remaining frequencies have been calculated according to the curves of $\sqrt{\Delta}$ given in Arnold and Warburton's paper (4), a slightly less accurate but considerably more convenient technique. The results are plotted in Fig. (AI.1) for the lower vibrational frequencies as are tabulated on the following page.

m Axial Mode	n Radial Mode	λ Wavelength Factor	$\sqrt{\Delta}$ Frequency Factor	Frequency $= \dfrac{\sqrt{\Delta}\,x10^4}{c/s}$
1	2	.1891	.025	67.8
	3		.070	189
	4		.129	349
	5		-	573
2	2	.350	.036	97.5
	3		.070	189
	4		.131	355
3	2	.508	.055	149
	3		.075	203
	4		.133	360
4	2	.667	.087	235
	3		.087	235
	4		.14	379
5	2	.8271	.130	351
	3		.102	276
	4		.155	415

APPENDIX II

STRESS ANALYSIS

Hoop Stresses

The derivation of the hoop stress and dynamic stress function, summarized in the main text in Eqs. (1) to (4), is given below in full for the example of the sawtooth input waveshape.

With reference to the diagram showing the forces and stresses on a small segment of a cylinder, Fig. 2, a force balance in the radial direction will give the radial acceleration, i.e. $\Sigma F_r = m\ddot{r}$ and leads to the equation of motion:

$$-2\sigma_\theta \left(\sin\frac{d\theta}{2}\right)h\,dz + p(r\,d\theta\,dz) = \rho h r\,d\theta\,dr\frac{d^2u}{dt^2} \qquad \text{(A2.1)}$$

where m is the mass of the element, ρ is its density, $\ddot{r}$ its radial acceleration, h its thickness, and $d\theta$ and dz its circumferential and axial lengths respectively. σ_θ is the hoop stress acting on the element due to the radially acting internal pressure, p, which is time variant and will be represented by $p(t)$ here onward. The radial acceleration is the second derivative of the radial displacement, u, which is given by

$$u = (r - r_0)/r_0$$

where r_0 is the initial mean radius of the cylinder, and r the radius at a subsequent time, t.

For small displacements, Eq. (A2.1) can be simplified by writing $\sin d\theta/2$ and $d\theta/2$, then:

$$p(t)/h - \sigma_\theta/r = \rho \, d^2u/dt^2 \tag{A2.2}$$

The hoop stress, σ_θ may be replaced by an expression for the displacement, u, provided that the assumptions are made that the cylinder is long and that each element is in a state of plane stress, i.e. $\sigma_\theta = E\epsilon_\theta = Eu/r_0$, where ϵ_θ is the hoop strain, and E the modulus of elasticity. Equation (A2.2) then becomes:

$$p(t)/h - Eu/r \cdot r_0 = \rho\ddot{u} \tag{A2.3}$$

For small displacements, we can assume that $u \approx 0$, $r \approx r_0$, $h \approx$ constant, and $\rho \approx$ constant, which leads to:

$$p(t)/h - Eu/r^2 = \rho\ddot{u}$$

or

$$\ddot{u} + \left(E/\rho r^2\right)u = p(t)/\rho h \tag{A2.4}$$

From the second term in this equation we can define a natural hoop frequency, ω_θ as:

$$\omega_\theta = \sqrt{E/\rho r^2} \tag{A2.5}$$

so that Eq. (A2.4) may be written simply as

$$\ddot{u} + \omega_\theta^2 u = p(t)/\rho h \tag{A2.6}$$

The Laplace transform method was chosen as the most convenient means of solution of this equation of motion for the particular boundary conditions encountered in this application. Thus, the Laplace transform of Eq. (A2.5) for initial conditions $u(0) = \dot{u}(0) = 0$ is:

$$(s^2 + \omega_\theta^2)\, \bar{u}(s) = \frac{1}{\rho h}\, \bar{p}(s)$$

Solving for $\bar{u}$ we have:

$$\bar{u}(s) = \frac{1}{\rho h} \left(\frac{\bar{p}(s)}{s^2 + \omega_\theta^2} \right) \tag{A2.7}$$

where $\bar{u}(s) = \mathcal{L}[u(t)] = \int_0^\infty e^{-st}\, u(t)\, dt$

and $\bar{p}(s) = \mathcal{L}[p(t)]$

It now only remains to find $\bar{p}(s)$ to obtain the full solution. Each of the various mathematical approximations for blast loads, as shown in Fig. 3, will yield a different solution. Here, the solution for the sawtooth function (B) will be demonstrated. The other solutions are given later.

The pressure function, $p(t)$, for the sawtooth waveshape, (B), is given by:

$$p(t) = \begin{cases} P_m(1 - t/T) & 0 \le t \le T \\ 0 & t \ge T \end{cases} \tag{A2.8}$$

where T is the total time of duration of the pressure pulse, and P_m the maximum pressure.

This can be transformed into a single expression by use of a unit step function $H(t-T)$ such that

$$H(t-T) = \begin{cases} 0 & \text{for } t < T \\ 1 & \text{for } t > T \end{cases}$$

then the loading function becomes:

$$p(t) = p_m H(t-T) \frac{T-t}{T} \tag{A2.9}$$

$\bar{p}(s)$ is then obtained by finding the Laplace transform of $p(t)$, thus:

$$\bar{p}(s) = \mathcal{L}\left[p(t) \right] = \frac{p_m}{s} - \frac{p_m}{t}\left(\frac{1 - e^{-st}}{s^2} \right)$$

Relating $\bar{u}(s)$ to $\bar{p}(s)$ by means of Eq. (A2.7) we have:

$$\bar{u}(s) = \frac{p_m}{\rho h}\left[\frac{1}{s} - \frac{1}{T}\left(\frac{1 - e^{-st}}{s^2} \right)\frac{1}{s^2 + \omega_\theta^2} \right]$$

$$= \frac{p_m}{\rho h}\left[\frac{1}{s(\omega_\theta^2 + s^2)} - \frac{1}{Ts^2(\omega_\theta^2 + s^2)} + \frac{e^{-st}}{Ts^2(\omega_\theta^2 + s^2)} \right]$$

The solution in terms of the displacement, $u(t)$, is obtained by taking the inverse transform of the above expression, thus:

$$\bar{u}(t) = \frac{p_m}{\rho h}\left\{ \frac{1}{\omega_\theta^2}(1 - \cos\omega_\theta t) - \frac{1}{T\omega_\theta^3}(\omega_\theta t - \sin\omega_\theta t) \right.$$

$$\left. + \frac{1}{T\omega_\theta^3}\left[\omega_\theta(t-T) - \sin\omega_\theta(t-T) \right]H(t-T) \right\}$$

Removing the part of the solution pertaining to the artificially introduced step function, $H(t-T)$, we obtain finally the following solution for the displacement:

$$u(t) = \begin{cases} \dfrac{P_m}{\omega_\theta \rho h} \left(1 - t/T - \cos\omega_\theta t + \dfrac{\sin\omega_\theta t}{\omega_\theta T} \right) & 0 \le t \le T \\[2em] \dfrac{P_m}{\omega_\theta \rho h} \left(\left[\dfrac{1-\cos\omega_\theta T}{\omega_\theta T} \right] \sin\omega_\theta t - \left[1 - \dfrac{\sin\omega_\theta T}{\omega_\theta T} \right] \cos\omega_\theta t \right) & t \ge T \end{cases}$$

(A2.10)

Equation (A2.10) consists, in each of its two parts, of a constant term representing the hoop displacement of a thin cylinder under constant static internal pressure, P_m , and a trigonometric time function representing the correction to the static pressure formula required for a dynamic pressure as specified in Eq. (A2.8). The time function will be here onward called the dynamic loading function. Thus, for the case of the sawtooth input function, the dynamic loading function, ϕ , is:

$$\phi_\theta = \begin{cases} \left[1 - t/T - \cos\omega_\theta t + \dfrac{\sin\omega_\theta t}{\omega_\theta T} \right] & \text{for } 0 \le t \le T \\[2em] \left[\left(\dfrac{1-\cos\omega_\theta T}{\omega_\theta T} \right) \sin\omega_\theta t - \left(1 - \dfrac{\sin\omega_\theta T}{\omega_\theta T} \right) \cos\omega_\theta t \right] & \text{for } t \ge T \end{cases}$$

(A2.11)

Equation (A2.10) for displacement can now be reduced to:

$$U_\theta = \frac{P_m}{\omega_\theta^2 \rho h} \cdot \phi_\theta$$

(A2.12)

Rewriting this in terms of strain, we have:

$$\epsilon_\theta = \frac{p_m r}{E h} \cdot \phi_\theta \tag{A2.13}$$

which, in terms of stresses, yields:

$$\sigma_\theta = \frac{p_m r}{h} \cdot \phi_\theta \tag{A2.14}$$

Thus in each case, the required parameter (displacement, stress, or strain) can be obtained by simply multiplying the expression for a thin cylinder under constant static internal pressure by the dynamic time function, ϕ .

Axial Stresses

In the main text, the equation of motion in the axial direction was obtained in the form of Eq. (6) as follows:

$$\frac{d^2 u_z}{dt^2} + \frac{k}{m} u = \frac{R \pi r^2 p(t)}{m} \tag{A2.15}$$

where u_z is the axial displacement of the cylinder's end flange, which is of mass   and is acted upon by a pressure $R p(t)$ where   is the ratio of the reflected to the incident pressures. The cylinder, of mean radius r has an axial spring constant k .

The form of Eq. (A2.15) can be seen to be similar to the equation for hoop motion (A2.6), especially if an axial natural frequency, ω_z , be defined such that

$$\omega_z = \sqrt{k/m}$$

Thus Eq. (A2.15) becomes:

$$u_z + \omega_z^2 \cdot u_z = \frac{R \pi r^2 p(t)}{m} \tag{A2.16}$$

By direct comparison, the solution for the axial dynamic loading function, ϕ_z , exactly comparable to ϕ_θ , is obtained:

$$\phi_z = \begin{cases} \left[1 - t/T - \cos\omega_z t + \dfrac{\sin\omega_z t}{\omega_z T}\right] & 0 \le t \le T \\[3mm] \left[\left(\dfrac{1-\cos\omega_z T}{\omega_z T}\right)\sin\omega_z t + \left(1 - \dfrac{\sin\omega_z T}{\omega_z T}\right)\cos\omega_z t\right] & t \ge T \end{cases}$$

(A2.17)

The complete solution for displacement, stress, and strain can then be written (again the coefficients of ϕ represent the values of the parameters corresponding to a statically loaded thin cylinder).

<u>displacement</u>:

$$U_z = \frac{R\pi r^2}{m\omega_z^2} - p_m \cdot \phi_z$$

(A2.18)

<u>strain</u>:

$$\epsilon_z = \frac{R p_m r}{2Eh} \cdot \phi_z$$

(A2.19)

<u>and stress</u>:

$$\sigma_z = \frac{R p_m r}{2h} \cdot \phi_z$$

(A2.20)

Solutions for Alternate Dynamic Loadings

The other dynamic loading forms shown in Fig. 3 will give different solutions for the dynamic loading functions ϕ_θ and ϕ_z but will not affect the other parts of the solution, i.e. the parameters for statically loaded thin cylinders, Eqs. (A2.12-14) and (A2.18-20).

Below are listed the solutions for the dynamic time functions, $\phi(t)$, for each of the input waveshapes shown in Fig. 3:

(A) Square wave input

waveshape;
$$p(t) = \begin{cases} p_m & \text{for } 0 \le t \le T \\ 0 & \text{for } t \ge T \end{cases}$$

solution,
$$\phi(t) = \begin{cases} (1 - \cos \omega t) & \text{for } 0 \le t \le T \\ 2 \sin\left(\frac{\omega T}{2}\right) \sin \omega\left(t - T/2\right) & t \ge T \end{cases} \quad (A2.21)$$

(B) Sawtooth input

waveshape,
$$p(t) = \begin{cases} p_m(1 - t/T) & \text{for } 0 \le t \le T \\ 0 & \text{for } t \ge T \end{cases}$$

solution, $\phi(t)$
$$\begin{cases} \left[1 - t/T - \cos \omega_m t + \frac{\sin \omega_m t}{\omega_m T}\right] & 0 \le t \le T \\ \left[\left(\frac{1 - \cos \omega_m t}{\omega_m t}\right) \sin \omega_m t \right. \\ \qquad \left. - \left(1 - \frac{\sin \omega_m T}{\omega_m T}\right) \cos \omega_m t\right] & t \ge T \end{cases} \quad (A2.22)$$

(C) <u>Exponential decay</u>

waveshape: $p(t) = p_m \cdot e^{-at}$

solution: $\phi(t) = \dfrac{\left(\frac{1}{\omega T}\right)\sin \omega t - \cos \omega t + e^{-t/T}}{1 + \left(\frac{1}{\omega T}\right)^2}$

$$(A2.23)$$

where $T = \frac{1}{a}$

(D) <u>Exponential multiplied by time</u>

waveshape: $p(t) = p_m\, a\, t\, e^{-at}$

solution: $\phi(t) = \left[\dfrac{e/\omega t_i}{[1+(\frac{1}{\omega T})^2]^2}\right]\left\{\left[\dfrac{2}{\omega T} + \left(1+\left[\dfrac{1}{\omega T}\right]^2\right)\omega t\right] e^{-t/T}\right.$

$\left. - \dfrac{2}{\omega T}\cos \omega t - \left(1\left[\dfrac{1}{\omega t}\right]^2\right)\sin \omega t\right\}$ $\qquad$ (A2.24)

where $T = \frac{1}{a}$

(E) <u>Linear rise with exponential decay</u>

waveshape: $p(t) = \begin{cases} p_m\, t/t_1 & \text{for } 0 \le t \le t_1 \\ p_m \cdot e^{-a(t-t_1)} & \text{for } t \ge t_1 \end{cases}$

solution: $\phi(t)' = \dfrac{e^{-t'/T}}{1+[\frac{1}{\omega T}]^2} + \left(\dfrac{(\frac{1}{\omega T})^2}{1+(\frac{1}{\omega T})^2} - \dfrac{\sin \omega t_1}{\omega t}\right)\cos \omega$

$+ \left(\dfrac{\frac{1}{\omega T}}{1+[\frac{1}{\omega T}]^2} + \dfrac{1-\cos \omega t_1}{\omega^+}\right)\sin \omega t'$ $\qquad$ (A2.25)

for $t > t_1$, and where $t' = t - t_1$ and $T = \frac{1}{a}$

Calculation of Dynamic Time Functions

The expressions for the dynamic time functions, Eqs. (A2.21) to (A2.25) give $\phi(t)$ as a function of three variables, ω, t, and T. In every case, ω can be combined with the time variables so that in effect $\phi(t)$ is a function only of the two composite variables (ωt) and (ωT).

Values of ϕ for various of the solutions have been plotted as functions of these composite variables, using an electronic computer to handle the calculations. In each case $\phi(t)$ has been plotted to a base of (ωt) for several values of (ωT), for $1.0 \leqslant \omega T \leqslant 100$ radians, the range of (ωt) plotted being $0 \leqslant \omega t \leqslant 32.0$ radians

The computer program is very similar for each of the dynamic time functions, and is explained in the following section. An example program is given in Table A2.3 for the sawtooth input, and alterations required for the other input functions are given in Table A2.4.

The computer output, in the form of graph plots is presented as follows:

Waveshape	Output Plot
(A)	Fig. AII.2
(B)	Fig. AII.1
(C)	Fig. AII.3
(D)	Fig. AII.4

(E)--not computed. The additional variable, t, rendered this function unsuitable for convenient presentation.

Computer Program for Stress Calculations

A program in FORTRAN computer language was constructed for running the stress calculations on an IBM 7090 computer feeding a CAL-COMP automatic graph plotter. The computer calculated the values of $\phi(t)$ at time intervals Δt for a variety of values of T . The output was stored on magnetic tape which then became the input for the graph plotter, resulting eventually in the set of automatically plotted curves shown in Figs. (AII.1-4).

With reference to Tables A2.1, A2.2 and A2.3, the explanations and translation of the FORTRAN language variables, the computer program flow chart, and the computer program respectively, the step by step computation process can be followed through.

For given boundary conditions ($\omega, \Delta t, t_{max}, \& T$) the steps involved are:

(i) selection of a value of T.

(ii) selection of a value of t

(iii) calculation of ωt and reduction of this to an angle between O and 2π radians.

(iv) calculation of ωT and similar reduction to $O < \omega T < 2\pi$

(v) selection of the relevant part of the $\phi(t)$ function for the particular value of t involved.

(vi) computation of $\phi(t)$

(vii) plotting of the value of $\phi(t)$ on the output curve.

(viii) selection of the next value of t or T .

(ix) repetition for the new value of t or T until the entire range has been covered.

Tables A2.1, A2.2, and A2.3 are for the sawtooth input function
(B), resulting in output curve AII.1. The programs for the other
inputs are exactly similar, using the alterations to the program
card-deck as given in Table A2.4.

APPENDIX III

SEMICONDUCTOR STRAIN GAUGES

In this appendix are given details of the properties and characteristics of semiconductor strain gauges, their installation, calibration, and their use. The particular gauges used in the present work were Baldwin-Lima-Hamilton, type SPB2-18-12, although the information which follows is applicable, in general, to all semiconductor gauges.

Background

The principle behind conventional resistance wire-grid strain gauges can be traced back to the time of Lord Kelvin who demonstrated the manner in which certain metallic conductors exhibited a change in electrical resistance when subject to mechanical strain. Such gauges are now in a highly developed state and are the basis of most experimental stress analysis. In recent years, however, a new strain sensitive device has been developed, very similar in every respect to the old wire-grid gauges, but exhibiting resistance changes in the order of 60 times those obtained from the wire-grid types. This device is the semiconductor strain gauge, superior to its older couterpart in its increased sensitivity, lack of hysteresis effects, and lack of zero shifting, and inferior in only one major aspect - its non-linear response to strain. The non-linear response hindered the development and popularity of

this new gauge for many years; in fact it was only in 1960 that a serious attempt was made to explain the mechanism of operation of the gauges from a knowledge of their crystallographic character- istics (10). A reliable theory is now established, and with the aid of an electronic computer to handle the rather lengthy calibration calculations, there is no reason why semiconductor gauges should be regarded as any more problematic than wire-grid gauges.

Theory

The "many-valley" theory of semiconductors, as is presented in the appendix to Ref. 10, shows that for a semiconductor with its maximum sensitivity along the 111 axis, the resistance-strain relation can be expressed in the form:

$$\frac{\Delta R}{[R_o]_T} = c_1 \epsilon + c_2 \epsilon^2 + c_3 \epsilon^3 + \dots \tag{A3.1}$$

where ϵ is the strain level, $[R_o]_T$ is the characteristic gauge resistance at temperature T (to be explained later), and ΔR is the resistance change in straining the gauge from $\epsilon = 0$ to $\epsilon = \epsilon$. The constants c_1, c_2, c_3, etc., are basic properties of the semiconductor material, depending on its material, its crystallo- graphic orientation and the level of doping.

A word of explanation on the crystallographic terms would perhaps be appropriate here: Introduction of a foreign element into the semiconductor crystal is known as "doping". This is a common practice in manufacture of semiconductor strain gauges, as it has an advantageous effect on strain-resistance linearity and on temperature stability. In the case of silicon gauges, doping

levels up to 10^{20} atoms of boron per cc have been advantageously used (10).

Selection of the best crystal axis along which to cut semi-conductor gauges is indicated by the many valley theory as being the 111 axis. For a crystal of silicon, which grows in the form of a long hexagonal bar, this axis is the longitudinal center line.

A semiconductor material's resistance will be a function of the following parameters: T, temperature; ϵ, the strain level; ρ, the resistivity; and $[R_o]_T$ the basic gauge resistance at T. For a semiconductor strain gauge of given resistivity, cut on a given axis, and of a given shape, then, the resistance will be a function only of T, ϵ, and $[R_o]_T$:

$$\frac{\Delta R}{[R_o]_T} = f\left[\frac{\epsilon}{T}, \frac{\epsilon^2}{T^2}, \frac{\epsilon^3}{T^3}, \cdots\right] \tag{A3.2}$$

Utilizing a reference temperature of 298°K, (A3.2) can be non-dimensionalized with regard to temperatures, and an equality established:

$$\frac{\Delta R}{[R_o]_T} = C_1'\left(\frac{298}{T}\right)\epsilon \cdots C_2'\left(\frac{298}{T}\right)^2\epsilon^2 + C_3'\left(\frac{298}{T}\right)^3\epsilon^3 \tag{A3.3}$$

The prime mark used on any constants here onward indicates that values are referred to the 298°K reference temperature.

In practice it transpires that only the first two terms in Eq. (A3.3) are necessary for quite accurate analysis. In Ref. 11 it is shown that the effect of C_3' at the high strain level of

10,000 $\mu"/"$ is less than 1%, and can justifiably be neglected, i.e.

$$c_3' = c_4' = c_5' \, , \text{ etc.} \rightarrow 0$$

This leaves us with the equation of a parabola: (see Fig. AIII.1)

$$\left[\frac{\Delta R}{R_o}\right]_T = c_1' \left(\frac{298}{T}\right)\epsilon + c_2'\left(\frac{298}{T}\right)^2\epsilon^2 \qquad (A3.4a)$$

To bring semiconductor strain gauge theory into line with theory for conventional wire gauges, the concept of a "gauge factor" G.F., is introduced. For wire gauges;

$$\frac{\Delta R}{R_g} = \text{G.F.} \times \epsilon \qquad (A3.4b)$$

is the governing equation for operation, R_g and G.F. both being constants for a particular gauge.

The non-linear response to strain and the fact that the basic gauge resistance, R_o , is a function of temperature makes a simple relation of this type meaningless in the case of semiconductor gauges. However, use of a similar constant (G.F.)' is useful in formulating the more complex expressions for these gauges. (G.F.)' is defined as the gauge factor determined at reference temperature 298°K and at zero strain, i.e.;

$$\left[\text{G.F.}\right]' = \frac{\Delta R}{\left[R_o\right]_{298}} \times \frac{1}{\epsilon} \qquad \text{as } \epsilon \rightarrow 0 \qquad (A3.5)$$

From Eq. (A3.3), it may be seen that $c_1' = (\text{G.F.})'$. Thus, the equation describing the behavior of semiconductor strain

gauges in its most convenient form is:

$$\frac{\Delta R}{[R_0]_T} = [G.F.]' \left(\frac{298}{T}\right) \epsilon + c_2' \left(\frac{298}{T}\right)^2 \epsilon^2 \qquad \text{(A3.6)}$$

Eq. (A3.6) is the basic expression governing the character-
istics of any semiconductor strain gauge, where ΔR is the output
for a change in strain ϵ . It must be understood that ϵ in this
equation is the total strain acting on the bar of silicon which
is the gauge's sensing element. Three separate and distinct
strains act on the silicon bar at any given time:

(i) ϵ_B - a large compressive strain due to bonding.

(ii) ϵ_T - a tensile or compressive strain due to differen-
tial temperature expansion or contraction between
the gauge element and the specimen.

(iii) ϵ_S - the strain in the specimen, the magnitude of which
we are attempting to determine.

The total strain on the gauge element, ϵ , is then:

$$\epsilon = \epsilon_B + \epsilon_T + \epsilon_S \qquad \text{(A3.7)}$$

The calculations involved in obtaining calibration curves for
the particular gauges used in these tests from formulae (A3.6 and 7)
will be discussed later. First it will be beneficial to examine
the effects of temperature and bonding on gauges, and to consider
some practical aspects of the use of semiconductor gauges - bonding
techniques, circuitry, calibration, etc.

Gauge bonding

It is not possible to bond a semiconductor strain gauge to any specimen without leaving a residual strain on the gauge element (the silicon rod in this case). The causes of this are twofold. Firstly, there is always a large compressive strain on the silicon rod from the backing material on to which it is mounted by the manufacturers. Additionally, almost any process for attaching the gauge to the specimen involves heating to cure the bonding compound. Differential temperature expansion between the silicon and the specimen material will result in a permanent strain on the silicon rod when cool.

Clearly, there is no time when the rod is unstressed except before the silicon rod is mounted on to its backing. As it is essential to determine the basic gauge constants under the condition of zero stress, these measurements must be made by the manufacturer at this time. Measurement is made of the silicon rod's resistance and resistivity at the reference temperature of 298°K. From the resistivity measurement comes the values for the constants $(G.F.)'$ and C_2' from Eq. (A3.6). In Fig. AIII.2 are reproduced the manufacturer's curves used to determine these constants. The value of resistance measured under these conditions is that of $[R_o]_{298}$, the unstressed gauge resistance at 298°K, also required in Eq. (A3.6).

After the calibration measurements, the silicon rod is bonded by the manufacturer into a thin strip of bakelite to act as backing support and aid in mounting the gauge on to the specimen

This process results in a compressive strain being permanently applied to the silicon rod by the bakelite surround.

It now remains only for the user to mount the backed gauge on to the specimen in which strains are to be measured. The practical aspects of this process will be described later, but it should here be noted that the Epoxy cement used in this process requires that heat and pressure be applied while curing. The heat puts a further compressive strain on the gauge due to differential expansion between specimen and silicon, thus, by the time the gauge is bonded and ready for use, it is in a state of compression of considerable, but unknown, magnitude.

Equations (A3.6) and (A3.7) show how the magnitude of the bonding strain may be determined:

$$\frac{\Delta R}{[R_o]_T} = [G.F.]^1 \left(\frac{298}{T}\right) \epsilon + C_2^1 \left(\frac{298}{T}\right)^2 \epsilon^2 \tag{A3.6}$$

where

$$\epsilon = \epsilon_B + \epsilon_T + \epsilon_s \tag{A3.7}$$

If the resistance of the gauge be determined with no strain on the specimen and at a temperature of 298°K, then Eq. (A3.7) becomes

$$\epsilon = \epsilon_B$$

and, if R_B is the gauge resistance measured under these conditions,

$$\frac{\Delta R}{[R_o]_{298}} = \frac{R_B - [R_o]_{298}}{[R_o]_{298}} = [G.F.]^1 \epsilon_B + C_2^1 \cdot C_3^2 \tag{A3.8}$$

Thus, this one measurement completes the calibration requirements of the gauge, leading as it does, directly to evaluation of ϵ_B, the bonding strain.

Temperature effects

Temperature variation affects semiconductor strain gauges in two ways; (i) in affecting the value of the "unstressed gauge resistance", $[R_o]_T$, and (ii) in changing the strain due to differential expansion between gauge and specimen, ϵ_T.

The differential expansion effect is easily dealt with, provided that the expansion coefficients of silicon and of the test specimen are accurately known. If α_G is the temperature expansion coefficient of silicon, α_S is the temperature expansion coefficient of the specimen, then

$$\epsilon_T = (T-298)(\alpha_S - \alpha_G)$$
$$= (T-298)\alpha$$

(A3.9)

where $\alpha = \alpha_S - \alpha_G$

When working with static strains, this expansion effect is undesirabl as the magnitude of ϵ_T often will exceed ϵ_S, the strain being measured, and thus reduce the accuracy of measurement unless ϵ_T is known very precisely. Compensation techniques, using another gauge as "dummy" are common in wire-grid strain gauge practice, but less popular with semiconductor gauges because of:

    a) the difficulty of matching gauges to give the same output for a given temperature change. For this it is necessary for the bonding strains to be nearly identical for the two gauges, and practical experience shows that

this is far from a simple matter.

b) the high cost of semiconductor gauges prevent too liberal use of them merely as "dummy" gauges.

The problem is not serious when measuring only dynamic strains, however. Knowledge of the gauge temperature to only reasonable accuracy was necessary to find the zero-point on the gauge characteristic from which measurements could be based. In practice, therefore, a thermocouple was installed with each gauge at the time of bonding, this giving a sufficiently accurate temperature measurement.

The effect of temperature on the "unstressed gauge resistance" $[R_o]_T$ is a basic property of the silicon material and could thus be determined from a temperature coefficient curve supplied by the manufacturer. This curve is reproduced in Fig. AIII.3.

With this curve and knowledge of the reference resistance $[R_o]_{298}$, $[R_o]_T$ can be determined in the range 0 to 400°F. Here we have another drawback in the use of these gauges. At the present time there are no data available to find the variation of $[R_o]_T$ in the sub-zero temperature range. The suppliers of the gauges, Baldwin-Lima-Hamilton Corporation, are at present collecting data in this range, but meanwhile it is only possible to estimate what will happen. Information received from the Semiconductor Division of BLH indicates that the temperature coefficient curve is parabolic, reflecting the same value at -200°F as at +75°F. Hence, the performance of the gauges at low temperatures can be estimated, but no reliable low

temperature measurements can be made until reliable calibration data is available.

Pictorial representation of semiconductor strain gauge characteristics

The effects of bonding and of temperature variations will be clarified by reference to Fig. AIII.4, a plot—not to scale— of typical gauge characteristic curves. The figure is an enlargement of the negative section of the parabola shown in Fig. AIII.1, the several curves indicating different temperatures. The history of the strain gauge, as covered in the previous pages, can be mapped out on Fig. AIII.4 as follows:

The plain bar of silicon before mounting and backing is represented by the origin; zero strain acts on the bar. The manufacturer mounts the bar on to bakelite, and we move down the 298°K characteristic toward B. The gauge user mounts the gauge on to his test specimen, and, on recovering the temperature of 298°K, reaches the point B, with a compressive strain of B set into the gauge.

Now, if measurements are made at some other temperature, T, we move along the expansion characteristic (broken line) to Z before any strain is applied to the specimen. If a tensile strain, ϵ_B, now be applied to the specimen, the gauge indicates a strain of $\epsilon_B + \epsilon_s + (T - 298)\alpha$. Now, at the "zero point" Z, at some temperature, with the strain on the specimen zero, it

follows from Eq. (A3.6) that the sensitivity is:

$$\frac{\Delta R_z}{[R_o]_T} = [G.F]' \left(\frac{298}{T}\right)\left(\epsilon_B + [T-298]\alpha\right) + c_2' \left(\frac{298}{T}\right)^2 \left(\epsilon_B + [T-298]\alpha\right)^2 \quad \text{(A3.10)}$$

Then, on applying strain ϵ_S to the specimen the sensitivity becomes (at point c):

$$\frac{\Delta R_c}{[R_c]_T} = [G.F]' \left(\frac{298}{T}\right)\left(\epsilon_B + \epsilon_S + [T-298]\alpha\right)$$

$$+ c_2' \left(\frac{298}{T}\right)^2 \left(\epsilon_B + \epsilon_S + [T-298]\alpha\right)^2 \quad \text{(A3.11)}$$

The gauge output due to a change in stress of ϵ_S will be given by the difference between (A3.10) and (A3.11). Expanding and combining the two equations:

$$\left(\frac{\Delta R_c - \Delta R_z}{[R_o]_T}\right) = [G.F]' \left(\frac{298}{T}\right)\epsilon_S$$

$$+ c_2' \left(\frac{298}{T}\right)^2 \left[\epsilon_S^2 + 2\epsilon_S\left(\epsilon_B + [T-298]\alpha\right)\right]$$

The output change in gauge resistance ΔR for strain ϵ_S is given by:

$$\Delta R = \Delta R_c - \Delta R_z$$

$$= \frac{[R_o]_T 298 \cdot \epsilon_S}{T^2} \left[[G.F]' T + 298 c_2'\left(\epsilon_S + 2\epsilon_B + 2[T-298]\alpha\right)\right] \quad \text{(A3.12)}$$

Practical Aspects

So far, only purely theoretical and general considerations have been presented on both the stress analysis and semiconductor strain gauge aspects of this work. It is now necessary to consider practical details and theoretical predictions applied to this specific project. Bonding procedure for the strain gauges will first be briefly considered, followed by some practical schemes for strain gauge circuitry, then details of the techniques used to calibrate the gauges and prepare them for use.

Gauge bonding

As was indicated at the beginning of the previous section, six strain gauges were mounted on the detonation tube — a radial and an axial gauge at each of three stations.

Scrupulous preparation of the surface was carried out at these points, consisting of:

    (a)   surface grinding with a rotary belt-grinder until the surface was smooth and free from all irregularities.

    (b)   wire-brushing to a high surface finish so that the surface may be easily in.pected for any imperfections.

    (c)   controlled surface scoring with No. 200 emery grit.

    (d)   scrubbing with acetone to remove all dirt and grease.

Guide lines were then scribed on to the vessel's surface to ensure accurate alignment of each gauge.

The strain gauge and its associated thermocouple were prepared by lightly washing in acetone.

A small quantity of Epoxy adhesive (EPY-400, manufactured by Baldwin-Lima Hamilton Corporation) was smeared on the vessel surface and the strain gauge and thermocouple positioned, ensuring that no air bubbles were trapped under the gauge.

The strain gauge and thermocouple were covered with a 0.001" film of Teflon - a plastic material to which Epoxy adhesives will not adhere. Over this was placed an 1/8" thick Neoprene rubber pressure pad and a small flat copper plate. Bearing down on this assembly, under spring pressure, was an adapted heavy soldering iron to apply heat and pressure for curing the Epoxy adhesive. The soldering iron was connected to a temperature controller which, using the thermocouple as sensing element, kept the supply of heat to the gauge such that its temperature was constant at 250°F. An overnight cure at this temperature ensured a satisfactory bond. Fig. AIII.5 shows diagrammatically the bonding setup described above.

After curing, the assembly was stripped down to the gauge, excess adhesive chipped away with a small chisel, and the extension leads to the strain gauge carefully soldered in place. The leads were insulated and taped into place. The whole assembly was then given several thick coats of Glyptal (a synthetic epoxy rubber insulating compound made by the General Electric Company) to ensure good electrical insulation and moisture proofing. Over this was fitted a cover plate of 0.005" thick copper film for electrical screening. The laboratory in which these tests were conducted is in the close proximity of a local radio transmitter

so that unscreened leads easily picked up a high level noise

signal at a frequency of about 1 Mc/s. The copper film adequately

screened off this interference.

A photograph of the gauge installation at station 7 taken

just prior to application of the Glyptal is shown in Fig. AIII.6.

Circuitry

The more usual type of strain gauges, that is, for example,

those using a resistive wire grid as their sensing element, may

be used conveniently with bridge circuitry such as the Wheatstone

bridge. Their change in gauge resistance under strain is very

small compared with the over-all resistance of the gauge. With

semiconductor gauges, however, the change in gauge resistance is

so large that the inherent non-linearity of Wheatstone bridge type

circuits must be considered.

In the course of planning the circuitry for the semiconductor

gauges, the possibility of utilizing some Wheatstone bridge cir-

cuits that had been employed previously with wire grid strain

gauges was investigated. The bridges essentially consisted of

the components shown in Fig. AIII.7.

For a resistance change ΔR in the strain gauge, the output,

ΔE_o , is given by:

$$\Delta E_o = E_i \left(\frac{120 + \Delta R}{120 + \Delta R + 237} - \frac{120}{120 + 237} \right) \tag{A3.13}$$

and the sensitivity is:

$$\frac{\text{output}}{\text{input}} = \frac{\Delta E_o}{E_i} = \frac{237 \, \Delta R}{357(357 + \Delta R)}$$

The plot of this, shown in Fig. AIII.8, indicates that at $\triangle R = 20\Omega$ the non-linearity of the bridge output is as much as 5.3%. Such a value of $\triangle R$ would be produced, at room temperatures, by a strain of approximately 1200 μ"/", which is certainly within the possible strain range for this application.

Correction of the bridge non-linearity is possible but inconvenient, and use of this technique was rejected in favor of constant current circuitry. In this case the <u>voltage</u> across the strain gauge is directly monitored, the supply <u>current</u> being kept as near constant as feasible. Constant current circuitry has several other advantages which make it desirable in this application. The output, for example, is up to double that for an equal arm bridge circuit. Noise level is very low, as the ground line is common for supply, gauge, and display equipment. To achieve near constant-current conditions, the simple technique of using a large ballast resistor across a high supply voltage was used, the magnitude of the voltage and ballast resistance being chosen to give a supply of approximately 20 milliamperes within 1/2% for a 120-Ω gauge operating between $\pm$ 1000 μ "/". The circuit shown in Fig. AIII.9, operates under the following conditions:

voltage across strain gauge $= \dfrac{300 \times 120}{15,120} = 2.39$ volts

current through strain gauge $= 2.39/120 = 0.0199$ amp

power dissipated by strain gauge $= 0.0475$ watts

The efficiency of the circuit in generating constant current, η_c is:

$$\eta_c = \frac{R_L}{R_L + R_{S.G.}} = \frac{15,000}{15,120} = 99.2\% \qquad (A3.14)$$

where R_L = resistance of ballast resistor = 15,000 ohms, and

$R_{S.G.}$ = resistance of strain gauge = 120 ohms.

Hence, for a change of resistance ΔR in the strain gauge, the circuit non-linearity, δ, is:

$$\delta = \frac{\left(\dfrac{\Delta R}{R_{S.G.}}\right)\left(1 - \eta_c\right)}{1 + \left(\dfrac{\Delta R}{R_{S.G.}}\right)\left(1 - \eta_c\right)} \qquad (A3.15)$$

For example, when ϵ_s = 1000 microinches/inch, the resistance change ΔR would be approximately $17\,\Omega$ for a $120\,\Omega$ gauge at room temperature. Thus

$$\delta = \frac{(17/120)(0.008)}{1 + (17/120)(0.008)} = 0.00113$$

or 0 113% non-linearity.

The circuit sensitivity, S, is defined as the voltage output for an input of 1 microinch/inch strain input:

$$S = \frac{v}{\epsilon} = \frac{V_{SG} \cdot \Delta R \cdot \eta_c (1-\delta)}{R_{SG} \cdot \epsilon} \qquad (A3.16)$$

where V_{SG} is the applied voltage across the strain gauge. Substituting the values found above:

$$S \simeq \frac{2.39 \times 0.015^* \times 0.992 \times 0.999}{120 \times 1}$$

$$= 296 \times 10^{-6} \text{ volts}/\mu\,''/''$$

---

*This figure for strain sensitivity is only approximate since the value for ΔR can only be roughly estimated at this stage. The exact value will, of course, be different for each strain gauge encountered

A strain of 100 μ "/" could thus be expected to produce a voltage output of approximately 0.03 volts. This would be within the reasonable sensitivity range of the oscilloscopes used on this project, their maximum amplifier sensitivity being 0.02 volts/cm.

The constant-current circuitry thus being regarded as satisfactory, a strain converter was constructed having six such circuits in parallel operation. Fig. AIII.10 gives the complete circuit diagram for the strain converter. The six circuits are only interlinked in that they share the same power supply — the large ballast resistors prevent any one circuit from affecting the others. Included in the same unit was a conventional Wheatstone bridge circuit specially constructed for measuring resistances in the order of 120 Ω . This facility is necessary for initial calibration of the gauges. The external appearance of the strain converter unit is shown in Fig. AIII.11, and the complete experimental setup — strain converter, power supply, oscilloscope is shown in Fig. AIII.12.

Calibration

It will be recalled that it is necessary for the manufacturer of semiconductor strain gauges to partially calibrate the gauges at an early stage in the manufacturing process. The gauges as supplied, then, are delivered complete with the values of the three gauge constants $\left[R_0\right]_{298}$, (G.F.)', and C_2', determined before the silicon rod was mounted on its bakelite backing. Complete details of the strain gauges as supplied are given in Fig. AIII.13.

The constants $(G.F.)'$ and C_2' are inserted into Eq. A3.12 as they stand, but from the given value of $(R_o)_{298}$ it is necessary to construct a curve of $(R_o)_T$ over the required temperature range, using the temperature coefficient curve (Fig. AIII.3). The resulting curve of $(R_o)_T$ versus temperature is given in Fig. AIII.14, and it will be noticed that this is given for a wider range of temperatures than for which Fig. AIII.3 supplies data. Data for the temperature range 300 to 400°K is accurately known from the B-L-H curve supplied with the strain gauges, and for the range 150 to 300°K can be fairly well estimated using the parabolic assumption discussed earlier. For the remaining ranges 20 to 150°K and 400 to 460°K data can be estimated by extrapolation. It was considered more advantageous now to present insecure data with a wide estimated error band than to give no results for temperatures below 300°K. The error bands are marked on Fig. AIII.14 and shown in a clearer format in Fig. AIII.15.

One further calibration constant is required before the performance of the gauges can be completely predicted - measurement of the bonding strain, ϵ_B , for each individual gauge.

This constant is found by accurately measuring the resistance of each gauge after installation is completed at a temperature of precisely 298°K (77°F). It was found that the resistance at 298°K could be most accurately found by determining the gauge's resistance over a small range of temperatures around 298° and picking off the precise value from the curves of R versus T obtained. The curves for the four gauges at stations 7 and 9 are given in Fig. AIII.16.

Substitution of the resistance values in Eq. (A3.8) led immediately to the following values for the bonding strains:

Station 7:	Gauge XX (axial)	ϵ_B	$= -899 \; \mu"/"$
	Gauge YY (hoop)	ϵ	$= -744 \; \mu"/"$
Station 9:	Gauge AA (axial)	ϵ_o	$= -264.5 \; \mu"/"$
	Gauge BB (hoop)	ϵ_B	$= -1347.5 \; \mu"/"$

Now, together with the relevant properties of the material of the test vessel that are given in Table AIII.1, all the constants required for calibration are known.

Substituting into Eq. (A3.12) we have:

$$\text{Output} = \Delta R = \frac{[R_o]_T \cdot 298 \cdot \epsilon_s}{T} \left[122T \right.$$

$$\left. + (298 \times 3700) \left\{ \epsilon_s + 2\epsilon_B + 2[T - 298] \left(\% [9.7 \times 2.5] \times 10^{-6} \right) \right\} \right] \tag{A3.17}$$

The most convenient form in which to use this calibration equation was found to be in tables of output resistance, ΔR, versus strain level, ϵ_s, for various temperatures and for each value of bonding strain ϵ_B. This quite considerable calculation being ideally suited to automatic computation, and an IBM 7090 electronic computer was utilized.

Computer program for strain gauge output calculations

With reference to Tables AIII.2 – 4, the list of FORTRAN symbols, computer flow chart, and computer program respectively, the various stemps composing the program can be followed through:

    (a) Data input. Values of the bonding strains, estimated errors, and values of $(R_o)_T$ (and errors) over the

temperature range required are fed into the computer
on punched cards. Table AIII.5 shows how each data
card was made up, and Table AIII.6 gives an example
of the data input for the four gauges XX, YY, AA, and BB.

(b) The first "do loop" assimilates the data input, prepares
the output printer for operation, then selects the first
gauge for calculation.

(c) The second "do loop" performs the calculation for succes-
sive values of temperature, T, calculating for each
value the gauge output and estimated error over the
strain range -1500 to +1500 μ"/" at intervals of
100 μ"/". (Error estimation is considered in the
following section.)

(d) Completion of the second do loop operation returns the
computer to the first do loop where the next strain
gauge is considered and the whole calculation repeated.

(e) When both do loops are complete, the computer is stopped
and the output, which is printed out in the form of the
four-column table shown below, collected.

Temperature	Strain Level, ϵ_g	Output Resistance Change, ΔR	Error in ΔR
°K		ohms	ohms
Range 20° to 460° in 20° intervals	Range -1500 to +1500μ"/" in 100 μ"/" intervals		

Error Analysis

The probable error involved in computation of ΔR for known errors in each of the variables involved is calculated by use of a "normal error" analysis on Eq. (A3.12).

The normal error theory gives

$$S_r^2 = \sum_{i=1}^{n} \left(\frac{\delta R}{\delta i}\right)^2 S_{x_i}^2 \tag{A3.18}$$

where S_r is the total error, S_x is the standard error of each variable, and R is a function of the i individual variables involved.

Repeating Eq. (A3.12), then partially differentiating with respect to each variable in turn:

$$\Delta R = \frac{[R_o]_T \cdot 298 \cdot \epsilon_s}{T^2} \left[[G.F.]' T + 298 C_2' (\epsilon_s + 2\epsilon_B + 2[T-298]\alpha) \right]$$

(a) $\quad \dfrac{\delta \Delta R}{\delta [R_o]_T} = \dfrac{298 \cdot \epsilon_s}{T^2} \left[[G.F.]' T + 298 C_2' (\epsilon_s + 2\epsilon_B + [T-298]\alpha) \right]$

(b) $\quad \dfrac{\delta \Delta R}{\delta [G.F.]'_T} = \dfrac{[R_o]_T \cdot 298 \cdot \epsilon_s}{T}$

(c) $\quad \dfrac{\delta \Delta R}{\delta C_2'} = \dfrac{[R_o]_T \cdot 298 \cdot \epsilon_s}{T} \left[\epsilon_s + 2\epsilon_B + 2[T-298]\alpha \right]$

(d) $\dfrac{\delta \Delta R}{\delta \epsilon_B} = \dfrac{[R_o]_T \cdot 298 \times \epsilon_S}{T^2} \left(298 \times C_2' \times 2 \right)$

(e) $\dfrac{\delta \Delta R}{\delta T} = \dfrac{[R_o]_T \cdot 298 \times \epsilon_S}{T^2} \left(-[G.F.]' - (298\alpha \times C_2') \right)$

The error in ΔR can be found then from Eq. (A3.18):

$$S_R = \sqrt{ \sum \left(\dfrac{\delta \Delta R}{\delta [R_o]_T} \right)^2 S_{[R_o]_T}^2 + \left(\dfrac{\delta \Delta R}{\delta [G.F.]'} \right)^2 S_{[G.F.]}^2 + \left(\dfrac{\delta \Delta R}{\delta C_2'} \right)^2 S_{C_2'}^2 }$$

$$ + \left(\dfrac{\delta \Delta R}{\delta \epsilon_B} \right)^2 S_{\epsilon_B}^2 + \left(\dfrac{\delta \Delta R}{\delta T} \right)^2 S_T^2 $$

This expression was transferred to the computer program so that the error could be calculated for each value of ΔR computed.

TABLE 1

COMPUTER PROGRAM FOR CALCULATION OF THE DYNAMIC
TIME FUNCTION FOR HOOP STRESSES

```
*   NOTE AT PAUSE 1 MOUNT REEL   893 WRITEABLE ON B5
*   NOTE AT PAUSE 2 DISMOUNT AND SAVE B5 FOR PRINTING ON
        1 CAL'COM PLOTTER
*   TAPE B5,      REEL 893,      WRITE
*       LIST
*       LABEL
*       FORTRAN
C       DYNAMIC STRESS FUNCTION FOR HOOP STRESSES
        DIMENSION XX(30),CX(40),C(30)
        CALL PAUSE(6HPAUSE1)
        REWIND 6
     1 FORMAT (12A6)
     2 FORMAT (F8.3)
        OMEGA = 16.316
        ATIM = 0.02
        RTIM = 2.0
    12 TAX = -1.0
        CALL GRAPH(11.00,8.50,1.00)
        CALL FRAME(0.0,0.0)
        CALL XLN(1.50,9.50,3.5,0.4)
        CALL YLN(5.50,1.50,1.50,-0.20)
        READ2,Z
        DO 22 I = 1,4
        READ 2,XX(I)
        READ1,(C(J),J=1,12)
        CALL LTR(Z,3.35,1,0,C)
    22 Z = Z + XX(I)
        READ2,Z
        DO 23 I = 1,5
        READ2,XX(I)
        READ1,(C(J),J=1,12)
        CALL LTR(1.0,Z,1,0,C)
    23 Z = Z - XX(I)
        READ 1, (CX(I),I=1,12)
        CALL LTR(0.7,2.40,1,1,CX)
        READ 1, (CX(I),I=1,12)
        CALL LTR(9.80,3.35,1,0,CX)
        READ 1, (CX(I),I=1,12)
        CALL LTR(4.75,0.6,1,0,CX)
    25 TAX = TAX + 2.0
        GO TO 27
    26 TAX = TAX + 5.0
    27 CALL CURVE(1,1,0,1,-0.375,2.375,-3.5,5.0,1)
        TIM = 0.
    28 TIM = TIM + ATIM
        R = OMEGA*TIM
        S = OMEGA*TAX
    35 IF(R-6.2832)45,45,46
```

```
    45  IF(S-6.2832)55,55,47
    46  R = R - 6.2832
        GO TO 35
    47  S = S - 6.2832
        GO TO 45
    55  IF(TAX-TIM)75,75,65
    65  TFUN = 1.-TIM/TAX-COS(R)+SIN(R)/(OMEGA*TAX)
        GO TO 101
    75  TFUN = SIN(R)*((1.0-COS(S))/(OMEGA*TAX))-COS(R)
       1*(1.0-SIN(S)/(OMEGA*TAX))
   101  CALL PLOTPT(TIM,TFUN)
   110  IF(RTIM - TIM)115,115,28
   115  IF(10.0-TAX)130,130,120
   120  IF(5.00-TAX)26,26,25
   130  CALL NDPLOT
        ENDFILE 6
        ENDFILE 6
        CALL REWUNL(6)
        CALL PAUSE(6HPAUSE2)
        CALL EXIT
        END

*       DATA
3.35
2.05
(3H0.5
1.95
(3H1.0
2.0
(3H1.5
2.0
(3H2.0
5.45
1.00
(4H 2.0
1.00
(4H 1.0
1.00
(4H   0
1.00
(4H-1.0
1.00
(4H-2.0
(23HDYNAMIC STRESS FUNCTION
(7HTIME MS
(28HHOOP STRESS DYNAMIC FUNCTION
```

TABLE 2

Measured and Calculated Natural Frequencies of the Vessel

AXIAL Natural Frequency   Calculated Value = 191.0 Cycles/sec.

Test No.	Gauge No.	Measured Frequency
CD251	AA	170 c/s
CD251	XX	172.5 c/s

HOOP Natural Frequency   Calculated Value = 2,597 Cycles/sec.

Test No.	Gauge No.	Measured Frequency
CD149	BB	2,730 c/s
CD149	YY	2,780 c/s
CD150	BB	2,750 c/s
CD150	YY	2,690 c/s

TABLE 3

Measured and Calculated Values of Stress Amplitudes

Test No.	Conditions	Position	Gauge No	P_m	Static Stress	ϕ max	σ max	Measured Strain	Measured Stress
CD149	100 mmHg	9	BB	36.5 psi	1185 psi	1.90	2250 psi	55.5 $\mu''/''$	1610 psi
CD147	100 mmHg	9	AA	350.0	5660	1.00	5660	36.3	1050
CD251	100 mmHg	9	AA	350.0	5660	1.00	5660	29.6	860
CD251	100 mmHg	9	BB	36.5	1185	1.90	2250	70.0	2030
CD251	100 mmHg	7	XX	350.0	5660	1.00	5660	20.6	598
CD251	100 mmHg	7	YY	36.0	1170	1.90	2220	64.0	1850
CD150	200 mmHg	9	BB	73.0	2370	1.90	4500	139.0	4040
CD150	200 mmHg	7	YY	72.0	2340	1.90	4440	102.0	2960

TABLE AII.1

Dynamic Time Function Calculation

List of Variables for Computer Program

FORTRAN NAME	SYMBOL	MEANING
OMEGA	ω	Natural Frequency of Vibration
TIM	t	Time
TAX	T	Decay Time
ATIM		Increment of Time t
RTIM		Maximum Value of t to be Calculated
TFUN	ϕ	Dynamic Time Function

Graph Plotting Subroutine: Library Number J6 BC XYP2
Author: P. H. Thrower,
    I. B. M.,
    Oakland, California
    May, 1963.

OMEGA
ATIM
RTIM
TAX

CALL
GRAPH

TAX = TAX + 9.0

TAX = TAX + 90.0

28
TIM = TIM + ATIM

R = OMEGA x TIM

S = OMEGA x TAX

46
R = R - 2π   0<   35
                                R - 2π   ≤ 0

(35)

                    0<   45
                                S - 2π   ≤ 0

47
S = S - 2π   TAX - TIM

(45)   0<   ≤ 0

65
TFUN = 1 - TIM/TAX-COS(R)+SIN(R)/(OMEGAxTAX)

(101)

75
TFUN=SIN(R) x ((1-COS(S))/(OMEGA x TAX))
     -COS(R) x (1-SIN(S)/(OMEGA x TAX))

>0   101
        RTIM - TIM   CALL
                            PLOTPOINT
        ≤ 0   TIM, TFUN

>0   115
        100 - TAX   ≤ 0

        120
        10 - TAX   END

        ≤0   >0
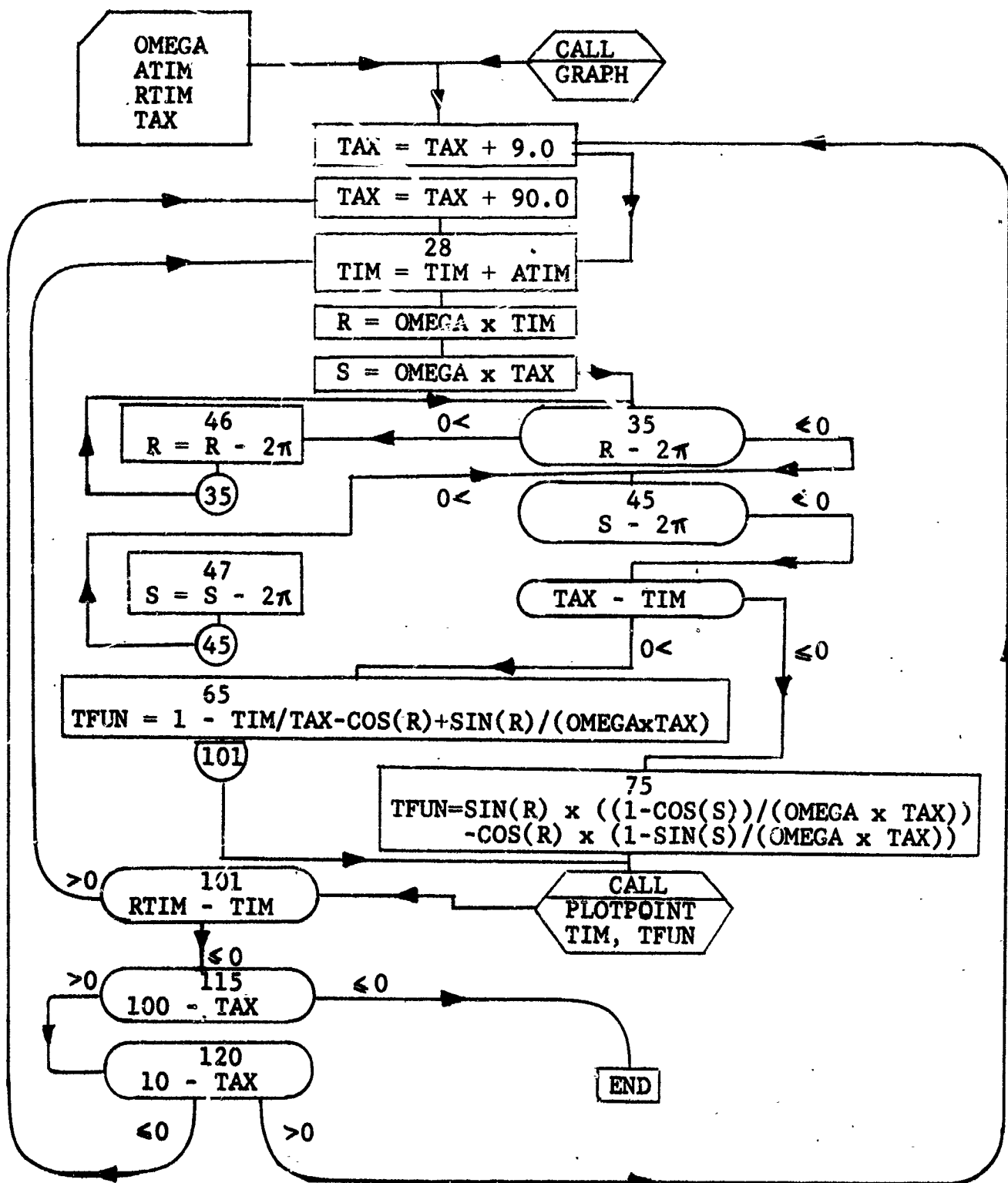
Table AII.2 Computer Flow Chart for Dynamic Time Function

TABLE AII.3   DYNAMIC TIME FUNCTION

COMPUTER PROGRAM FOR SAWTOOTH INPUT FUNCTION

```
* NOTE AT PAUSE 1 MOUNT REEL  893 WRITEABLE ON B5
* NOTE AT PAUSE 2 DISMOUNT AND SAVE B5 FOR PRINTING ON
    1 CAL'COM PLOTTER
* TAPE B5,    REEL 893,    WRITE
*    LIST
*    LABEL
*    FORTRAN
C    GENERAL DYNAMIC FUNCTION FOR SAWTOOTH INPUT
     DIMENSION XX(30),CX(40),C(30)
     CALL PAUSE(6HPAUSE1)
     REWIND 6
   1 FORMAT (12A6)
   2 FORMAT (F8.3)
     ATIM = 0.4
     RTIM = 32.0
     TAX = 0.0
     CALL GRAPH(11.00,8.50,1.00)
     CALL FRAME(0.0,0.0)
     CALL XLN(1.50,9.50,3.5,0.25)
     CALL YLN(5.50,1.50,1.50,-0.20)
     READ2,Z
     DO 22 I = 1,3
     READ 2,XX(I)
     READ1,(C(J),J=1,12)
     CALL LTR(Z,3.35,1,0,C)
  22 Z = Z + XX(I)
     READ2,Z
     DO 23 I = 1,5
     READ2,XX(I)
     READ1,(C(J),J=1,12)
     CALL LTR(1.0,Z,1,0,C)
  23 Z = Z - XX(I)
     READ 1, (CX(I),I=1,12)
     CALL LTR(0.7,2.40,1,1,CX)
     READ 1, (CX(I),I=1,12)
     CALL LTR(9.80,3.35,1,0,CX)
     READ 1, (CX(I),I=1,12)
     CALL LTR(4.75,0.6,1,0,CX)
  24 TAX = TAX + 1.0
     GO TO 27
  25 TAX = TAX +6.0
     GO TO 27
  26 TAX = TAX + 90.0
  27 CALL CURVE(1,1,0,1,-6.0,38.0,-3.5,5.0,1)
     TIM = 0.
  28 TIM = TIM + ATIM
     R = TIM
     S = TAX
  35 IF(R-6.2832)55,55,46
  45 IF(S-6.2832)55,55,47
  46 R = R - 6.2832
```

```
      GO TO 35
   47 S = S-6.2832
      GO TO 45
   55 IF(TAX-TIM)75,75,65
   65 TFUN = 1.-TIM/TAX-COS(R)+SIN(R)/TAX
      GO TO 101
   75 TFUN = SIN(R)*((1.-COS(S))/(TAX)-COS(R)*(1.-SIN(S)/TAX
  101 CALL PLOTPT(TIM,TFUN)
  110 IF(RTIM - TIM)115,115,28
  115 IF(100.0-TAX)130,130,120
  120 IF(10.0-TAX)26,26,121
  121 IF(3.0-TAX)26,25,24
  130 CALL NDPLOT
      ENDFILE 6
      ENDFILE 6
      CALL REWUNL(6)
      CALL PAUSE(6HPAUSE2)
      CALL EXIT
      END
*     DATA
 3.95
 2.50
(2H10
 2.50
(2H20
 2.50
(2H30
 5.45
 1.00
(4H 2.0
 1.00
(4H 1.0
 1.00
(4H  0
 1.00
(4H-1.0
 1.00
(4H-2.0
(23HDYNAMIC STRESS FUNCTION
(7HRADIANS
(35HGENERAL DYNAMIC STRESS FUNCTION (A)
```

TABLE AII.4

PROGRAM DECK ALTERATIONS FOR ALTERNATE
INPUT FUNCTIONS

(B)   SQUARE WAVE INPUT

```
55 IF(TAX-TIM)75,75,65
65 TFUN = 1.0 - COS(R)
   GO TO 101
75 TFUN = 2.0*(SIN(P)*SIN(Q))
```

(C)   EXPONENTIALLY DECAYING INPUT

```
55 TFUN = (SIN(R)/(OMEGA*TAX)-COS(R)+2.7183**
   1(ATIM/TAX))/(1.0+1.0/(OMEGA*TAX)**2.0)
```

(D)   EXPONENTIAL * TIME FUNCTION

```
55 TFUN = ((2.7183/TAX)/(1.0+1.0/TAX**2.0)**2.0)*
   1(2.7183**('TIM/TAX)*(2.0/TAX+TIM*(1.0+1.0/TAX**2.0))
   2-2.0*COS(R)/TAX-SIN(R)*(1.0-1.0/TAX**2.0))
```

TABLE AIII.1

Properties of the Test Vessel Material

Type 304 Stainless Steel

Structure:	Austenitic
Density:	0.287 lb/cu.in.
Modulus of Elasticity:	29×10^6 psi
Specific Heat:	0.12 Btu/°F/lb
Thermal Conductivity:	9.4 Btu/hr/ft^2/°F/ft, at 200°F
Thermal Expansion Coefficient:	9.6 μ in/in/°F, 32 to 312°F
	9.9 μ in/in/°F, 32 to 600°F
Ultimate Tensile Strength:	85,000 psi
Yield Strength:	35,000 psi
Brinell Hardness:	146

TABLE AIII.2

Variable Names for Computer Program

Variable Description	Symbol	Variable Name
Bonding Strain	ϵ_B	XBOND
Error in Value of Bonding Strain		EXBOND
Unstressed Gauge Resistance	$[R_o]_T$	XZERO
Error in Unstressed Gauge Resistance		EXZERO
Number of Strain Gauges		MBMAX
Number of Incremental Temperatures		MZMAX
Temperature °K	T	TEMP
Bonding Strain	ϵ_B	RBOND
Unstressed Gauge Resistance	$[R_o]_T$	RZERO
Strain Due to Thermal Expansion	ϵ_T	TEXP
Strain Level in Specimen	ϵ_S	STRAIN
Sum of Strains on Gauge	ϵ	SUMSTR
Intermediate Variable		COEFF
Output Resistance Change	ΔR	OUTRES
Partial Derivatives of the Output	$\delta \Delta R / \delta [R_o]_T$	DELZRO
Resistance Change	$\delta \Delta R / \delta [G.F.]'$	DELCCR
ΔR	$\delta \Delta R / \delta C_2'$	DELGFR
with respect to its	$\delta \Delta R / \delta \epsilon_B$	DLBOND
Constituent Variables	$\delta \Delta R / \delta T$	DLTEMP
Error in	Error in $[R_o]_T$	ERZRO
the above	" " $[G.F.]'$	ERGFR
Constituent	" " C_2'	ERCCR
Variables	" " ϵ_B	ERBOND
	" " T	ERTEMP
Calculated Error in Output Resistance	" " ΔR	ERROR
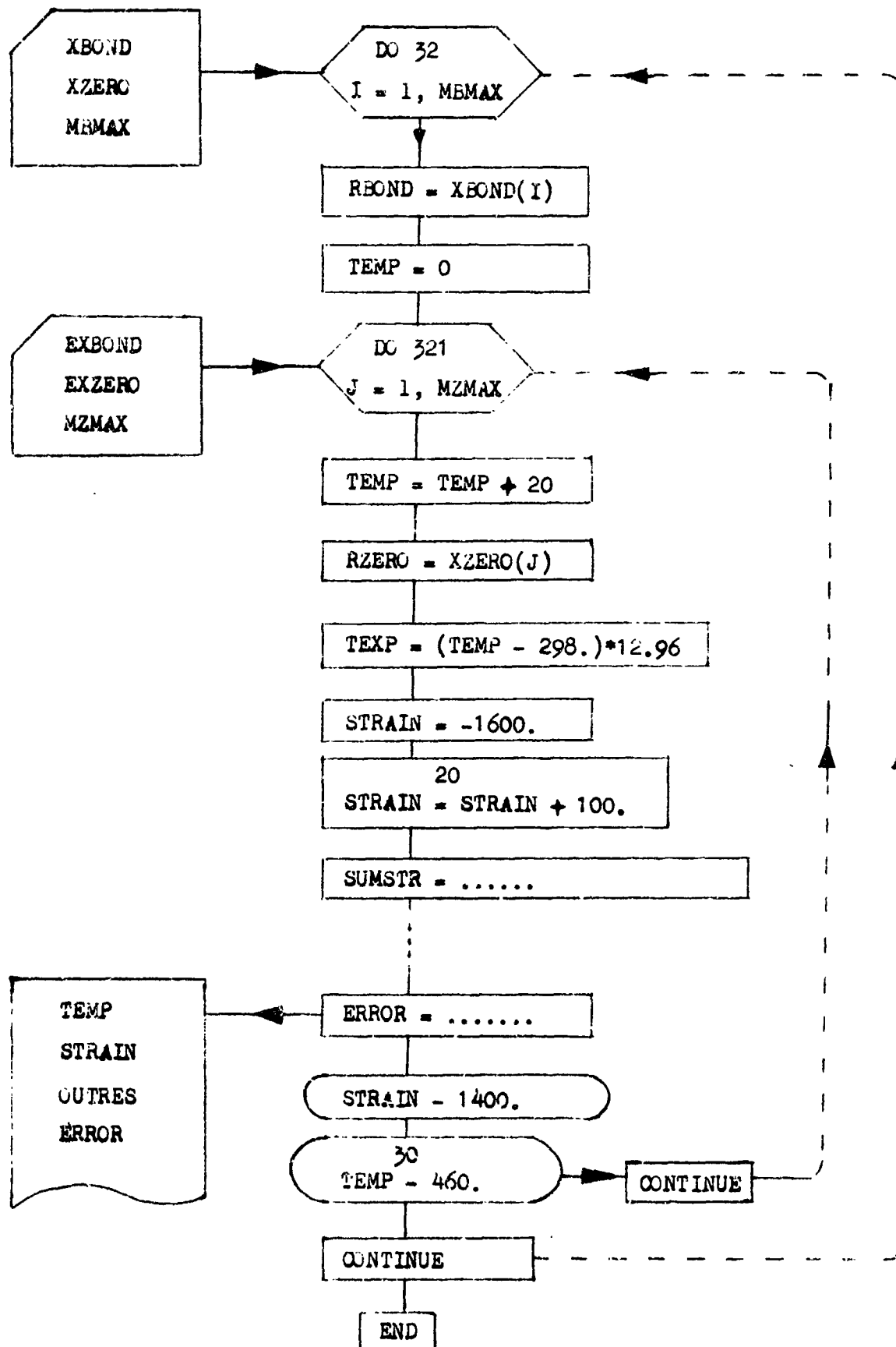
Table AIII.3 Flow Chart for Strain gauge characteristics program.

TABLE AIII.4

STRAIN GAUGE CHARACTERISTICS   COMPUTER PROGRAM

```
*       JOB 1072, TIME 2, PAGES 60, NAME ROBERT D WING
*       FORTRAN
*       LABEL
*       LIST
C       SEMICONDUCTOR STRAIN GAUGE CHARACTERISTICS
        DIMENSION XBOND(10),EXBOND(10),XZERO(30),EXZRO(30)
    2 FORMAT(4X,F5.1,10X,F7.1,10X,F10.3,10X,F10.5)
    3 FORMAT(2I3)
    4 FORMAT(4E10.3)
    5 FORMAT(E10.3)
  131 FORMAT(4X,5HTEMP.,10X,6HSTRAIN,11X,10HRESISTANCE,
     112X,5HERROR)
  132 FORMAT(1H1)
        READ3,MBMAX,MZMAX
        READ4,(XBOND(I),I=1,MBMAX)
        READ4,(EXBOND(I),I=1,MBMAX)
        READ5,(XZERO(J),J=1,MZMAX)
        READ5,(EXZRO(J),J=1,MZMAX)
        DO32 I=1,MBMAX
        RBOND = XBOND(I)
        PRINT 132
        PRINT 131
        TEMP=0.
        DO 321 J=1,MZMAX
        TEMP = TEMP + 20.
        RZERO = XZERO(J)
        TEXP = (TEMP-298.)*12.96
        STRAIN = -1600.
   20 STRAIN = STRAIN + 100.
        SUMSTR = 1.1026(STRAIN+2.*RBOND+2.*TEXP)
        COEFF = RZERO*298.*STRAIN/(1000000.*TEMP**2.)
        OUTRES = COEFF*(122.*TEMP+SUMSTR)
        DELZRO = 298.*STRAIN*(122.*TEMP+SUMSTR)/(1000000.
     1*TEMP**2.)
        DELGFR = COEFF * TEMP
        DELCCR = COEFF*SUMSTR/3700.
        DLBOND = COEFF*2.205
        DLTEMP = -122.286*COEFF
        ERZRO = EXZRO(J)
        ERGFR = 2.44
        ERCCR = 185.
        ERBOND = EXBOND(I)
        ERTEMP = 2.
        ERROR = SQRTF((DELZRO*ERZRO)**2.+(DELGFR*ERGFR)**
     12.+(DELCCR*ERCCR)**2.+(DLBOND*ERBOND)**2.+
     2(DLTEMP*ERTEMP)**2.)
        PRINT 2,TEMP,STRAIN,OUTRES,ERROR
        IF(STRAIN-1400.)20,20,30
   30 IF (TEMP -460.) 321,321,32
  321 CONTINUE
   32 CONTINUE
        CALL EXIT
```

TABLE AIII 5

Data for Computer Program

The information on each data card is laid out in the following
format:

*DATA

MBMAX	MZMAX		
XBOND, I=1	XBOND, I=2	XBOND, I=MBMAX	
EXBOND, I=1	EXBOND, I=2	EXBOND, I=MBMAX	
XZERO, J=1			T = 20°K
XZERO, J=2			T = 40°K
XZERO, J= MZMAX			T = 460°K
EXZERO, J = 1			T = 20°K
EXZERO, J = 2			T = 40°K
EXZERO, J = MZMAX			T = 460°K

----

* The following table (AIII.6) gives an example of the data card
  listing for strain gauges AA, BB, XX, and YY.

TABLE AIII.6
STRAIN GAUGE CHARACTERISTICS DATA INPUT LISTING

```
*       DATA
   4 23
   -264.5      -1347.5      -899.0      -744.0
       5.0        10.0         8.0         8.0
160.6                                    20
156.6                                    40
153.0                                    60
149.7                                    80
146.6                                   100
144.0                                   120
141.6                                   140
139.7                                   160
138.2                                   180
137.4                                   200
137.3                                   220
137.4                                   240
138.0                                   260
139.3                                   280
141.2                                   300
143.5                                   320
146.2                                   340
149.1                                   360
152.4                                   380
156.1                                   400
160.3                                   420
164.5                                   440
168.8                                   460
6.0                                      20
5.4                                      40
4.7                                      60
4.1                                      80
3.5                                     100
3.0                                     120
2.4                                     140
2.0                                     160
1.6                                     180
1.2                                     200
0.9                                     220
0.6                                     240
0.4                                     260
0.2                                     280
0.2                                     300
0.2                                     320
0.2                                     340
0.2                                     360
0.2                                     380
0.3                                     400
0.5                                     420
0.7                                     440
1.1                                     460
```

(a) Extensional vibrations :
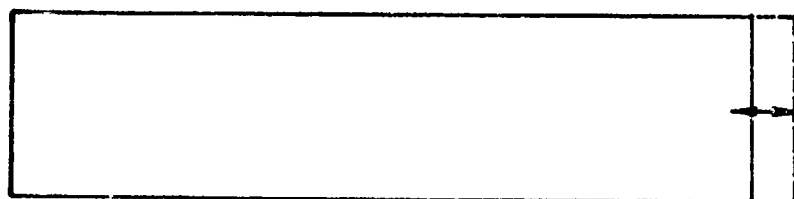
Axial
extensional
motion
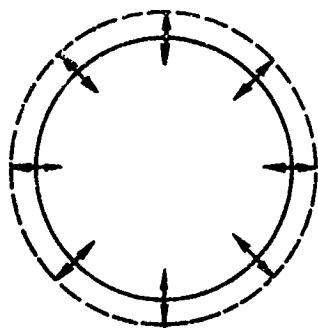
Radial
extensional
motion

(b) Bending modes :
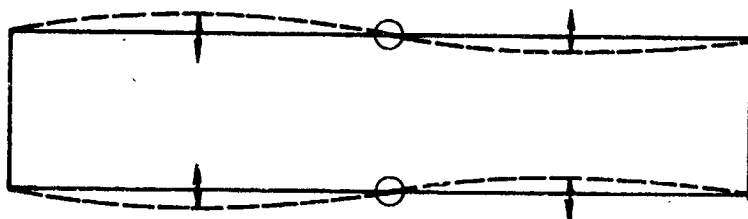
An axial mode - 2nd. axial mode shown as example

Radial modes

2nd radial mode

3rd radial mode

nodes
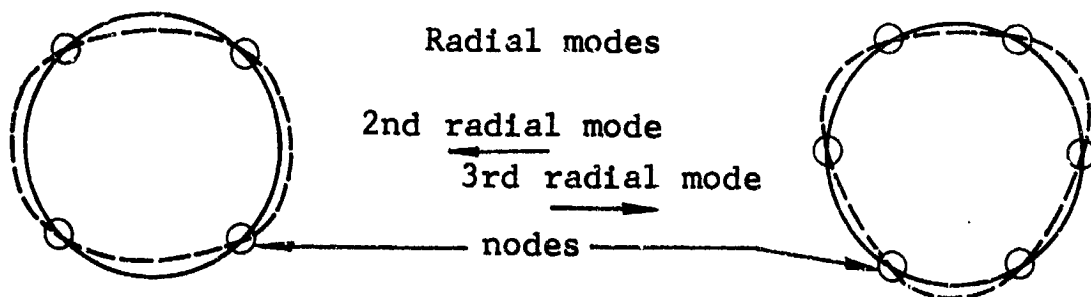
Figure 1. Vibrational forms of a thin cylinder
with closed ends.
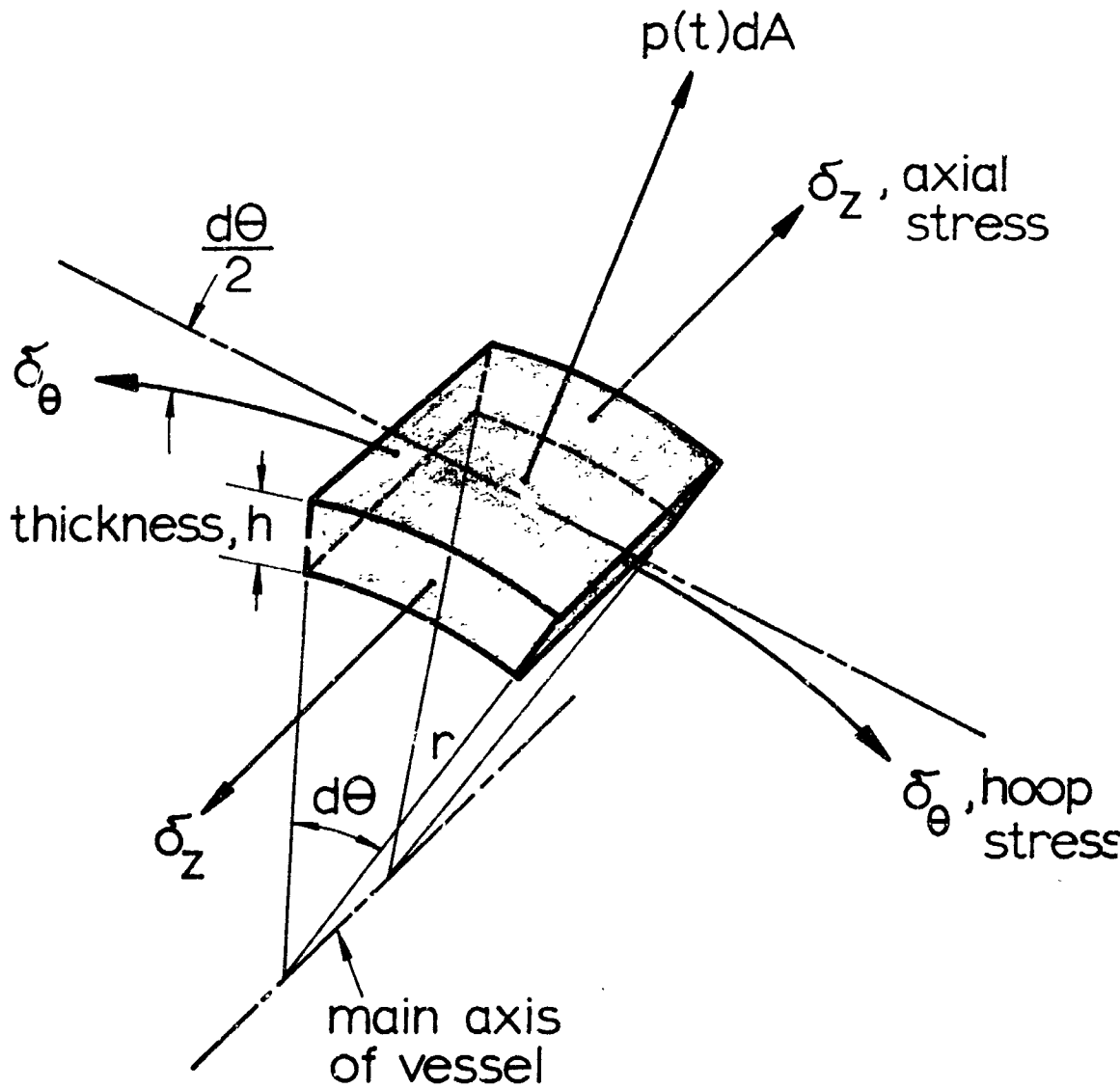
Fig. 2   Hoop and axial stresses acting on an element of the
cylinder as a result of a radially acting pressure, p(t).

P_m
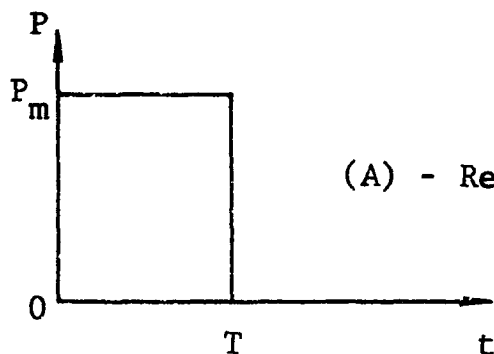
(A) - Rectangular step function
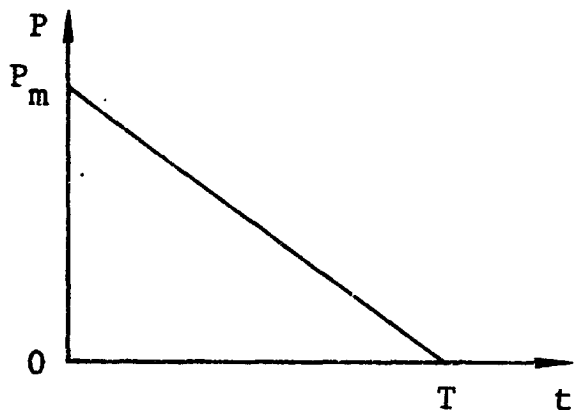
(B) Linear decay

$$p(t)=p_m(1-t/T) \quad \text{for } 0 \ t \ T$$
$$= 0 \qquad \text{for } \ t \ T$$
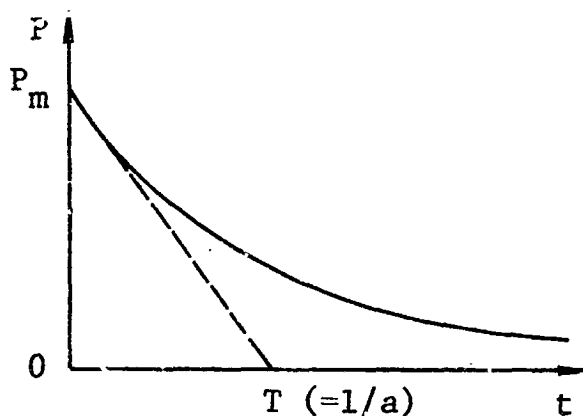
(C) Exponential decay

$$p(t)=p_m \cdot e^{-at}$$
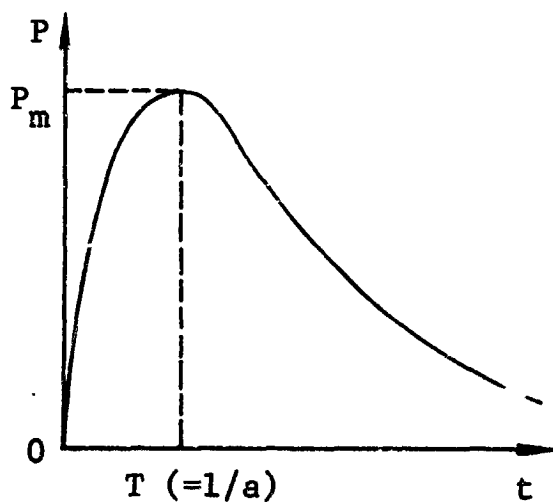
(D) Exponential x time

$$p(t)=p_m aet \cdot e^{-at}$$
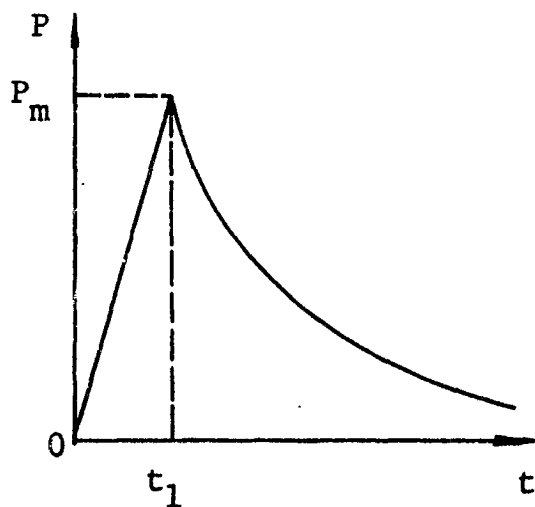
(E) Linear rise, exp. decay

$$p(t)=p_m t/t_1 \qquad \text{for } 0 \ t \ t_1$$
$$=p_m \cdot e^{-a(t-t_1)} \quad \text{for } \ t \ t_1$$

Figure 3. Typical approximate mathematical forms for blast loading.
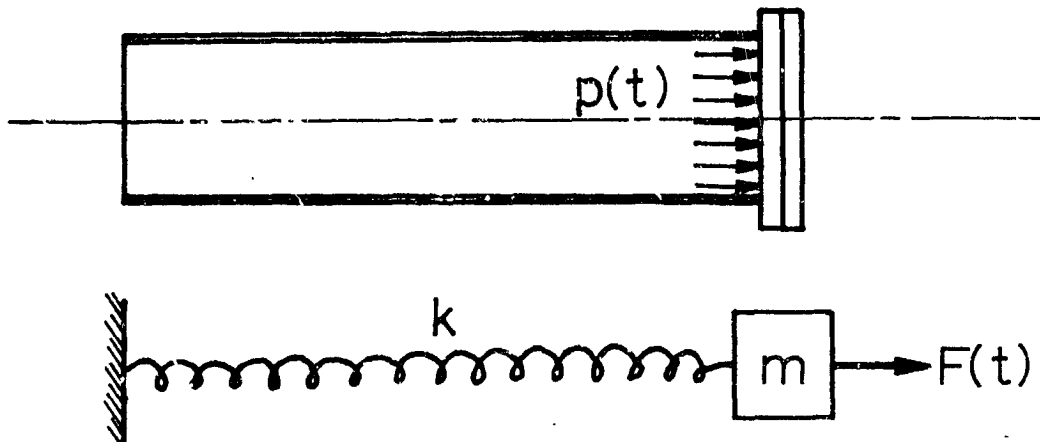
Fig. 4   Analogous dynamic systems.   Comparison of the cylinder and its heavy end cap to a simple spring-mass system.
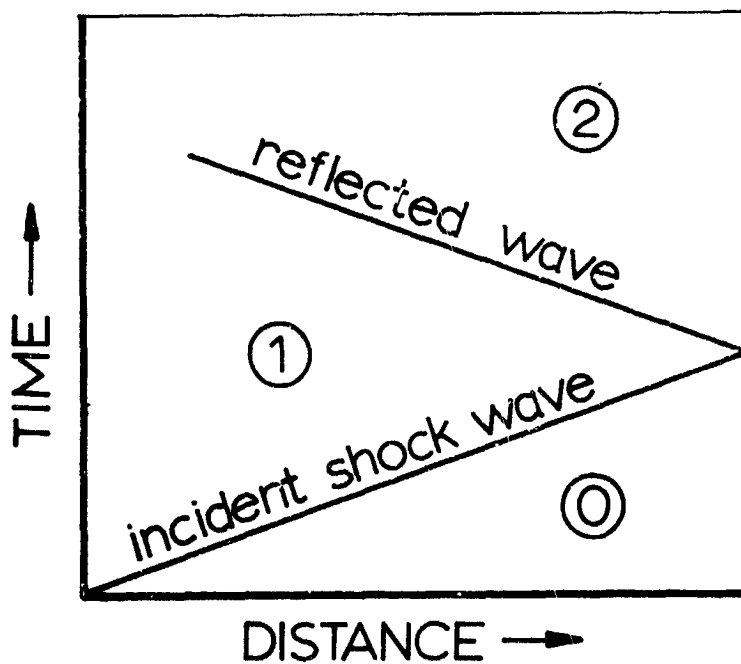
Fig. 5   Space-time diagram for shock wave reflection process.
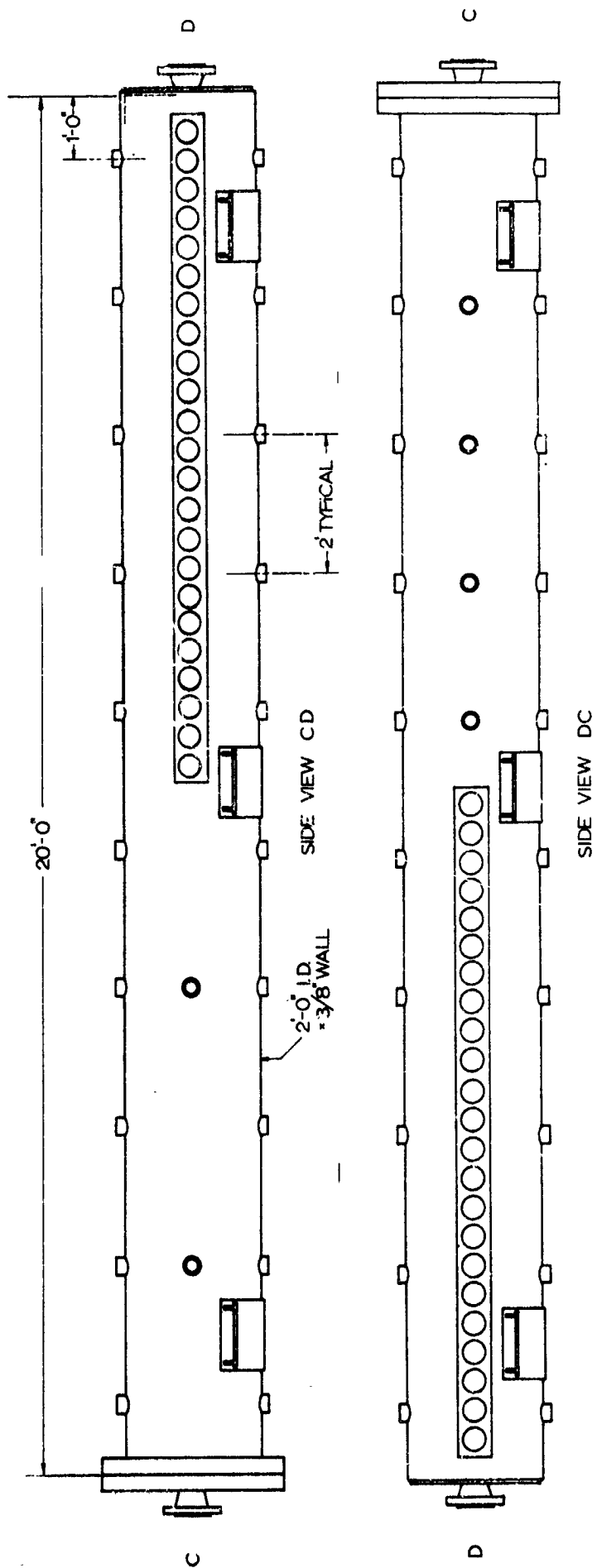
Fig. 6 Schematic drawing of the detonation tube, showing dimensions and locations of the ports for pressure transducers
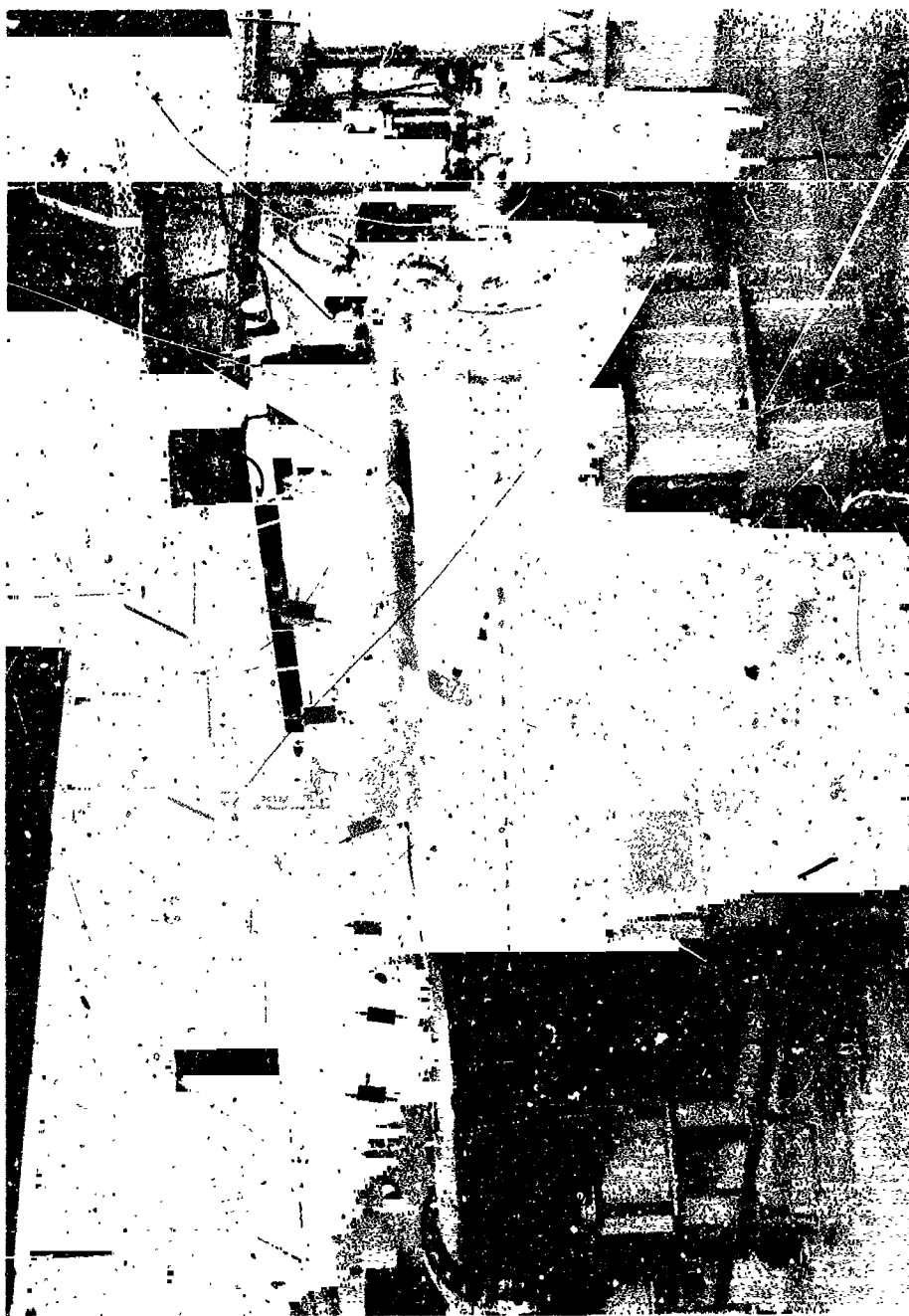
Fig. 7 Detonation tube with instrumentation
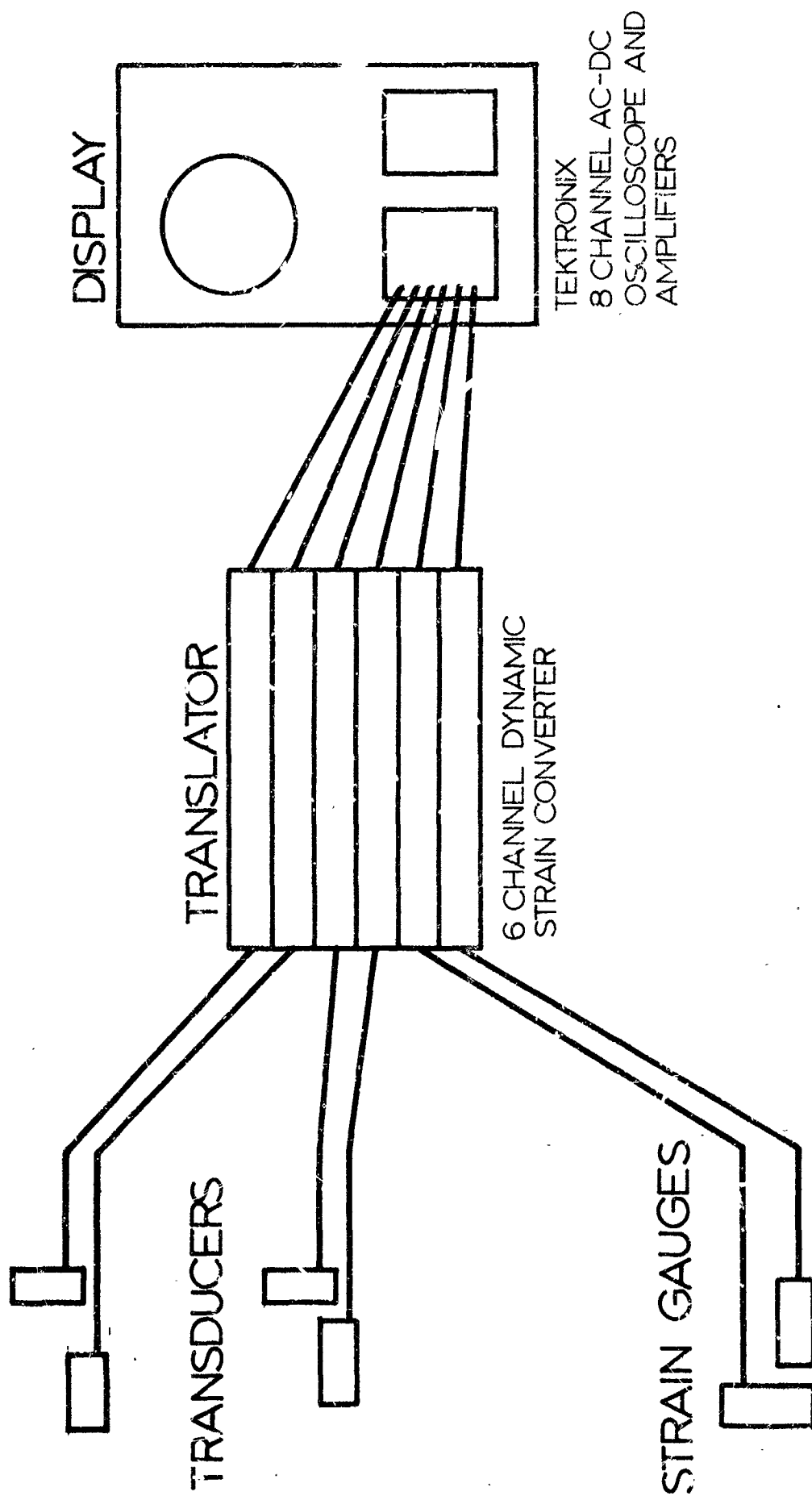
Fig. 8 Block diagram of strain recording system
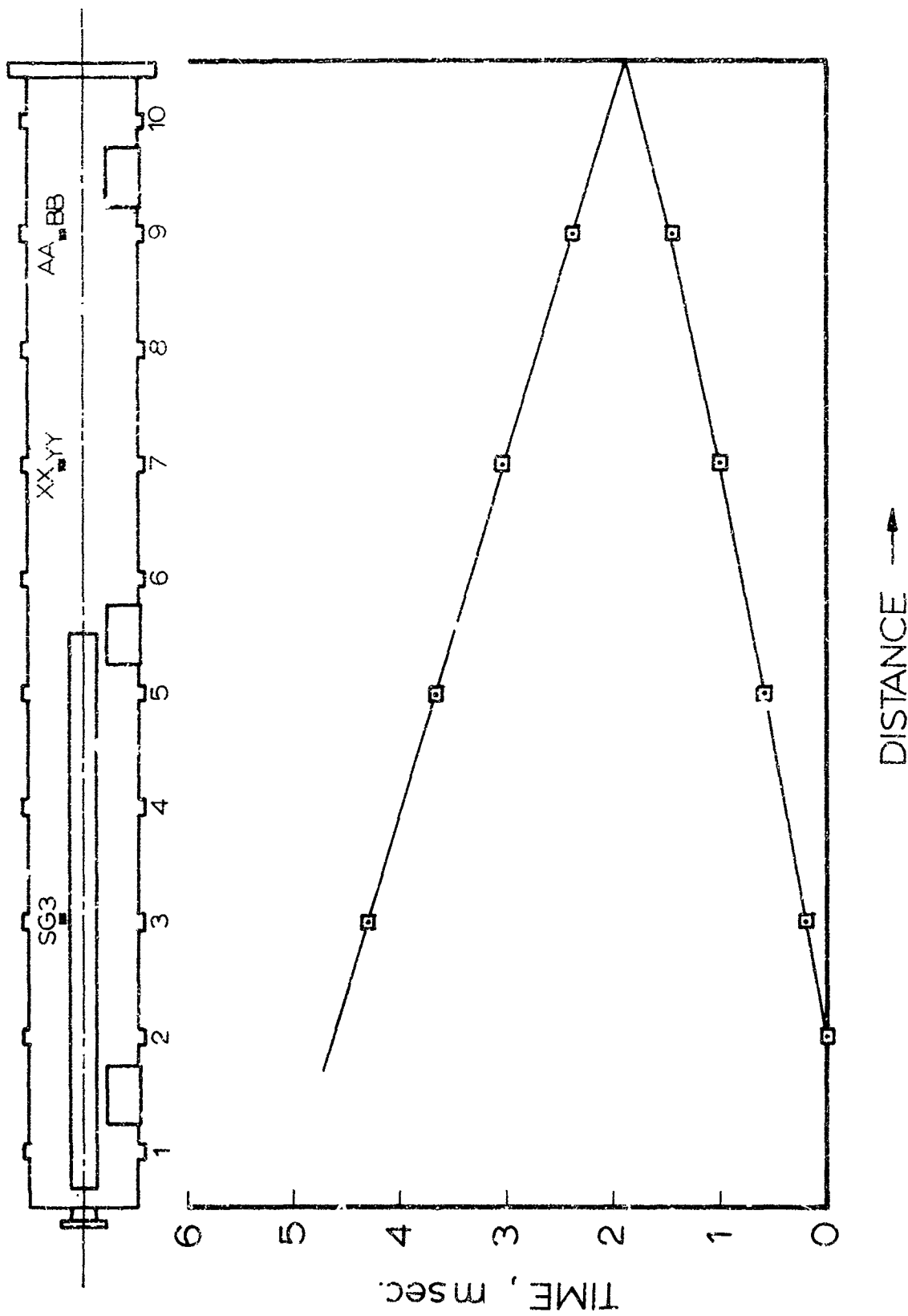
Fig. 9 Space-time diagram of detonation process in the
20' cylinder, plotted from pressure transducer records
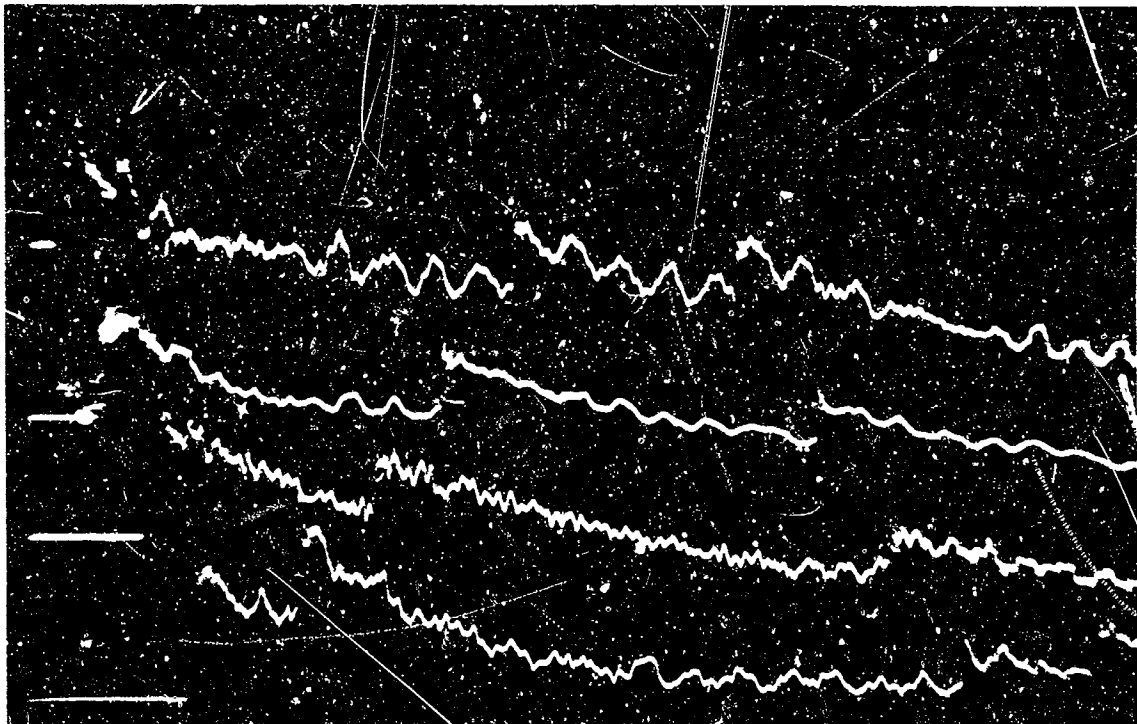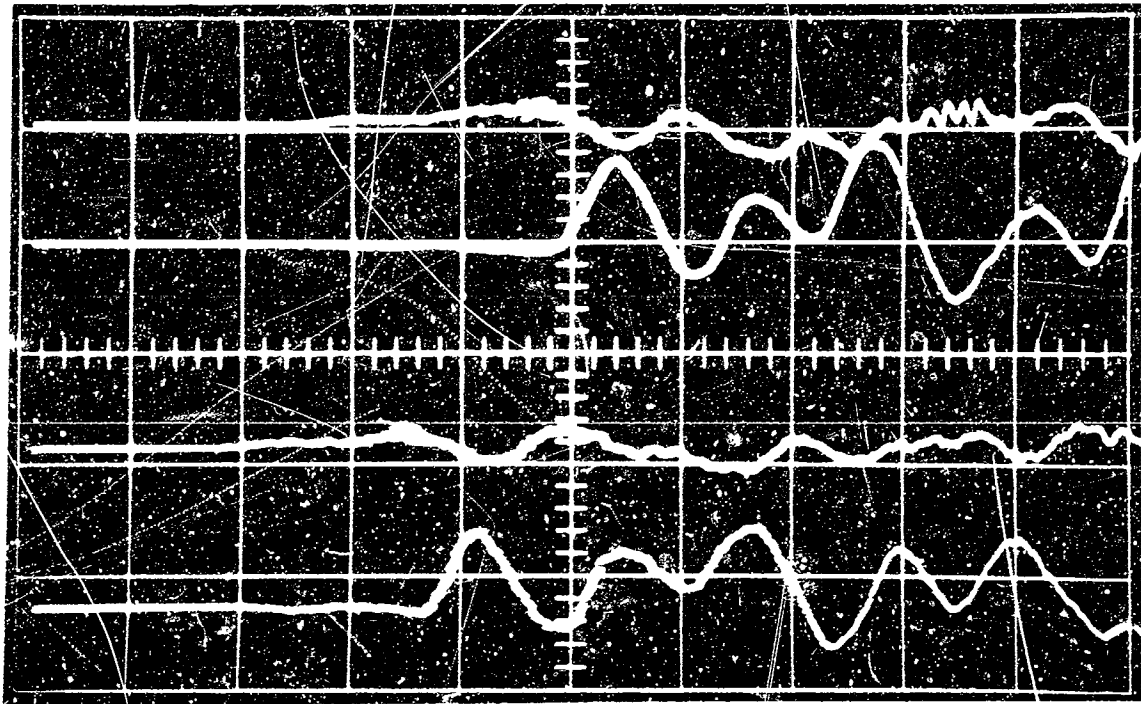
Fig. 10   Strain and Pressure records, Test # CD 149
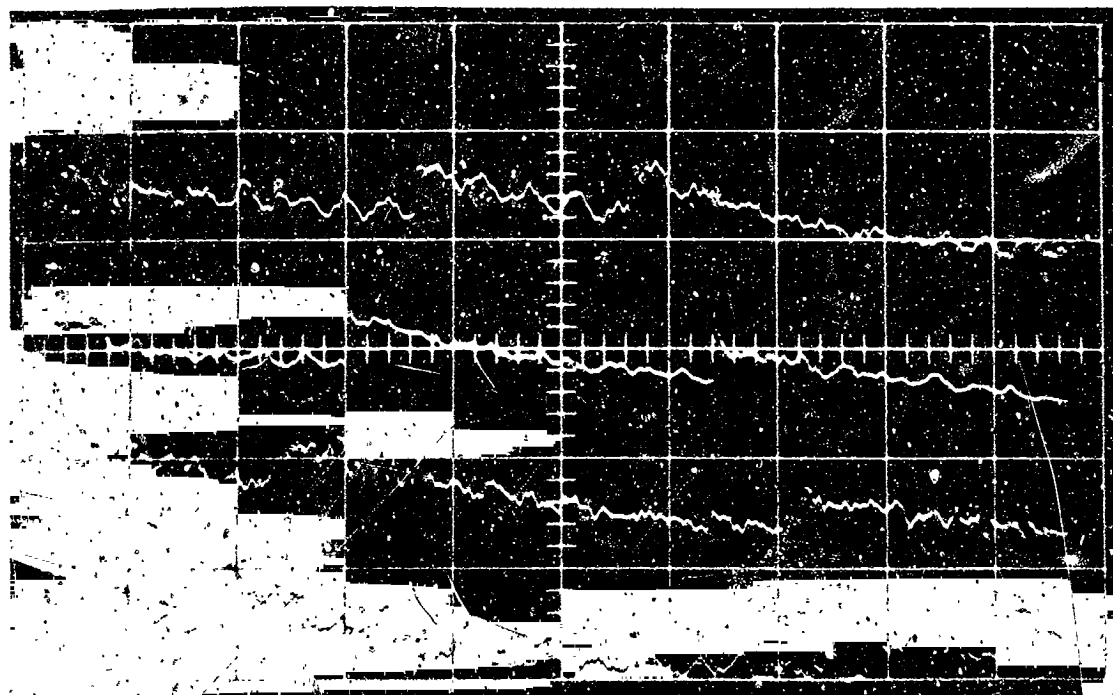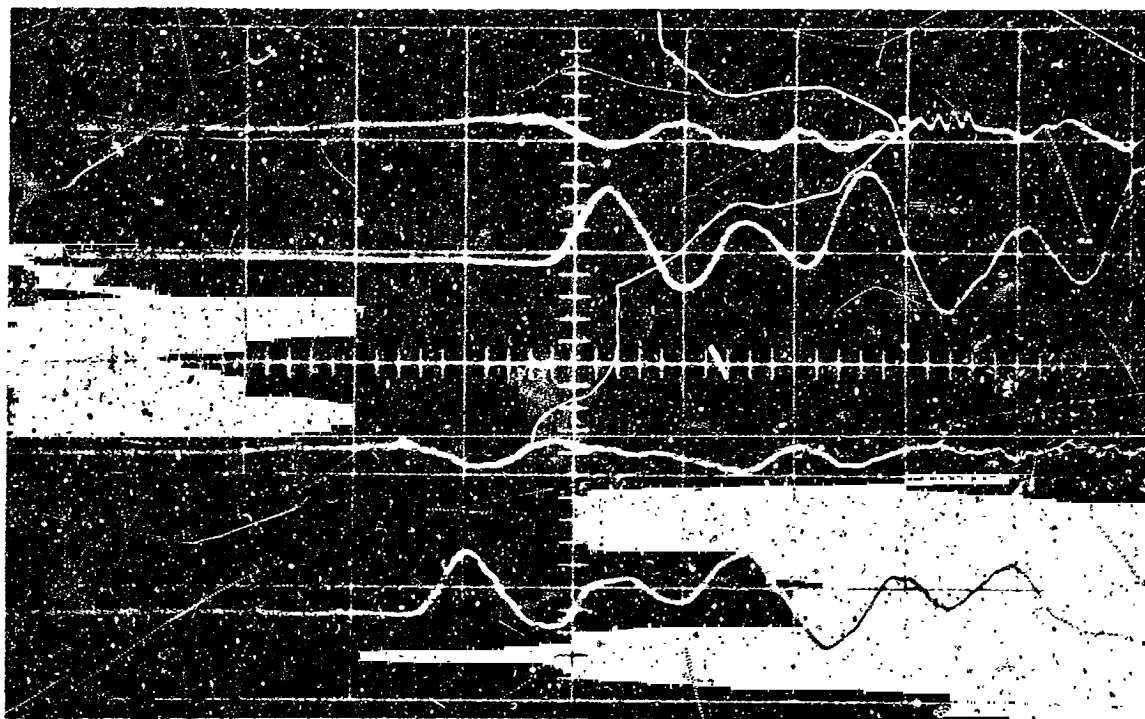
Fig. 11 Strain and Pressure records, Test # CD150

RECORD	TRACE	STRAIN GAUGE AND LOCATION	CALIBRATION	TEST CONDITIONS
Fig. 10 Upper Record	a	AA (9)	59.5 μ"/"/cm	Test No. CD 149 Mixture: $2H_2+O_2$ Initial Pressure: 100mmHg Ignitor: Primacord Trigger Position - 2 Sweepspeed: 0.3 ms/cm
	b	BB (9)	61.5	
	c	XX (7)	63.0	
	d	YY (7)	58.2	
Fig. 10 Lower Record	a	Pressure Gauge (3)	20.3 psi/cm	Test No. CD 149 Mixture: $2H_2+O_2$ Initial Pressure: 100mmHg Ignitor: Primacord Trigger Position - 2 Sweepspeed: 1.0 ms/cm
	b	" (5)	"	
	c	" (7)	"	
	d	" (9)	"	
Fig. 11 Upper Record	a	AA (9)	149.5 μ"/"/cm	Test No. CD 150 Mixture: $2H_2+O_2$ Initial Pressure: 200mmHg Ignitor: Primacord Trigger Position - 2 Sweepspeed: 0.3 ms/cm
	b	BB (9)	154.4	
	c	XX (7)	147.0	
	d	YY (7)	146.0	
Fig. 11 Lower Record	a	Pressure Gauge (3)	20.3 psi/cm	Test No. CD 150 Mixture: $2H_2+O_2$ Initial Pressure: 200mmHg Ignitor: Primacord Trigger Position - 2 Sweepspeed: 1.0 ms/cm
	b	" (5)	"	
	c	" (7)	"	
	d	" (9)	"	

Note: To distinguish between the four traces on each record, they are referred to as traces a,b,c, and d - lettering from the top down.

Figures 10 & 11 continued. Data to accompany photographic records
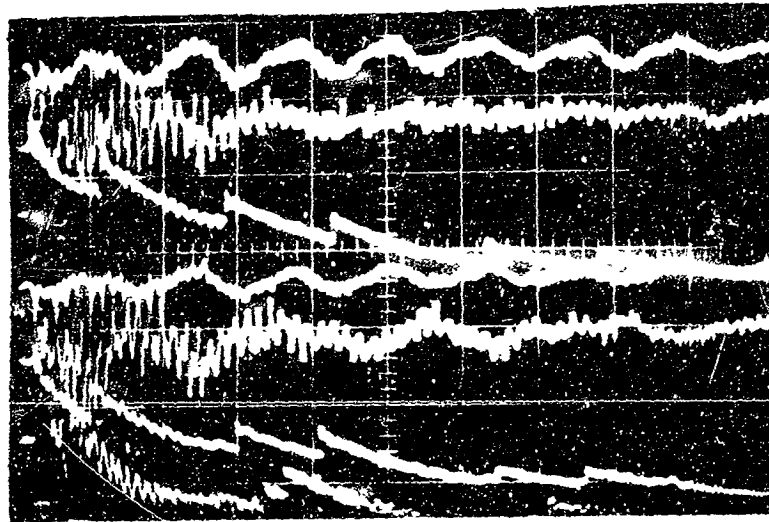
TRACE	STRAIN GAUGE NUMBER	LOCATION	CALIBRATION	
a	AA	9	66.0	"/"/cm
b	BB	9	72.4	"/"/cm
c	Pressure Gauge	9	20	psi/cm
d	XX	7	64.3	"/"/cm
e	YY	7	63.6	"/"/cm
f	Pressure Gauge	7	20	psi/cm
g	Pressure Gauge	2	20	psi/cm

Test No. CD 251; Mixture, $2H_2+O_2$; Initial Pressure, 100mmHg; Ignitor, Primacord; Trigger, Ionization Probe; Horizontal Sweep Speed, 5.0 ms/cm.

Fig. 12 Records and Data for Test No. CD251
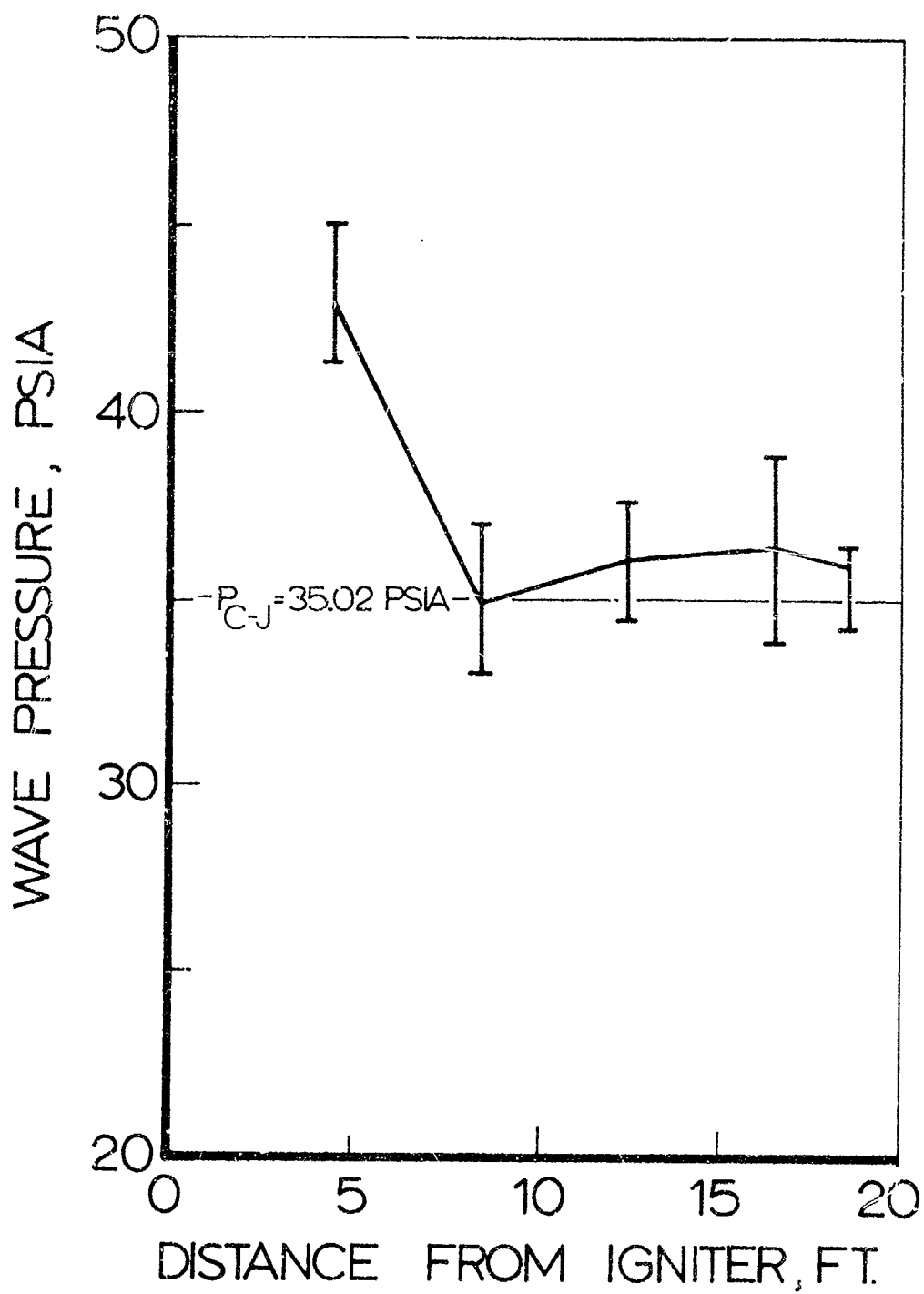
Fig. 13 Variation of incident wave pressure along the length of the detonation tube for $2H_2+O_2$ mixture initially at 100 mm Hg with Primacord ignition
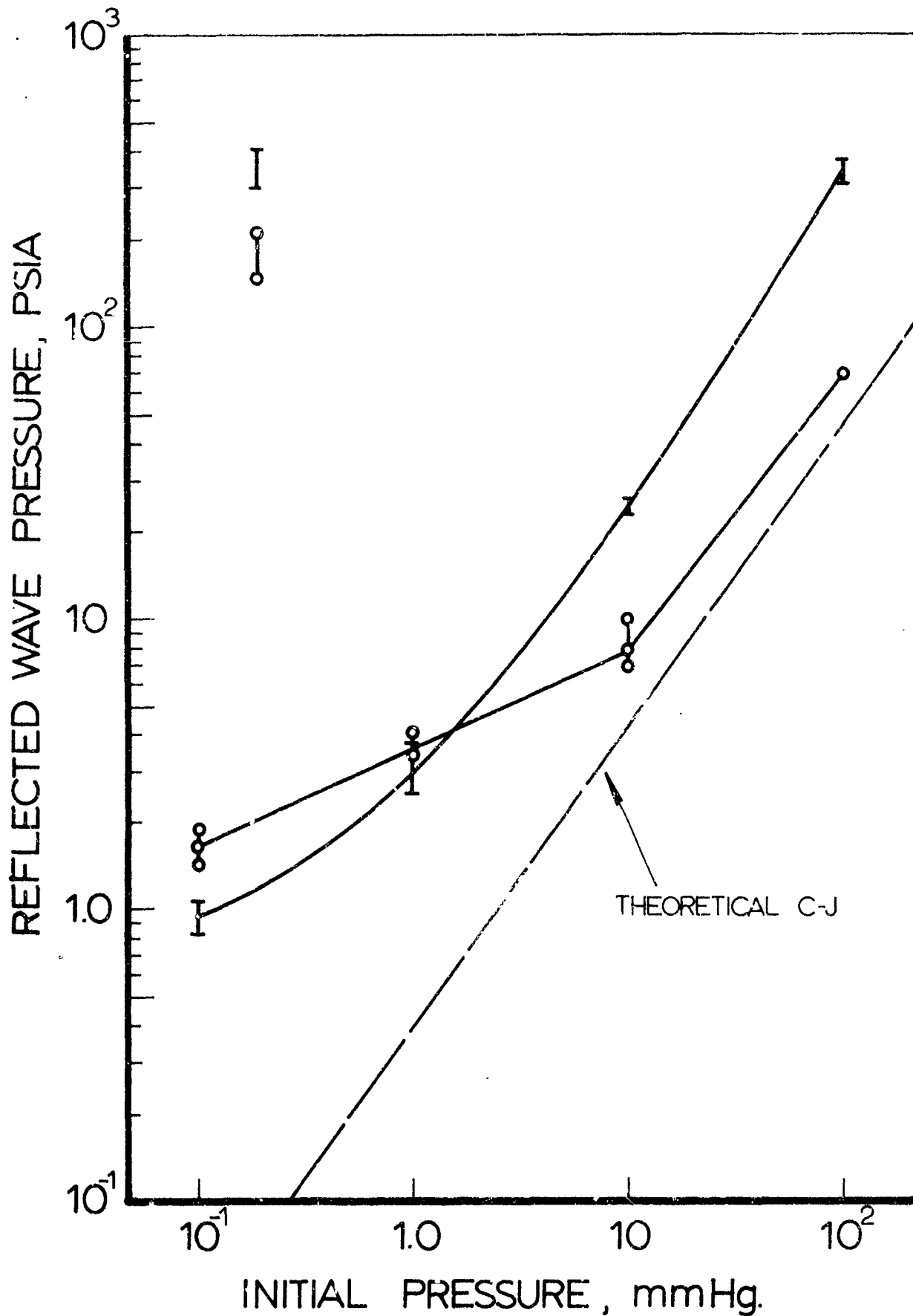
Fig. 14 Variation of reflected wave pressure with initial
mixture pressure for $2H_2+O_2$ mixture with Primacord
ignition.
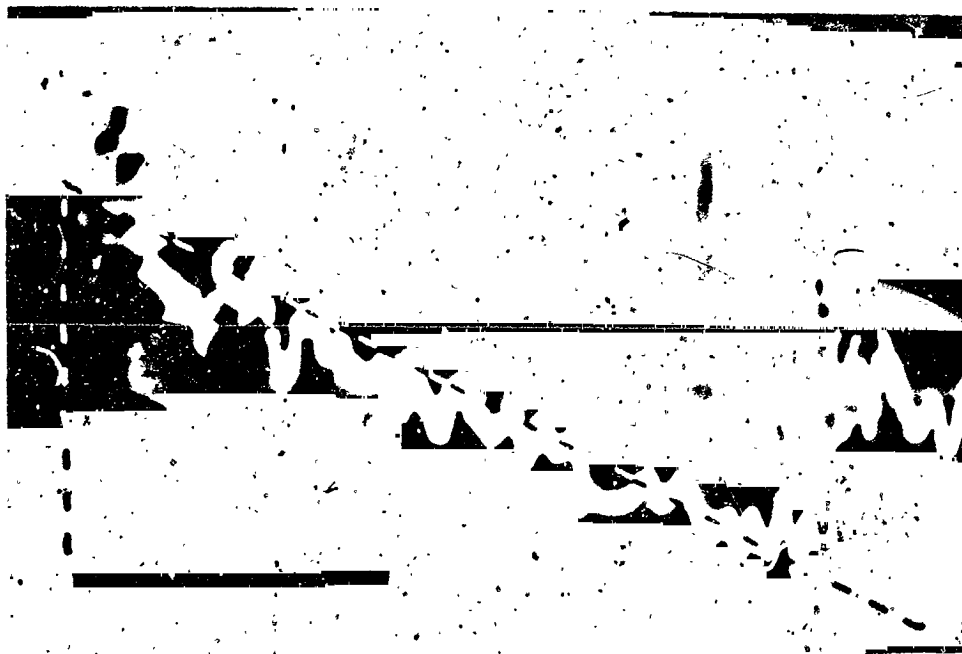
Fig. 15   Enlargement of typical pressure record

   Data: Trace from station 7, Test CD149
           100 mm Hg initial pressure
           Mixture $2H_2+O_2$ (stoichiometric)

   601 type pressure transducer with type 568 amplifier
   Oscilloscope sweep speed 1.0 millisecond/cm
       (left to right)
   Vertical calibration - 20.32 psi/cm

The above figure, an enlargement of one of the pressure
records from an actual test, is an example of the method used
to find an approximate mathematical form for the pressure
decay function. By simply drawing the best straight line
through the recording—and, as may be seen, this is not an
unreasonable approximation—the record can be reduced to
a function of the form:

$$p = p_m(1 - t/T) \qquad \text{for } 0 \ t \ T$$
$$= 0 \qquad\qquad \text{for } t \ T$$
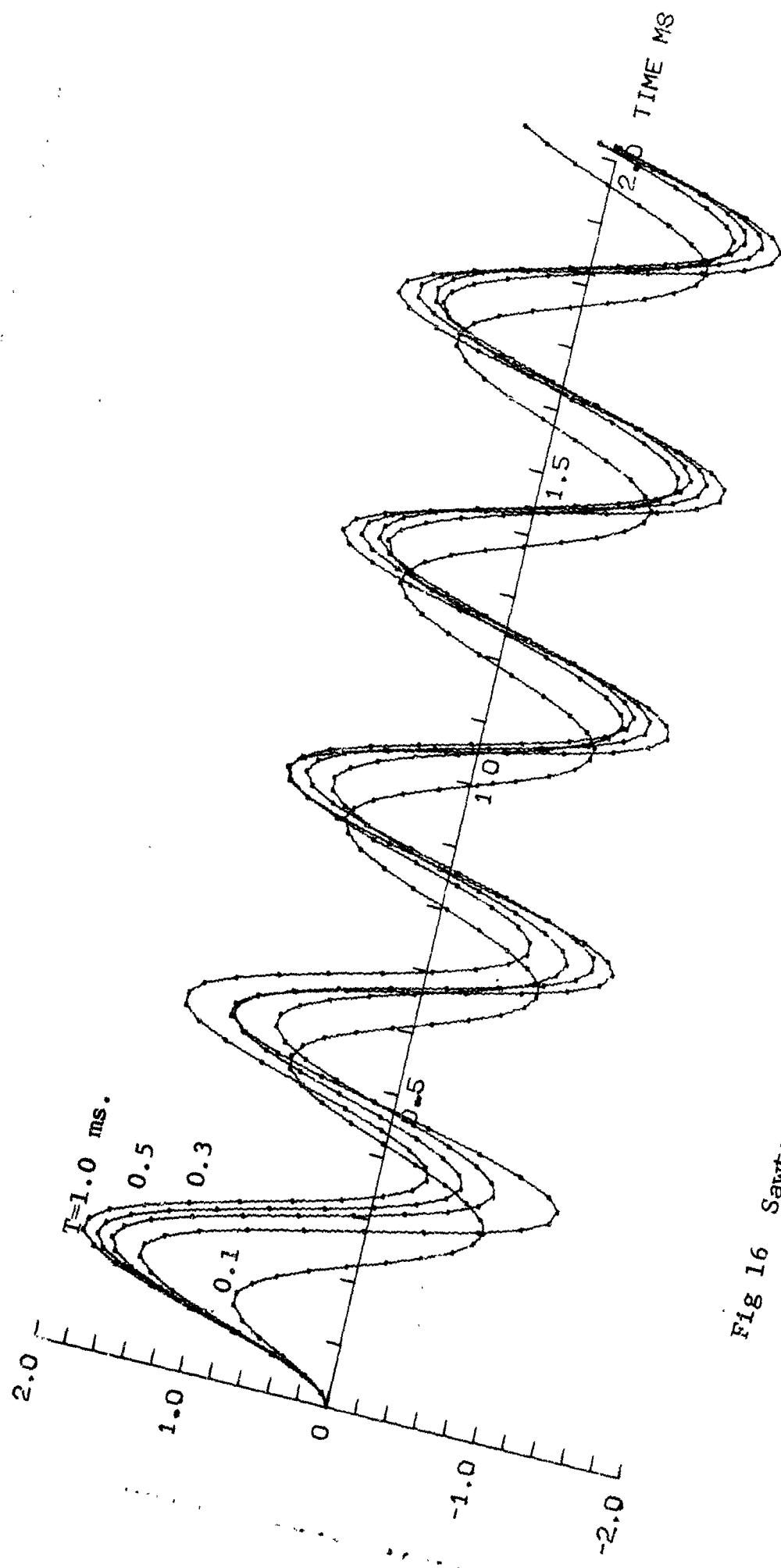
Fig 16 Sawtooth input: Pulse decay times 1.0 to 10 msec.

HOOP STRESS DYNAMIC FUNCTION
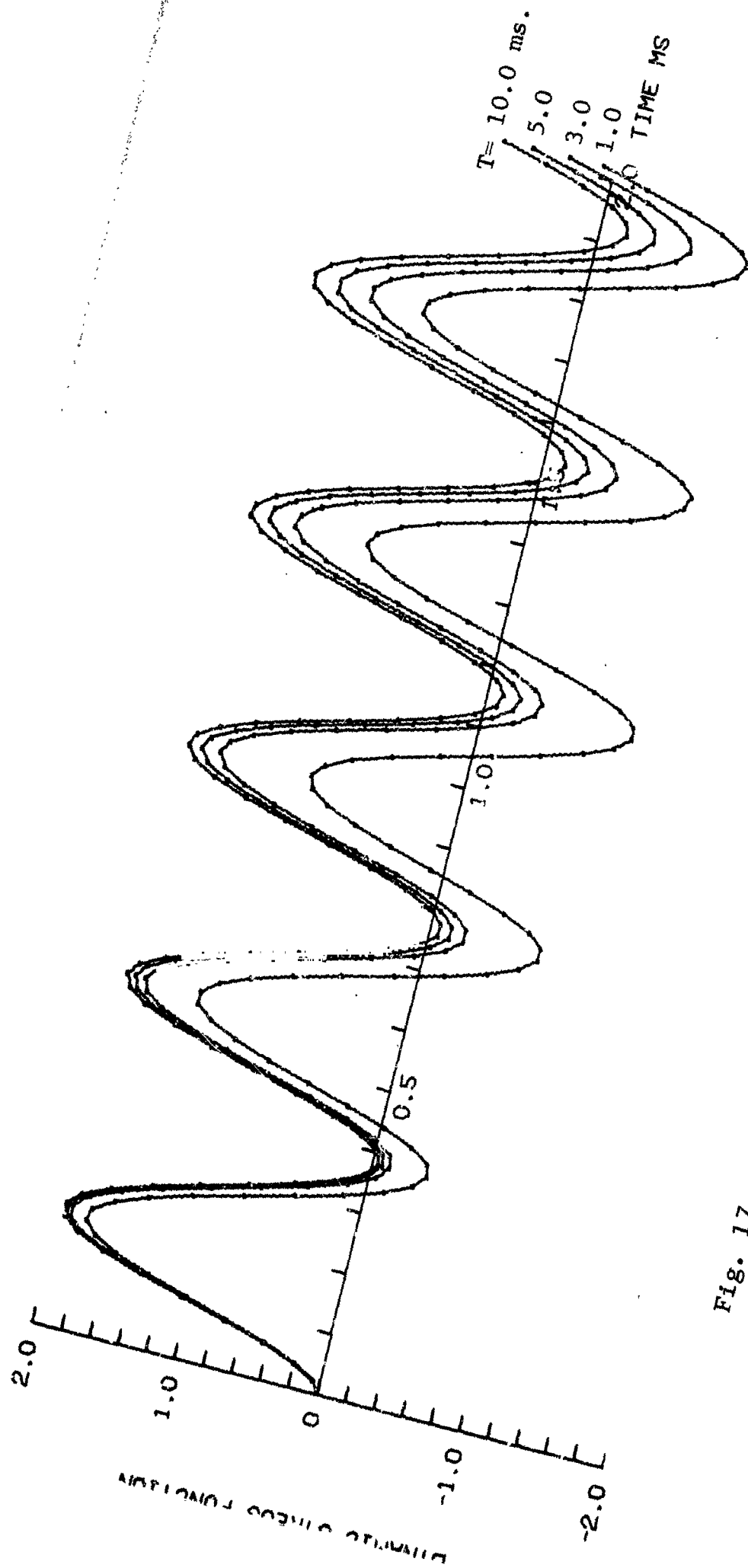
Fig. 17 Sawtooth input: Pulse decay times 0.1 to 1.0 msec

HOOP STRESS DYNAMIC FUNCTION
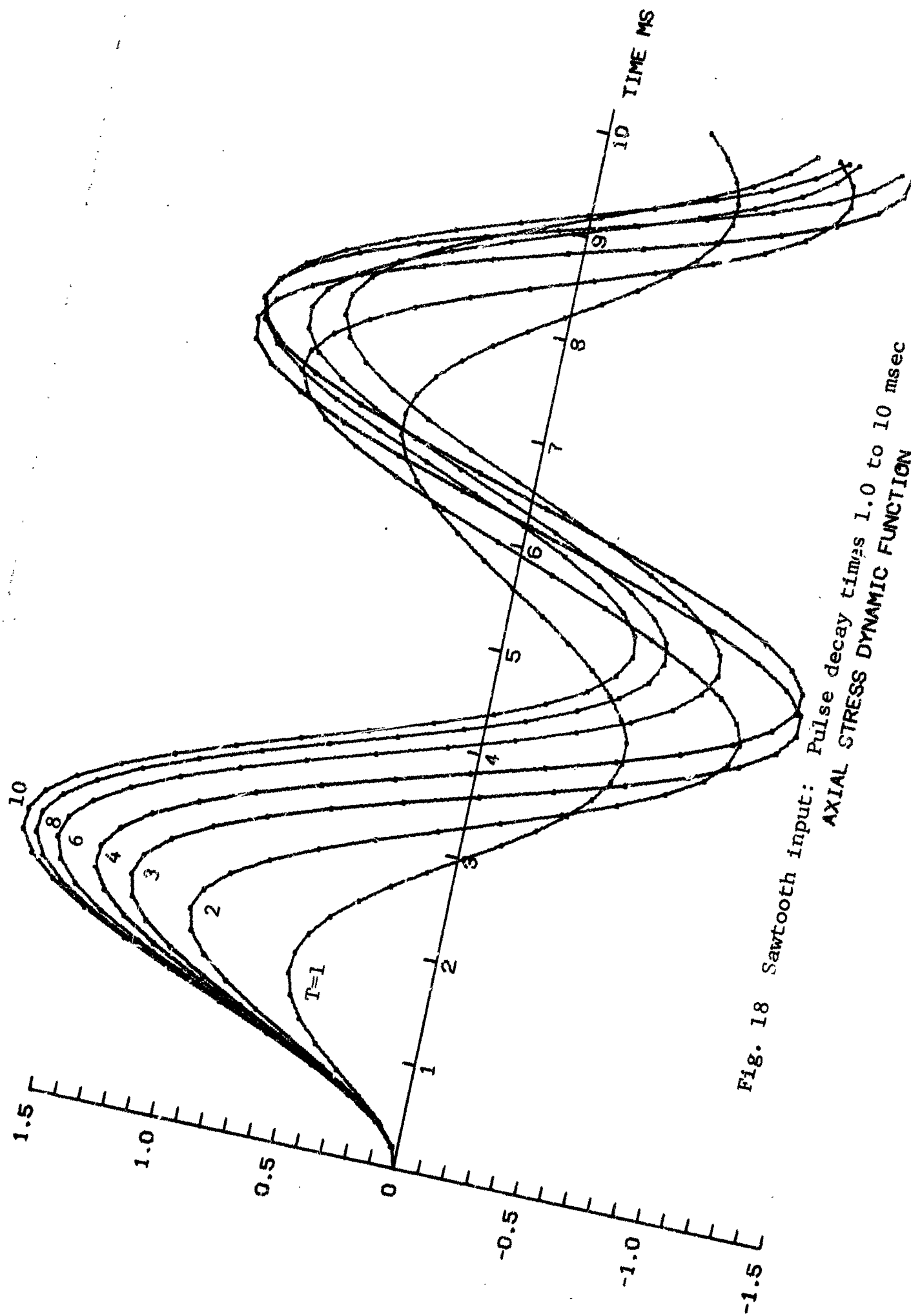
Fig. 18 Sawtooth input: Pulse decay times 1.0 to 10 msec

AXIAL STRESS DYNAMIC FUNCTION
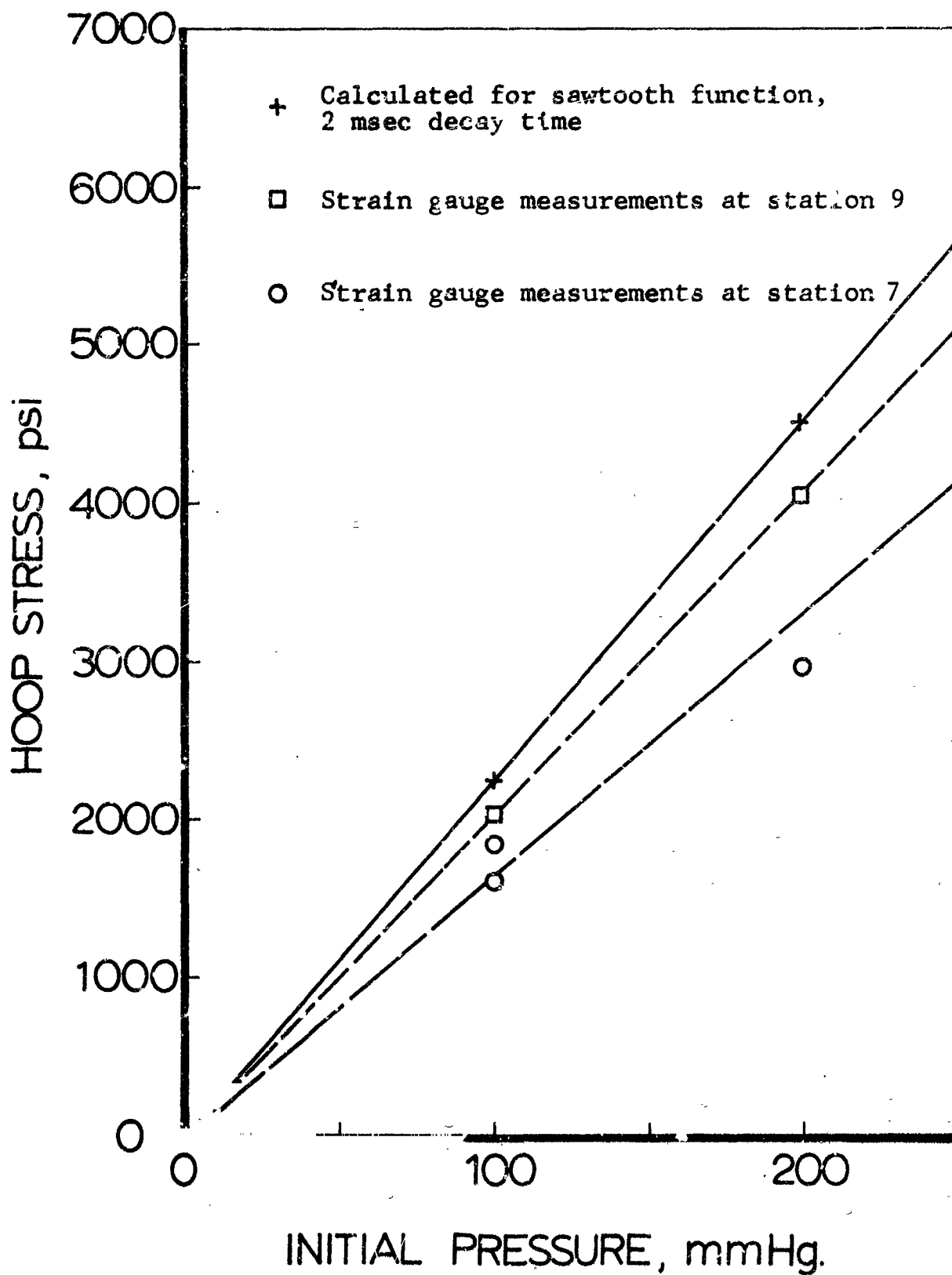
Fig. 19   Peak amplitudes of analytical and experimental hoop
stresses as a function of initial pressure

TEST CD149
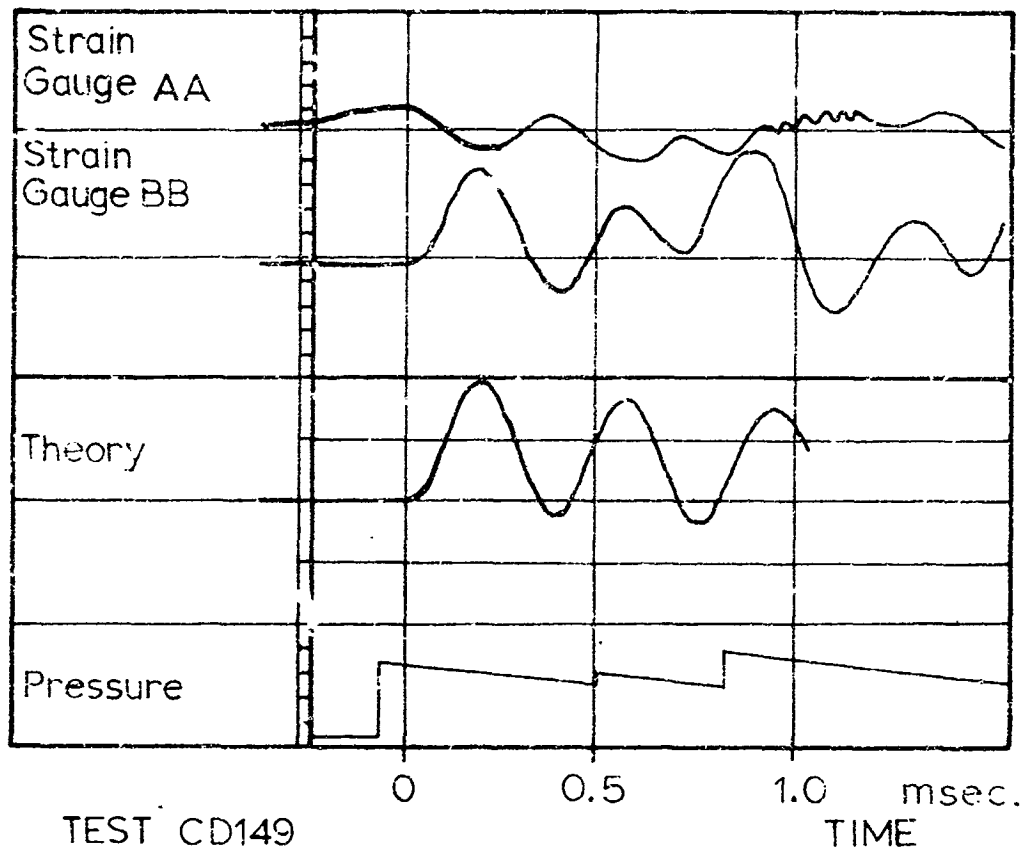
Calibration data:

    Strain gauge AA: 59.5 $\mu''/''/cm$

    Strain Gauge BB: 61.5 $\mu''/''/cm$

For the theoretical curve the sawtooth approximation
for blast loading was used, with pulse decay time,
T = 2 ms-c

Fig. 20 Dynamic hoop response of vessel--comparison of
        experimental and analytical results

24 bolts, 1"diameter

6"

240"
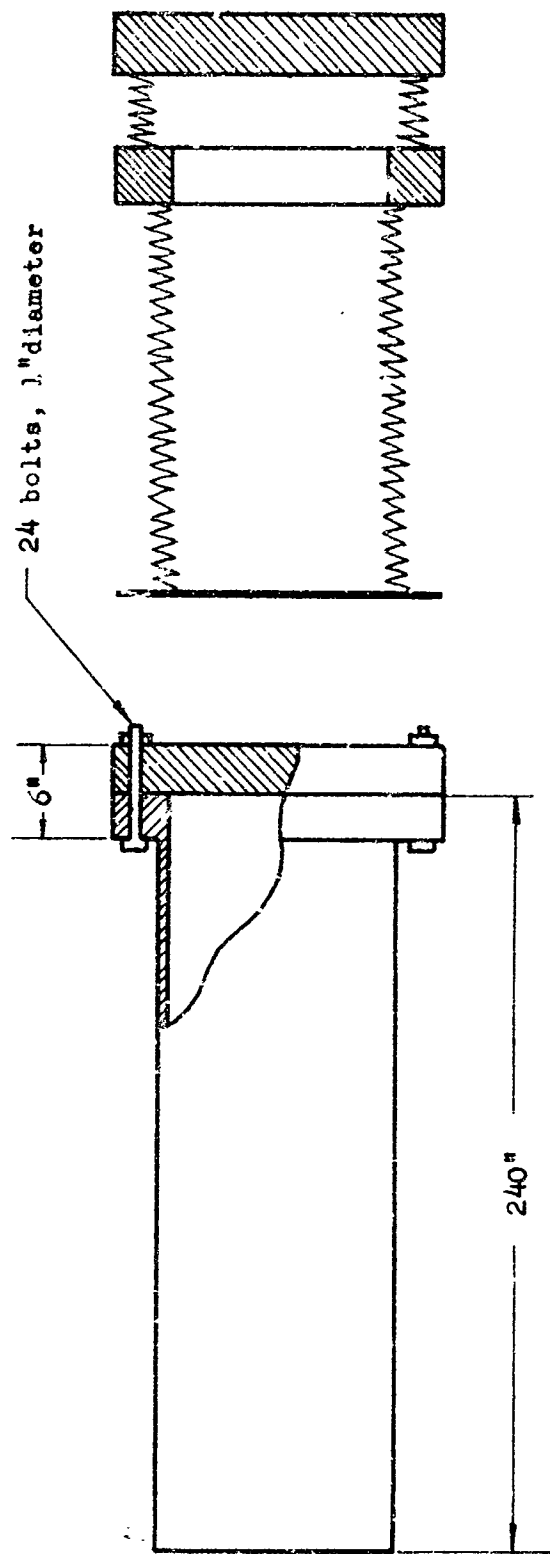
Spring constant of bolts, $k_b = A.E/L = 91.1 \times 10^6$ lb/in^2.

Spring constant of cylinder, $k_{cyl} = 2\pi r h.E/L = 3.47 \times 10^6$ lb/in^2.

Mass of end flange = 165 lb.

Mass of end cover plate = 714 lb.

Fig. 21   Two mass - two spring model for axial vibrations.
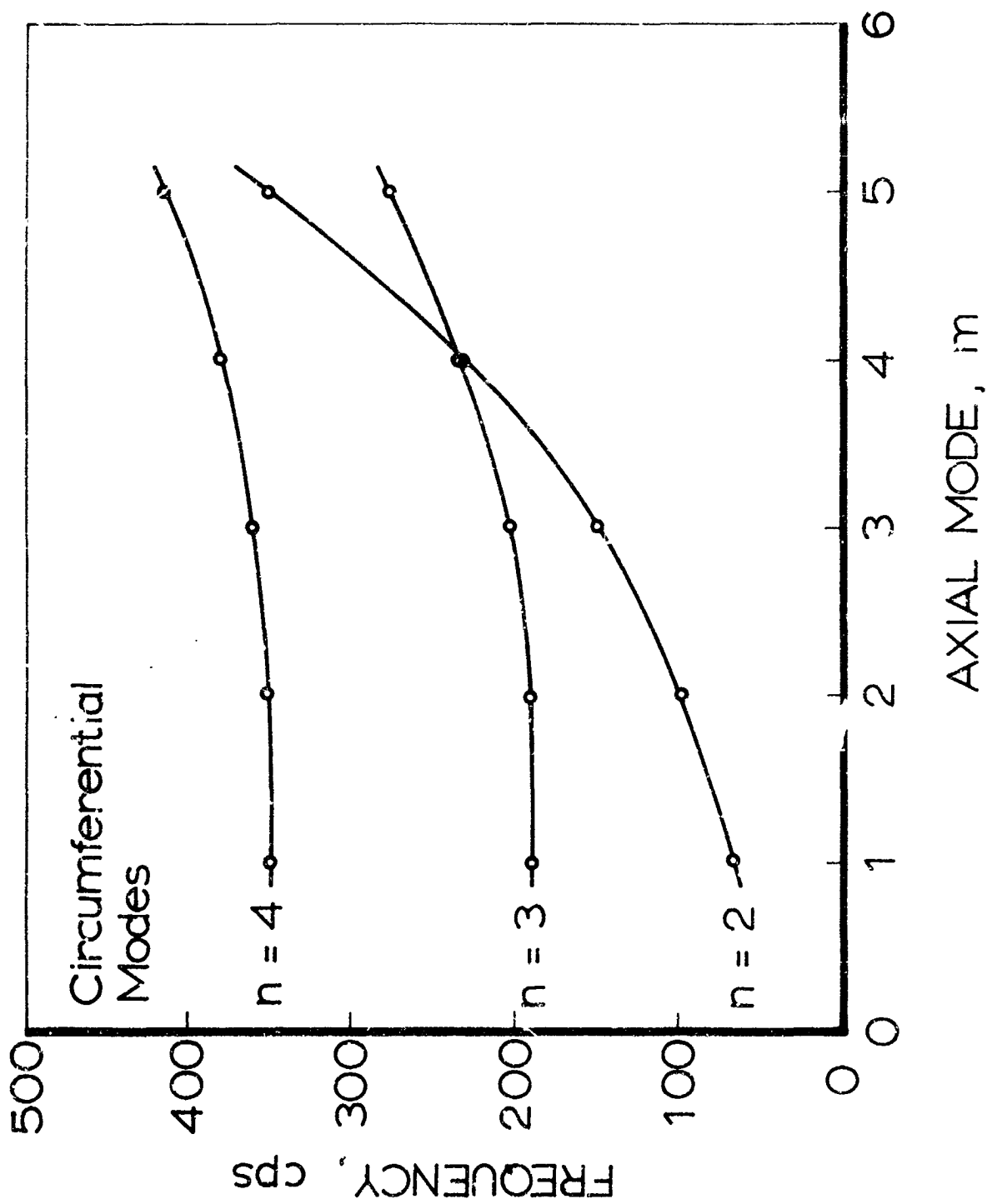
Fig. AI.1 Frequency predictions for lower modes of flexural vibration
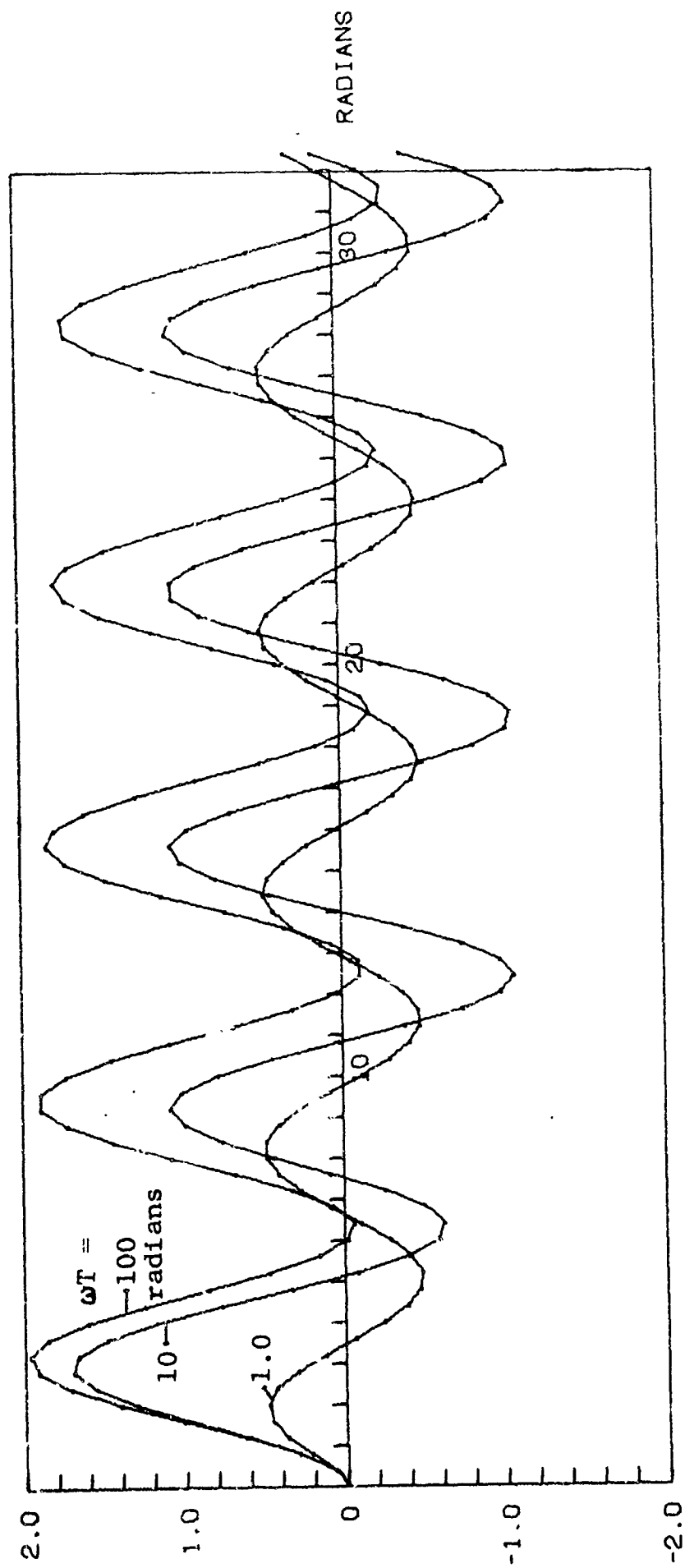
Fig. AII.1   GENERAL DYNAMIC STRESS FUNCTION (B)
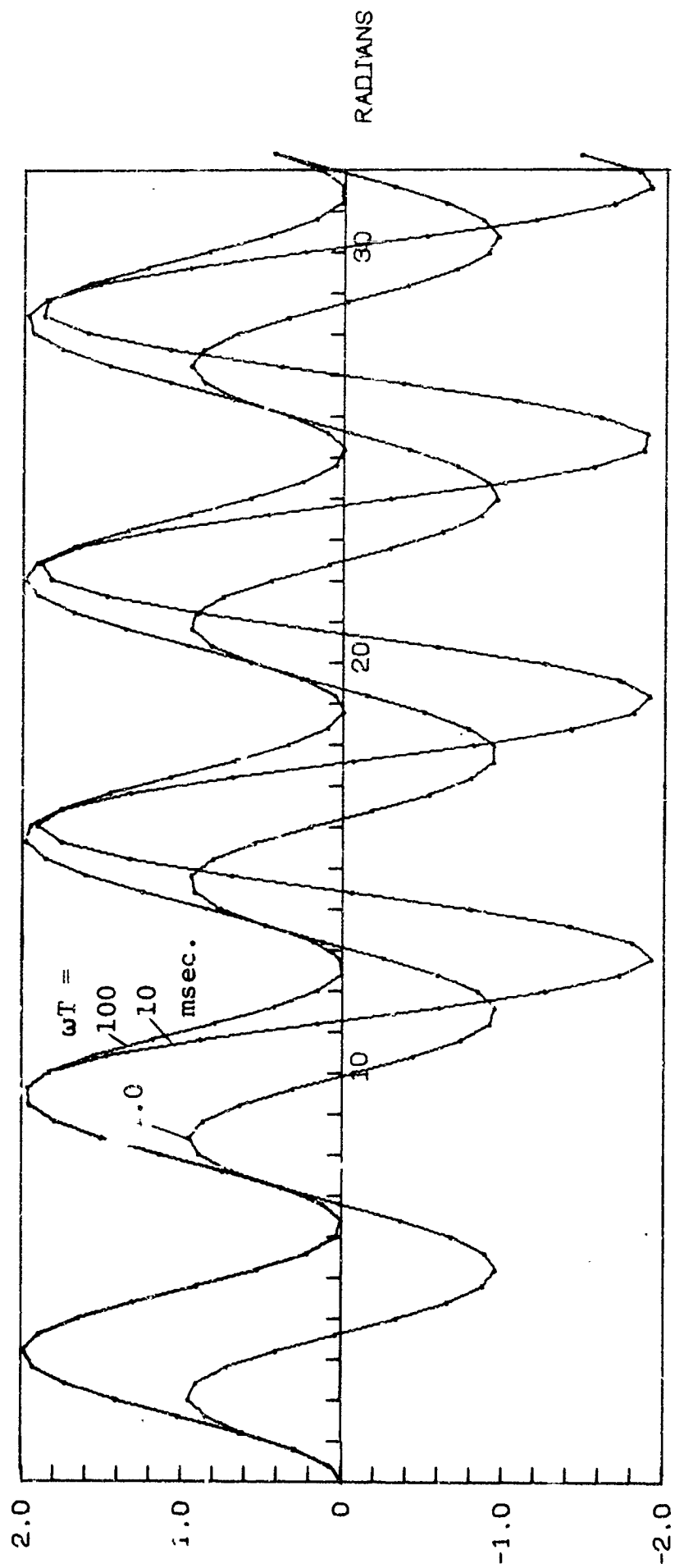
Fig. AII.2   GENERAL DYNAMIC STRESS FUNCTION (A)
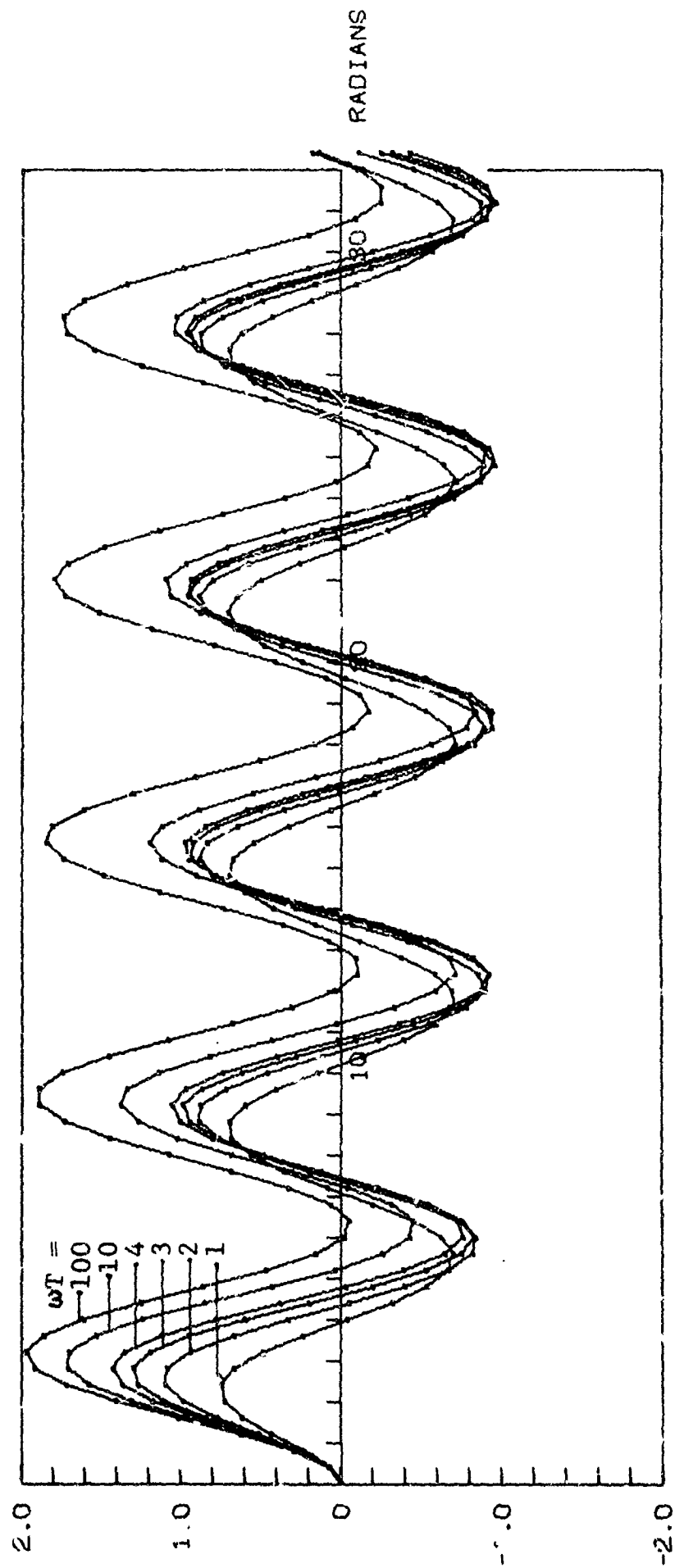
Fig. AII.3 GENERAL DYNAMIC STRESS FUNCTION (C)

Fig. AII.4

GENERAL DYNAMIC STRESS FUNCTION (D)

RADIANS

DYNAMIC STRESS FUNCTION

$\omega T =$
1.0
2.0
3.0
10.
100.
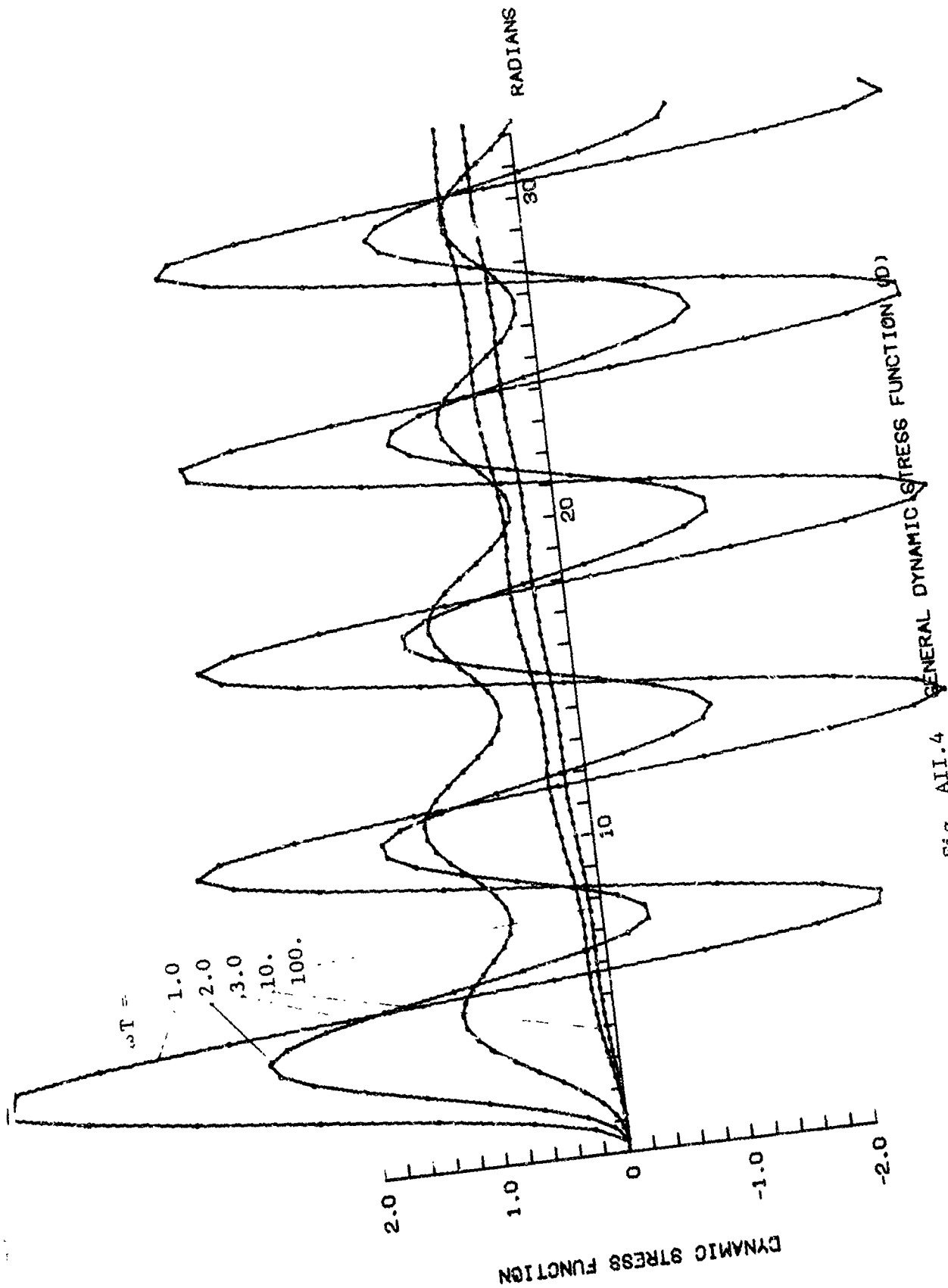
$$\frac{\Delta R}{[R_o]}_T \;=\; c_1' \left(\frac{298}{T}\right)\epsilon \;+\; c_2' \left(\frac{298}{T}\right)\epsilon^2$$
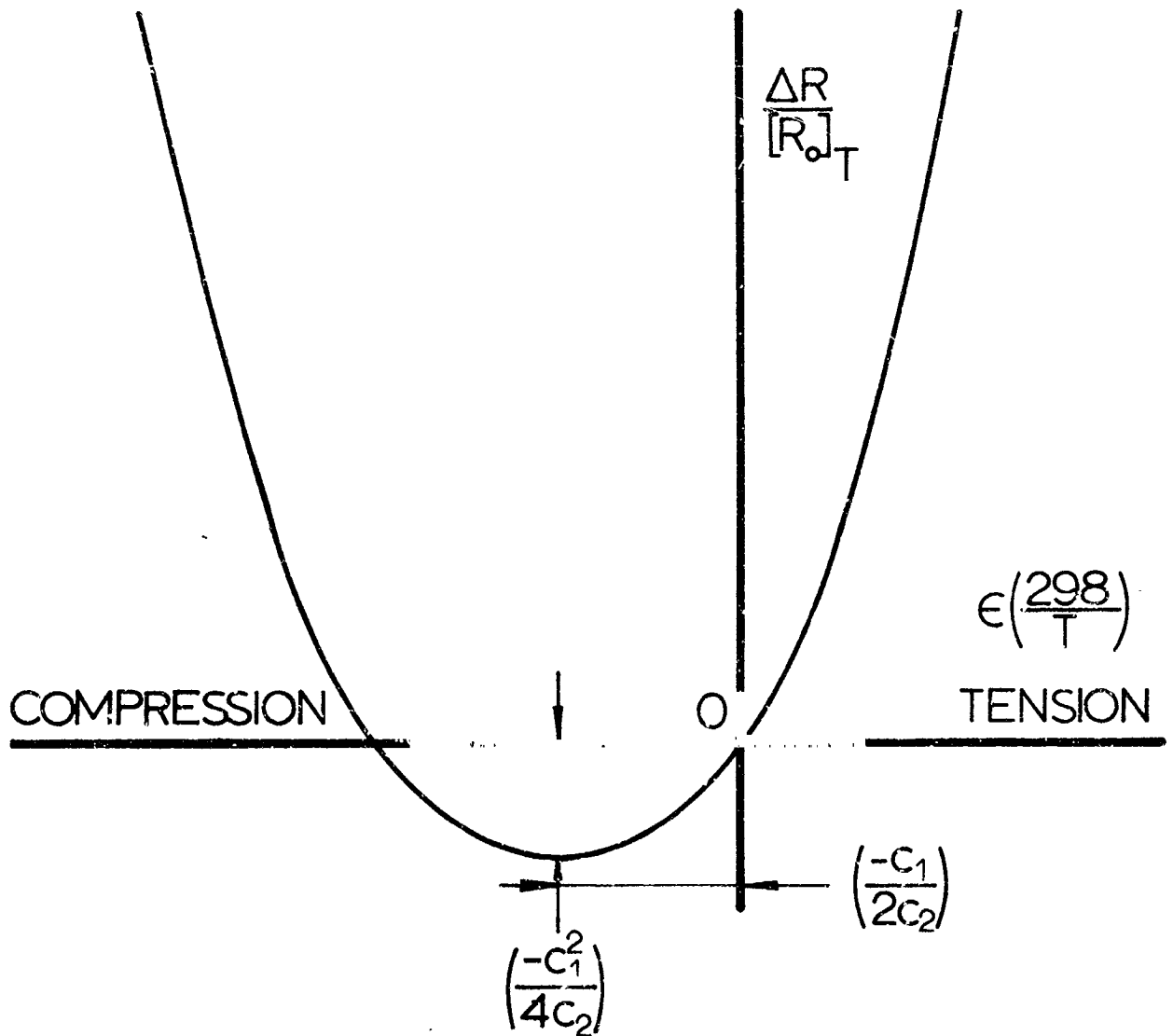
Fig. AIII.1   Strain and temperature sensitivity of a typical
semiconductor strain gauge
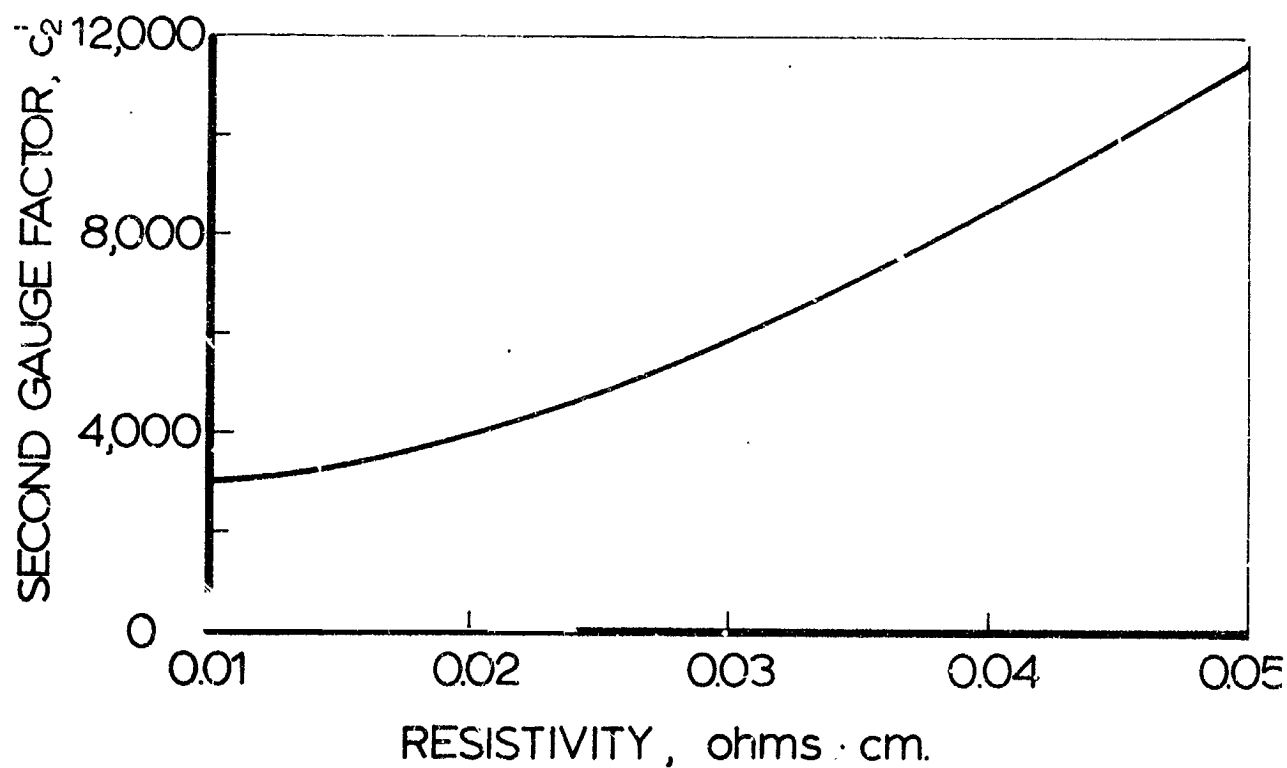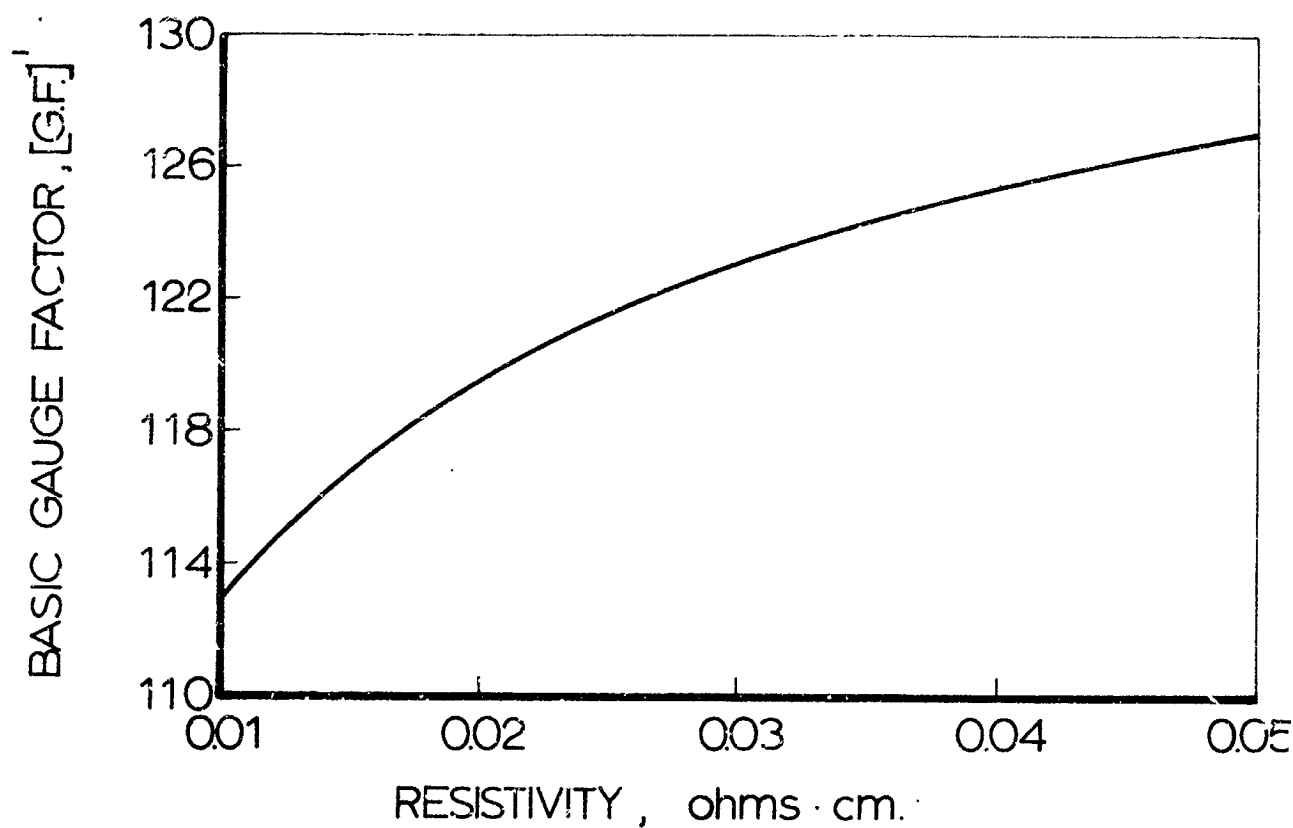
Fig. AIII.2   Gauge factor,   G.F. ', and gauge constant,
C_2', as a function of the resistivity of
a² silicon semiconductor strain gauge
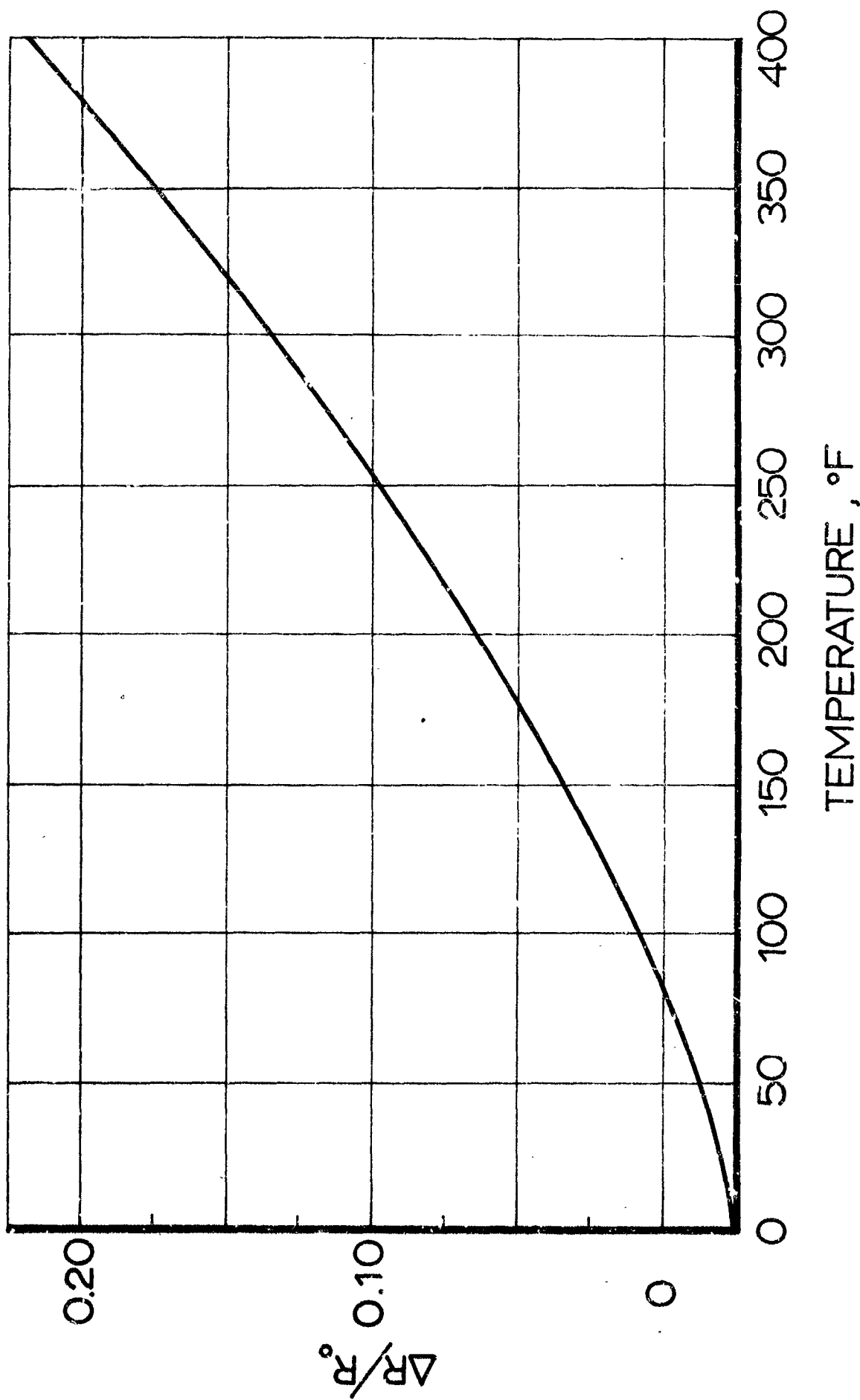
Fig. AIII.3   Temperature coefficient curve for silicon semiconductor strain
gauge of 0.02 ohm-cm resistivity
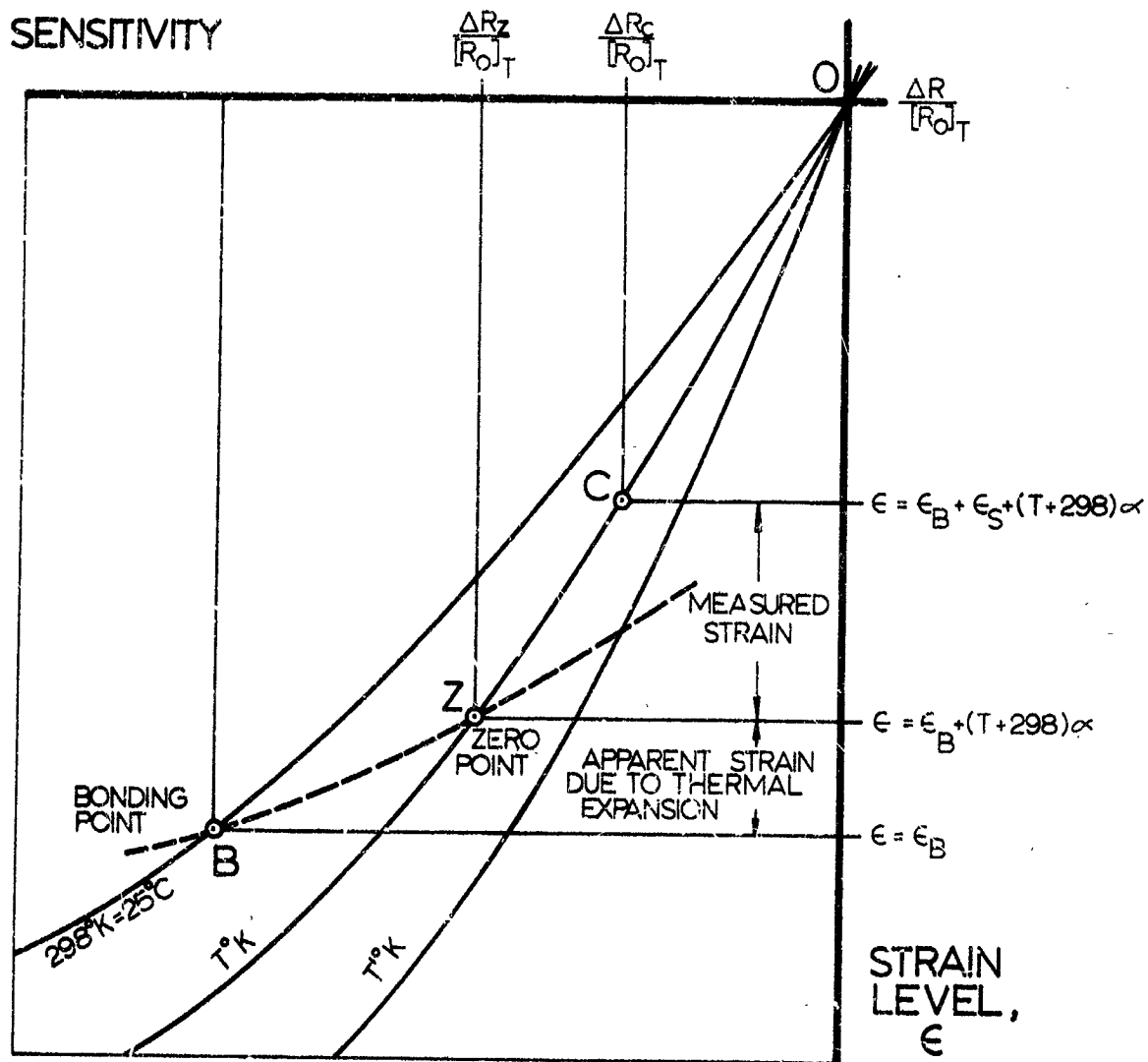
Fig.AIII.4 Characteristic strain - sensitivity curves for semiconductor strain gages

TENSIONING SCREWS AND SUPPORT WIRES

STRAIN GAUGE

TEFLON FILM

RUBBER

IRON

COPPER PLATE

THERMOCOUPLE

POWER LINE TO HEATER

THERMOCOUPLE

TEMPERATURE CONTROLLER

POWER INPUT
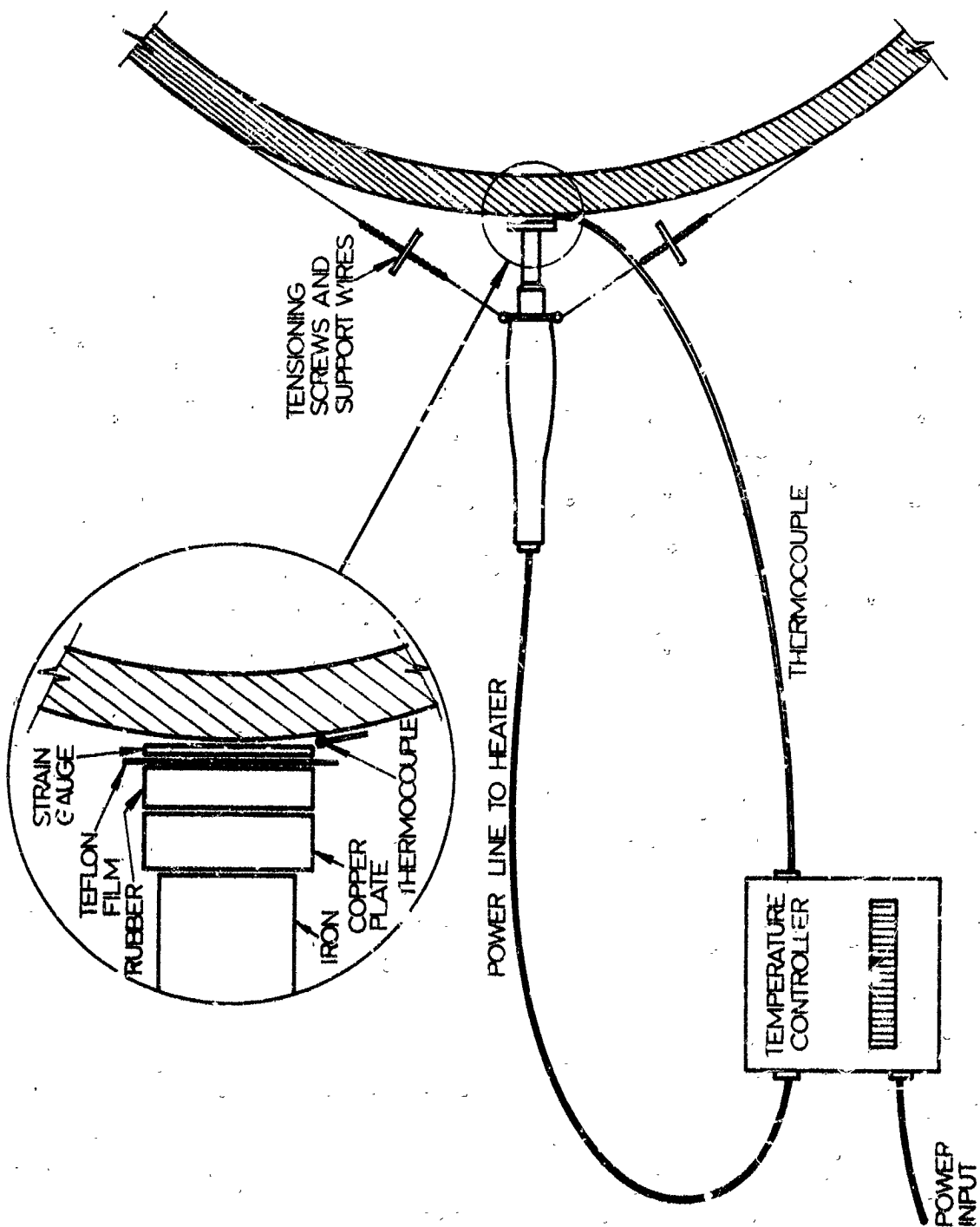
Fig. AIII.5 Bending rig for attaching strain gauge to specimen

Fig. AIII.6 Strain gauges and thermocouples after bonding, before sealing
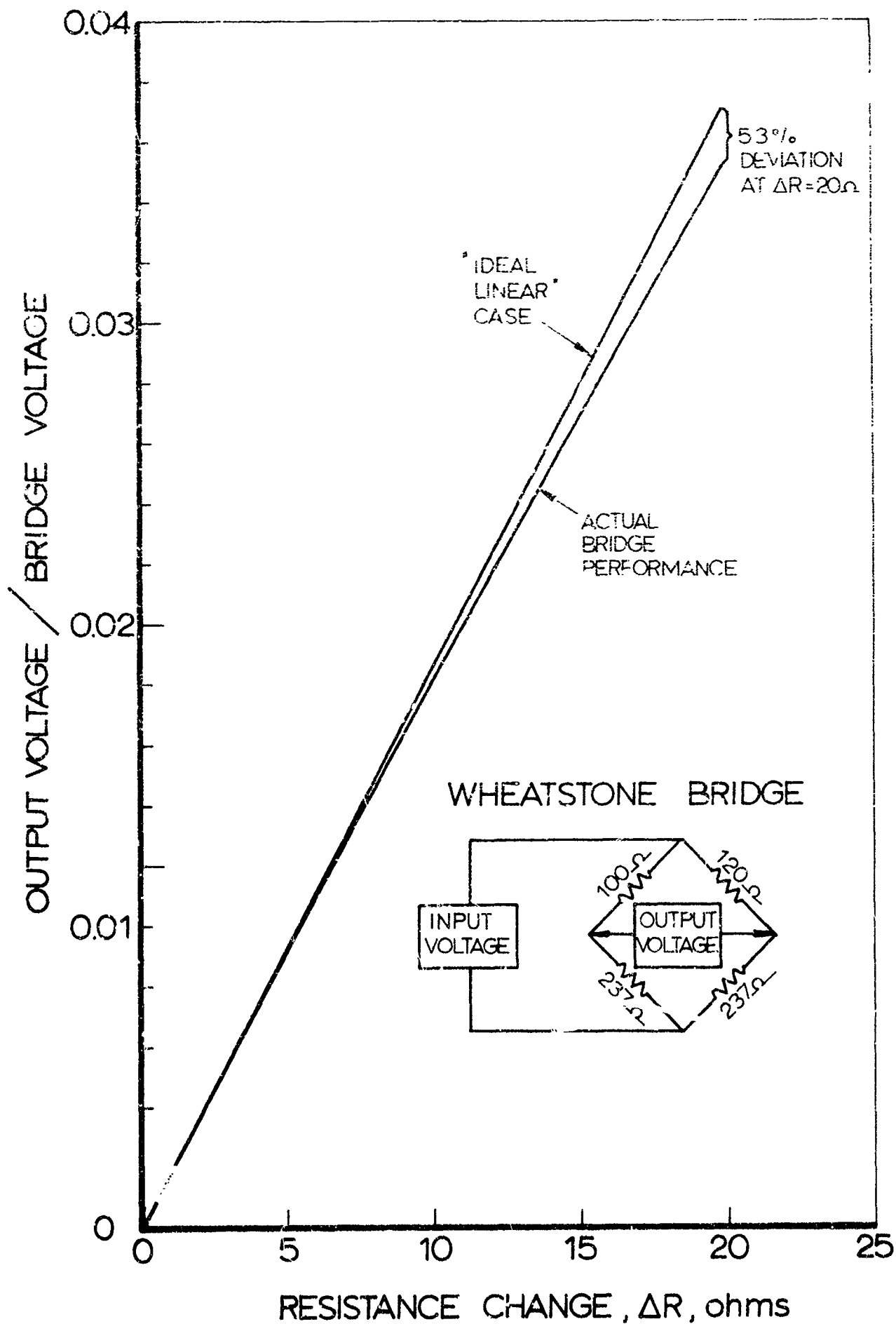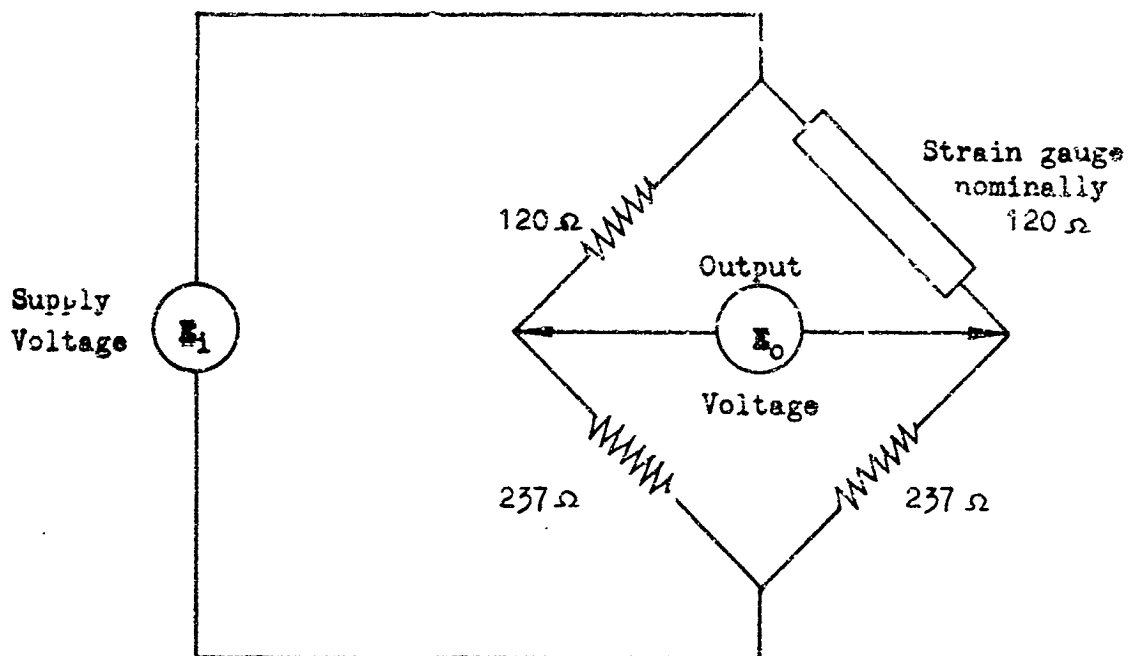
Fig. AIII.7 Wheatstone Bridge Circuit for 120 strain gauge.
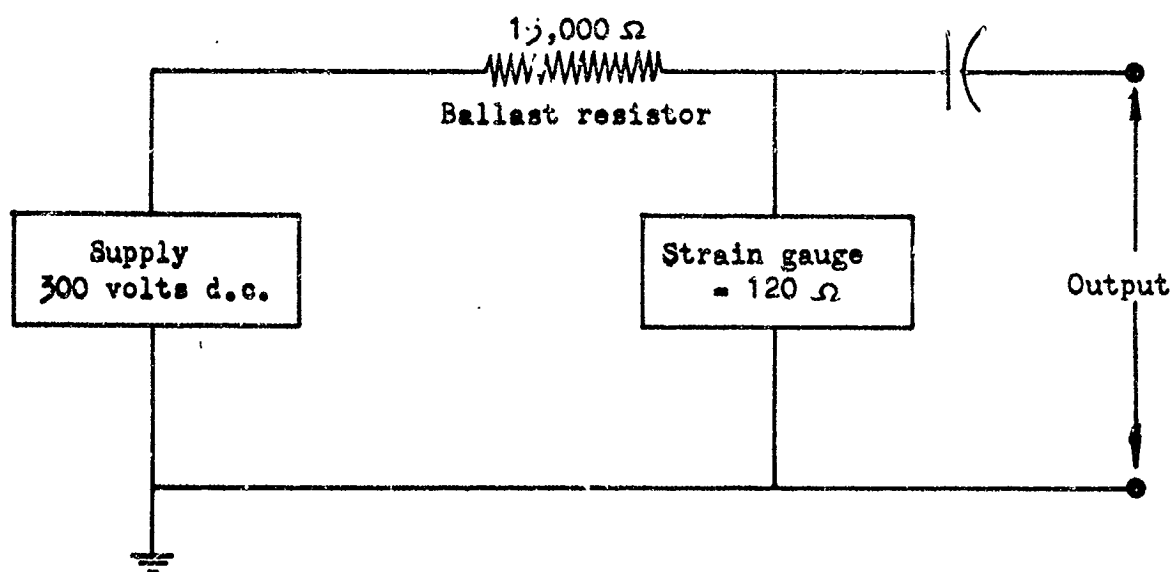
Fig. AIII.9 Constant current circuit for a 120 strain gauge.
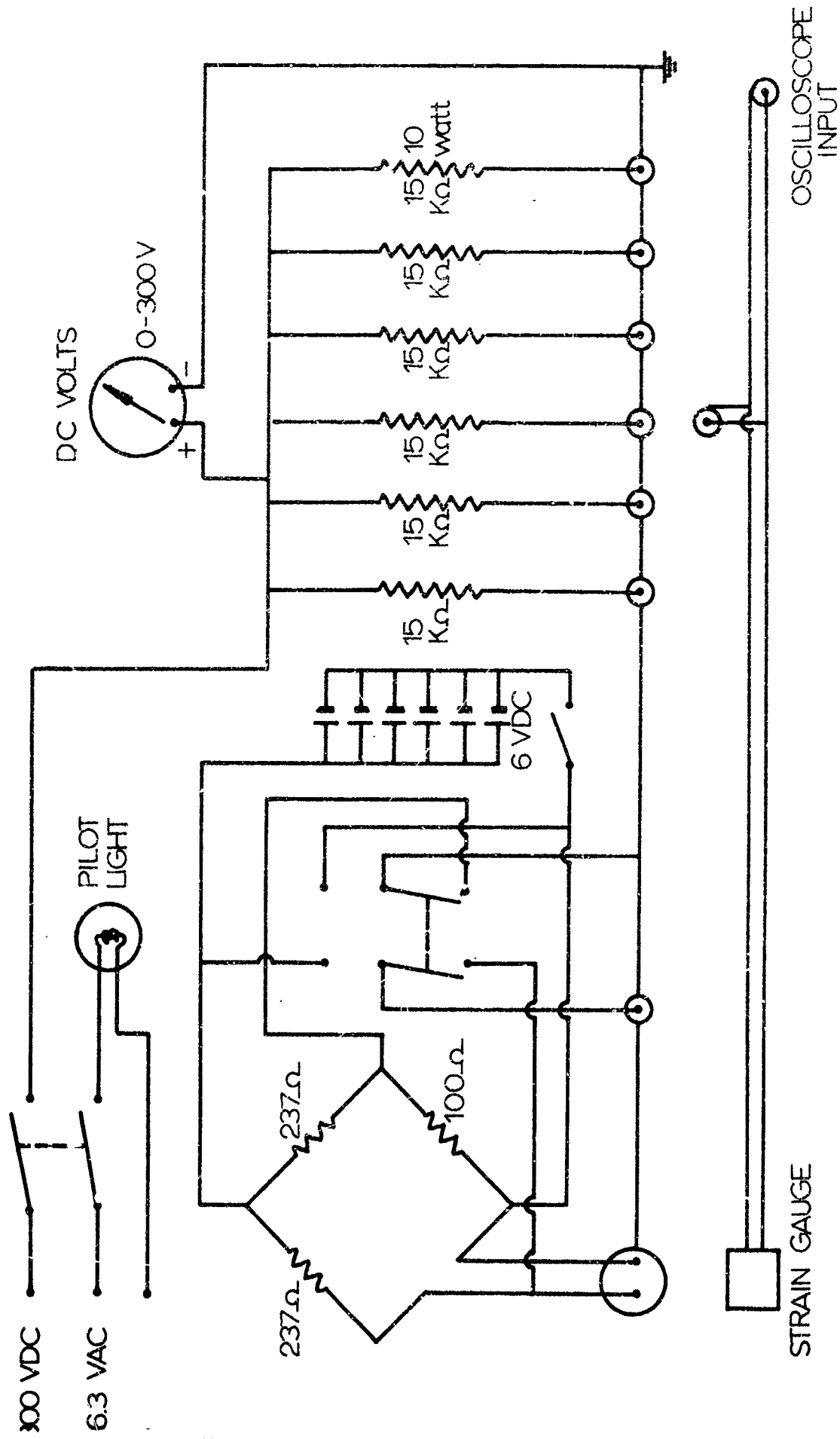
Fig. AIII.10 Circuit diagram for strain measurements, including calibration bridge circuit
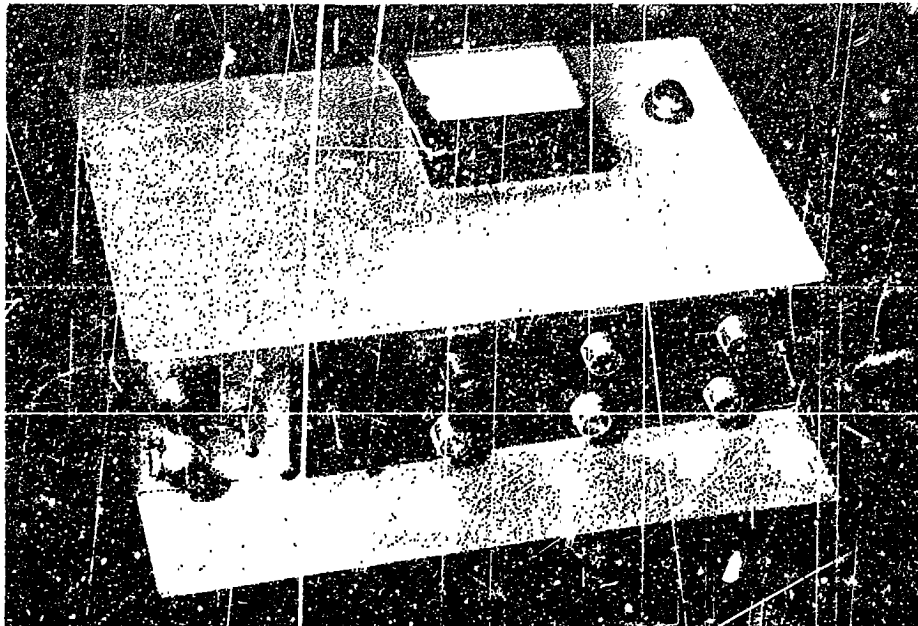
AIII.11 Photograph of the strain-gauge circuit, showing
calibration input-output on the left, and the inputs
for the six operational channels on the right
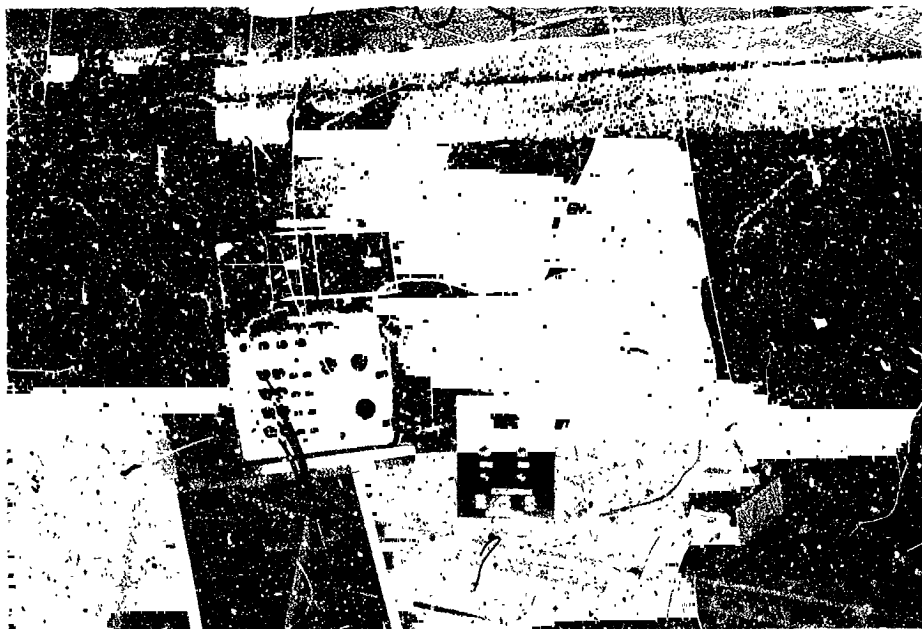
AIII.12 Experimental set-up for strain recording, showing the
strain gauge circuit, power supply, and oscilloscope
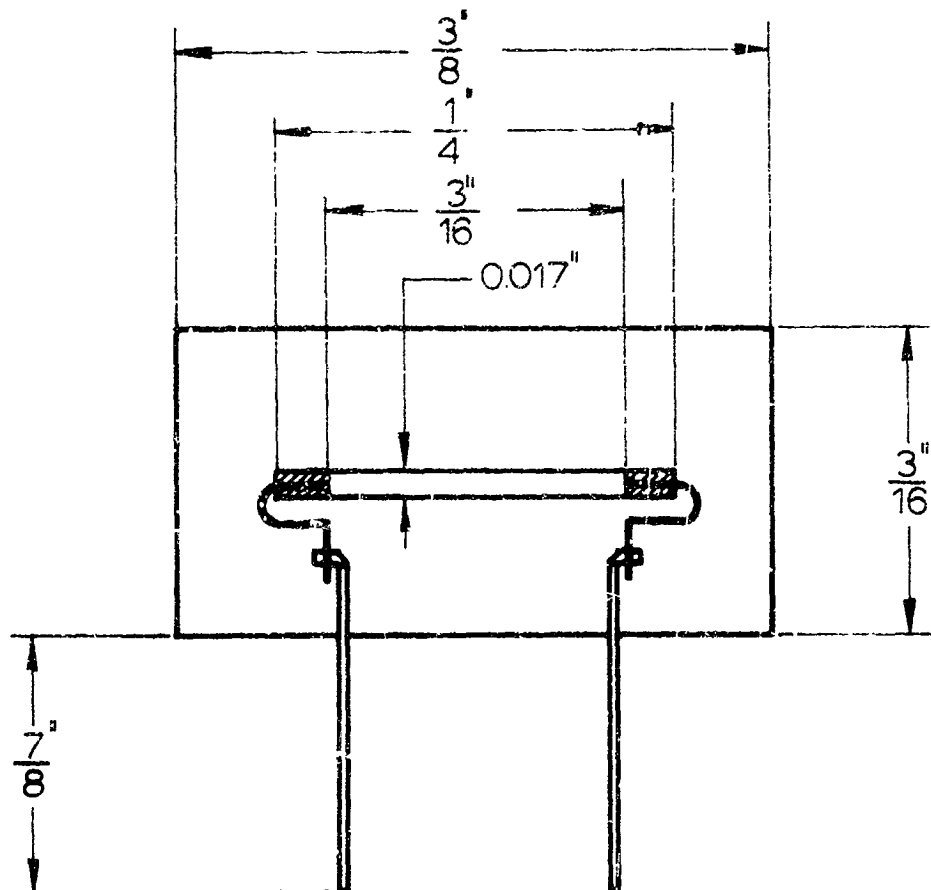
Fig. AIII.13 Baldwin-Lima-Hamilton type SPB2-18-12 Semiconductor Strain Gauge

Table of Gauge Properties

R   Unbacked, unbonded resistance - 141 ohms within 1%

G.F. ' Basic Gauge Factor - 122.0 within 2% at 25°C

C_2' Gauge constant - 3700 within 5% at 25°C

Thermal expansion coefficient - 2.5 in/in/°F

Material - Gauge element of P-type silicon (cut on the
        111 axis), mounted onto bakelite backing strip

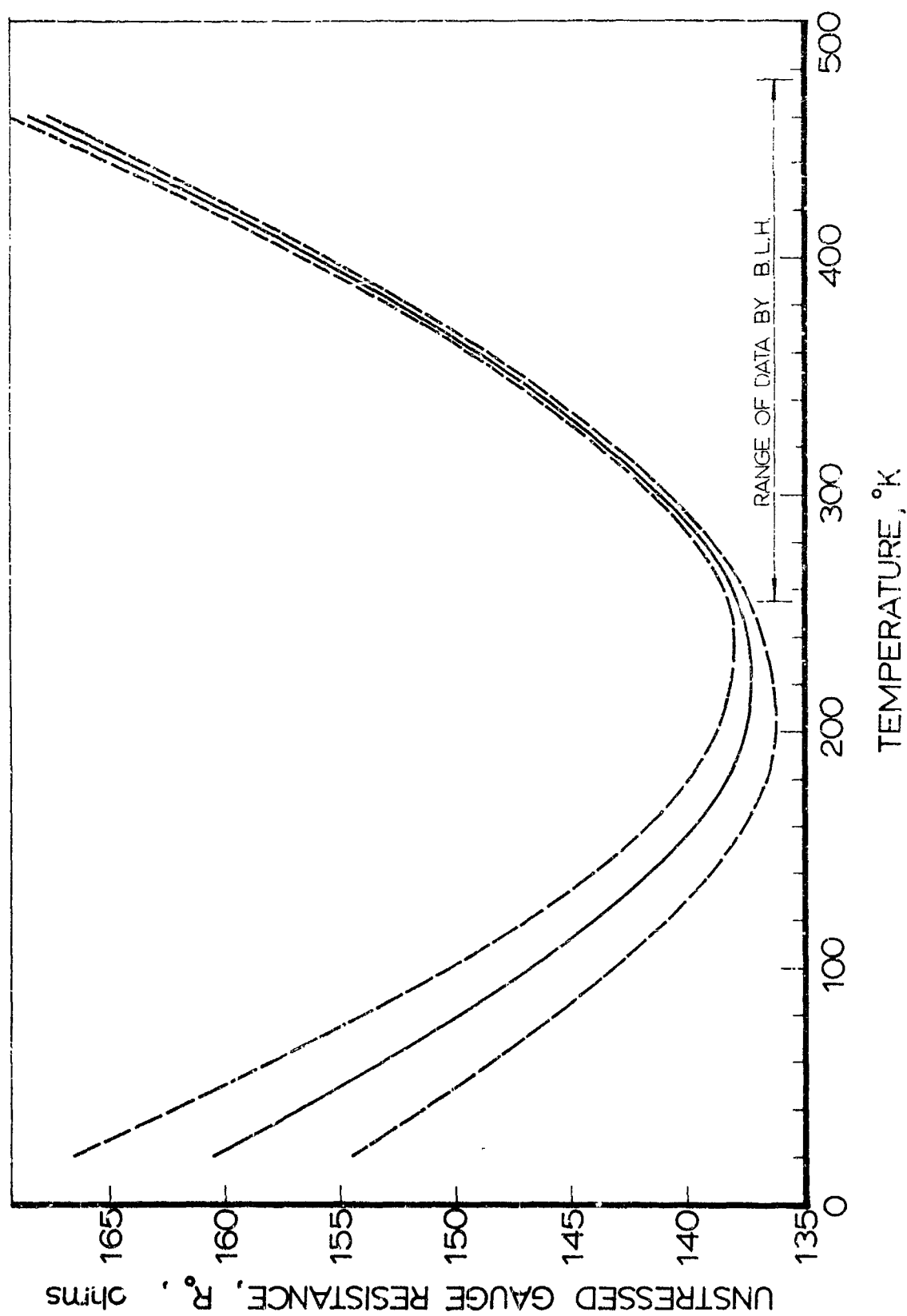Overall gauge length - 1/4 in

Backing dimensions - 3/8 x 3/16 in

Fig. AIII.14   Temperature variation of the unstressed gauge resistance Ro, for SPB2-18-12
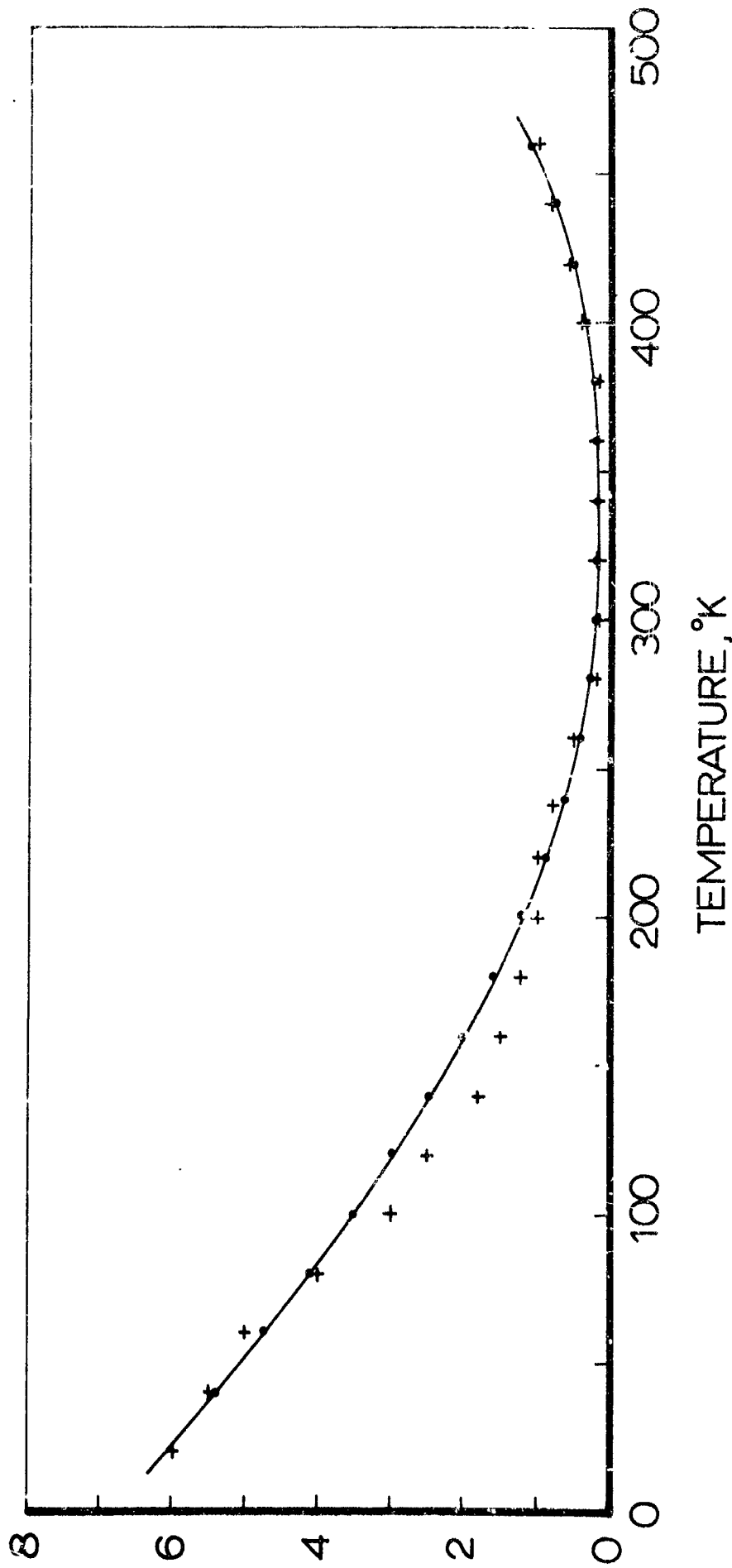strain gauges. The estimated error in gauge resistance is shown by broken lines.

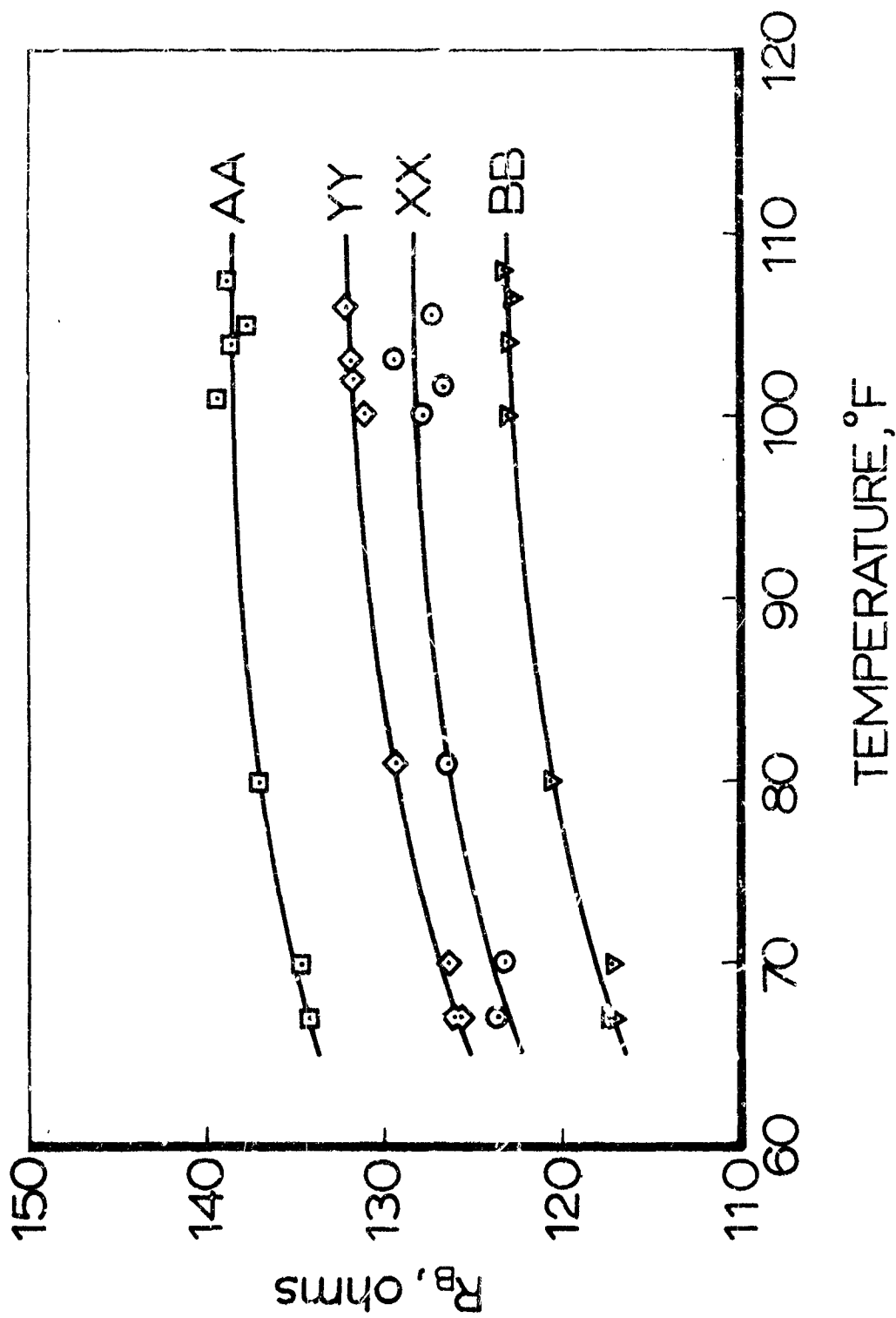Fig. AIII.15 Estimated error in values of unstressed gauge resistance Rl_t, plotted as a function of temperature

Fig. AIII.16 Experimental calibration curves of the variation of bonded resistance, R_B, with temperature for the semiconductor strain gauges